Université de Neuchâtel Faculté des Sciences

From Anticancer Complexes to Photoswitchable Assemblies: New Approaches in the Design and Synthesis of Arene Ruthenium Species

Thèse présentée à la Faculté des Sciences,

Pour l'obtention du grade de Docteur ès Sciences par

Thomas Cheminel

Titulaire d'un Master en Chimie Moléculaire de l'Université Pierre et Marie Curie de Paris, France

Membres du jury :

Prof. Bruno Therrien, Directeur de thèse, Université de Neuchâtel

Prof. Robert Deschenaux, Expert interne, Université de Neuchâtel

Prof. Riccardo Pettinari, Expert externe, Università di Camerino

Soutenue le 8 septembre 2016

UNIVERSITÉ DE NEUCHÂTEL

Faculté des sciences
Secrétariat-décanat de Faculté
Rue Emile-Argand 11
2000 Neuchâtel - Suisse
Tél: + 41 (0)32 718 2100
E-mail: secretariat.sciences@unine.ch

IMPRIMATUR POUR THESE DE DOCTORAT

La Faculté des sciences de l'Université de Neuchâtel
autorise l'impression de la présente thèse soutenue par

Monsieur Thomas Cheminel

Titre:

"From Anticancer Complexes to Photoswitchable Assemblies: New Approaches in the Design and Synthesis of Arene Ruthenium Species"

sur le rapport des membres du jury composé comme suit:

- Prof. ass. Bruno Therrien, Directeur de thèse, Université de Neuchâtel, Suisse
- Prof. Robert Deschenaux, Université de Neuchâtel, Suisse
- Prof. Riccardo Pettinari, Università di Camerino, Italie

Neuchâtel, le 20 septembre 2016 Le Doyen, Prof. R. Bshary

Acknowledgements

The present thesis was done at the University of Neuchâtel, in the group and under the supervision of Professor Therrien, and represents four years of work. While this document has my name on its front page, it would be fairly egocentric and inaccurate to say that it was something I achieved alone; many people deserve to be thanked for their contribution, whether professional, personal, or both.

First, I would like to express my sincerest thanks to Professor Bruno Therrien, for giving me the opportunity to work in his group and for presenting me with a challenging but exciting research project. Through our conversations, he provided advice on many aspects of chemistry as a whole and helped me better understand my project, as well as what it means to be a good scientist. I learned many important things during these four years, and Professor Therrien can be accredited for a good part of them.

I would like to thank Professor Robert Deschenaux and Professor Riccardo Pettinari for accepting to be part of my thesis jury, and for taking the time to read the manuscript and provide insightful comments and corrections about it during the examination. My thanks also go to Professor Georg Süss-Fink, for animating our group meeting sessions and for sharing his valuable experience and knowledge of ruthenium chemistry. I also thank Professor Reinhard Neier for our occasional but pleasant conversations, as well as for his commitment in the life of the chemistry department, especially regarding the doctoral program conferences.

During my PhD, I had the opportunity to work for a month at the University of Cluj, Romania, as part of the ruthenium hydrazinyl-thiazole complexes project. For that, I would like to thank Professor Adriana Grozav, for her supervision and for introducing me to the biological part of this project. I would also like to thank everyone I worked with in the chemistry department over there, especially Dr Balazs Brem, for their kindness and for making sure my stay in Cluj was pleasant.

During these four years in Neuchâtel, I worked alongside many people, some of them for quite some time. The connections and friendships I formed, and overall the everyday life in the chemistry department, are something I will always fondly remember. Many thanks go towards David, my lab and office neighbor for three years; our conversations, were they chemistry-related or far from that, happening near our lab benches or at a bar table, were always a delight and contributed greatly to our work atmosphere. I also have to thank Marie,

who David entrusted with the hard task of bearing with me when he left. Her patience and cheerfulness were deeply appreciated, and helped me finish my thesis in an enjoyable environment. Special thanks go to Virginie, who I often came to see in her lab whenever I had the chance; she always proved to be a very good friend, and I am grateful for that. Finally, I would like to thank William, who has been a coworker, a roommate, but most importantly a friend. We started – and finished – our doctoral studies roughly at the same time, and I think it was particularly beneficial for both of us to be road partners, both in fun and more serious times. I would also like to thank everyone I worked with: Julien, Manu, Raja M., Justin, Minghui, Amine, Bing, Jiri, Raja N., Gupta, Fan, Vidya, Johanna and Cristina in our group; Yovana, Luyen, Pauline, Steeve, Le Anh, Tung, Giao, Yassine, Damien, Christelle, Christian and Ewa in the other groups in the chemistry department.

Many thanks go towards my apprentices Csilla and Tracy, who did an outstanding job in the lab. I also have to thank all the NPAC staff for the analyses, and the administration staff for their help during these four years.

Outside the university environment, I would like to thank Mendes for being a great friend and roommate, and for all the good times when we would forget our work issues by getting angry at strangers – and sometimes at each other – over an online game. Of course, I would also like to thank my friends Adrien, Fabien, Aurélien and Alexandre back in Paris for their constant support and for being able to see a bunch of familiar faces whenever I decided to take a trip home.

Finally, I would like to acknowledge the two most important women in my life. I thank Seyran with all my heart, for being present on an everyday basis, and for supporting me during the last rough months of my thesis, as I am sure I must have been a pain in the neck sometimes. If it wasn't for you being here, all of this would have been much more difficult to finish. Thank you for making my life so nice to live.

These last words are for my mom. There are so many things I need to thank you for, it would be impossible to fit them all here. Thank you for making me, thank you for raising me, thank you for letting me make my own choices, even though you sometimes disagreed. You are the reason I am able to stand where I am today and write all of this. I can never say thank you enough, so the least I can do is dedicate this thesis to you, because it is every letter as much yours than it is mine.

Summary

The aim of the present thesis was to explore new approaches in the design and synthesis of new arene ruthenium species. This class of organometallic compounds has been the subject of much attention in the recent years due to their interesting properties in various fields, such as medicinal chemistry or supramolecular chemistry. In order to achieve this goal, this work was divided into two parts.

In the first part, the synthesis of ruthenium complexes containing hydrazinyl-thiazole ligands was studied. These organic molecules have indeed proved to be highly active against some types of cancer; the strategy of this project was then to combine the activity of the organic ligand and that of the arene ruthenium core. The first series of complexes, where the ligands contained phenyl derivatives in their structure, was tested on human cervical and ovarian cancer cell lines. The results were overall good when compared to platinum anticancer compounds cisplatin and oxaliplatin, and some of the complexes showed selectivity in favor of cancerous cells over healthy ones. This led to an optimization of the structure of the complexes, as well as the synthesis of two other series of complexes, where the ligands contained pharmacophore aromatics moieties – phenothiazine and indole derivatives.

In the second part, the design and synthesis of light responsive ruthenium assemblies was investigated. By using photoswitchable organic molecules as part of ruthenium metalla-assemblies, the goal was to create ruthenium entities capable of existing in two different states, thus potentially providing a novel means to control the encapsulation and release of guest molecules. Several classes of molecules – azobenzene, anthracene, and dihydropyrene derivatives – were used in this project. Results indicated that semi-functional photoswitchable assemblies could be obtained with some of those molecules, and gave insight on the functioning of such assemblies. Several compounds synthesized in this project also have the potential to be used as vehicles for the transport of singlet oxygen, making them interesting both in medicinal and supramolecular chemistry.

These results showed the versatility and relevance of arene ruthenium species in both the synthesis of a new family of anticancer complexes and the construction of novel light-triggered supramolecular assemblies.

Key Words

Arene ruthenium complexes, hydrazinyl-thiazole ligands, anticancer activity, supramolecular chemistry, photoswitches

Mots Clés

Complexes arène ruthénium, ligands hydrazinyl-thiazole, activité anticancéreuse, chimie supramoléculaire, photoswitches

Abbreviations

CPD	cyclophanediene
dcbq	2,5-dichloro-3,6-dihydroxy-1,4-benzoquinonato
dhbq	2,5-dihydroxy-1,4-benzoquinonato
dhnq	5,8-dihydroxy-1,4-naphtoquinonato
DHP	dihydropyrene
DMF	dimethylformamide
DMSO	dimethylsulfoxide
DNA	deoxyribonucleic acid
EPR	enhanced permeability and retention
ESI-MS	electrospray ionization mass spectrometry
HMBC	heteronuclear multiple-bond correlation spectroscopy
HSQC	heteronuclear single-quantum correlation spectroscopy
IC_{50}	inhibitory concentration of 50% of cells
IR	infrared
NMR	nuclear magnetic resonance
oxa	oxalato
PTZ	phenothiazine
RNA	ribonucleic acid
RPMI	Roswell Park Memorial Institute
RT	room temperature
THF	tetrahydrofuran
UV	ultraviolet

Table of Contents

Chapter 1: Introduction

1.1 History of Ruthenium

Ruthenium is a transition metal discovered in 1844 by Karl Klaus, as part of the residues left after dissolving platinum ores in aqua regia.[1] Named after Ruthenia, the Latin name of Russia, ruthenium is the element 44 of Mendeleev's periodic table, and is part of the Group VIII of this classification. It is a particularly rare element, its abundance in Earth's crustal rocks being estimated at only 0.0001 ppm. In the metallic state, ruthenium is generally found in ores along with other "platinum" metals, and after being separated, it is isolated as a hard white metal (Figure 1). As a metal, the main use of ruthenium is the hardening of platinum and palladium; however, its rarity and therefore high cost of production, with only about 20 tons produced each year,[2] make the industrial applications of ruthenium relatively limited.

Figure 1: Ruthenium crystals

Ruthenium shares a lot of properties with osmium, its neighbor in the periodic table, such as a high number – seven – of naturally occurring isotopes, and a wide range of available oxidation states, going from -II (d^{10}) to +VIII (d^0). This property is crucial and gives access to a variety of ruthenium compounds with different coordination modes and geometries. While the higher oxidation states are relatively unimportant in this regard and are mostly represented by oxides and halides,[3] oxidation states between 0 and +IV make for the most part of ruthenium coordination compounds, each electronic configuration of the metal being suited for different types of ligands. The diversity and tunability of compounds available make ruthenium a very interesting element and a promising candidate for traditional applications of

organometallic compounds, such as catalysis; but over the years, ruthenium has also proven to be a key element in other fields, as will be discussed here.

1.2 Uses of Ruthenium Organometallic Compounds

1.2.1 In Catalysis

Despite all of the interesting features described above, ruthenium organometallic chemistry is still fairly recent. Before the 1980s, ruthenium complexes were scarce and only used for the catalysis of organic reactions such as oxidations or hydrogenations. Since then, ruthenium chemistry has vastly expanded, and not only is ruthenium used as alternative to existent catalysts, but new organic reactions have also been developed using a ruthenium complex as catalyst. Nowadays, a large number of ruthenium species are used for a broad range of organic reactions, to the point that it is now of the same importance as palladium in the field of catalysis.[4] While it is not the goal of the present introduction to be comprehensive in that particular subject, some examples deserve to be mentioned.

Hydrogenation is one of the most important and challenging reactions in organic chemistry; it gives access to a lot of interesting molecules and is widely used in the industry. Ruthenium dioxide RuO_2 and the complex $RuCl_2(PPh_3)_3$ were the first ruthenium compounds used as catalysts for the hydrogenation of anilines and olefins, respectively. Ever since, dozens of ruthenium complexes were designed for the hydrogenation of unsaturated compounds such as olefins, carbonyls, and aromatic compounds. Some of the most well-known are the Ru-BINAP complexes, which are used in the enantioselective hydrogenation of alkenes.[5]

Another area of catalysis where ruthenium has proven to shine is carbon-carbon bond formation. This kind of reaction is of paramount importance in chemistry, and while palladium definitely stands out thanks to its popular use in coupling reactions, the number of ruthenium compounds used to catalyze such reactions has risen significantly over the last decades. Among these reactions, the one which development was most influenced by ruthenium is the olefin metathesis. Since the early 1990s,[6] Grubbs and co-workers have designed several ruthenium-centered complexes designed towards metathesis catalysis, some of them which are now commercially available are traditionally used in different metathesis processes (Figure 2).

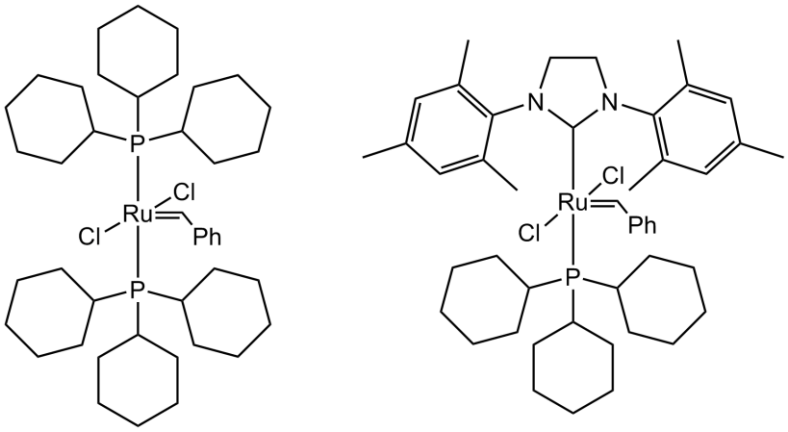

Figure 2: Grubbs Catalysts, 1st (left) and 2nd (right) generation

1.2.2 In Dye-Sensitized Solar Cells

Aside from catalysis, ruthenium also plays an important role in the preparation of dye-sensitized solar cells (DSC). Polypyridine ruthenium complexes are found to be some of the best dyes to be used; Grätzel and co-workers have investigated many of them and reported them for the accessibility of their synthesis and for their spectral and redox properties.[7] Indeed, these complexes exhibit very strong charge transfer transitions, which lead to an efficient absorption of light. While this area can still be improved and the structure of the dyes refined, some of these ruthenium complexes have become standards and are now used in commercially available solar cells (Figure 3).

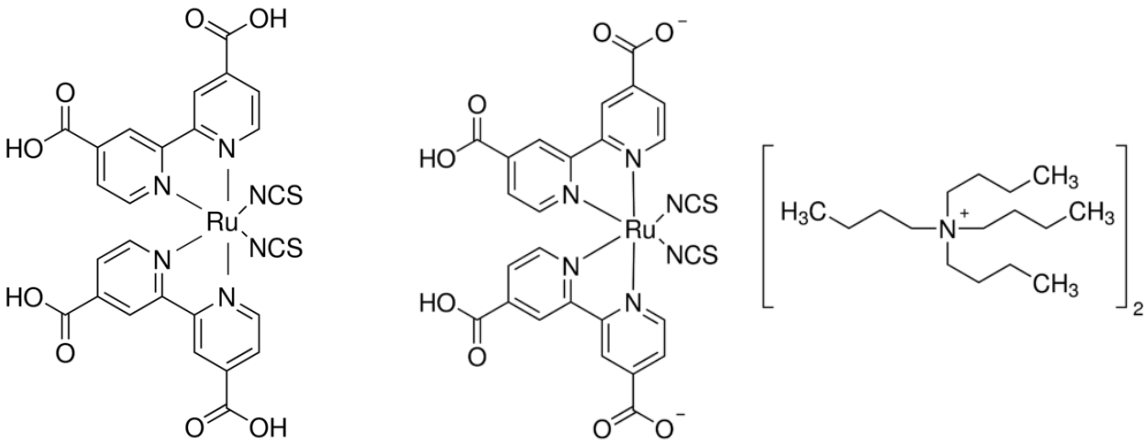

Figure 3: Ruthenium-based N-3 (left) and N-719 (right) dyes

1.2.3 In Biology

Ruthenium complexes are also extremely popular in medicinal chemistry, especially in the field of cancer treatment, with multiple compounds reported. However, they will not be discussed here, as it will be the topic of the introduction of Chapter 2 (see page 13).

1.2.4 In Supramolecular Chemistry

Supramolecular chemistry is a term coined by Jean-Marie Lehn and is defined as "the chemistry of molecular assemblies and of the intermolecular bond".[8] It is a field located at the boundaries between organic chemistry and coordination chemistry, and focuses on assemblies held together by weak interactions such as metal-ligand bonds, Van der Waals forces, π-π interactions or hydrogen bonds. Supramolecular chemistry spawned several important concepts, such as self-assembly, molecular recognition and host-guest chemistry. These topics, as well as the influence of ruthenium in this field, will be discussed here.

One of the first examples of molecular recognition is the encapsulation of metal cations inside crown ethers.[9] These complexes are stabilized thanks to the ion-dipole forces existing between the positively charged metal ion and the negatively charged oxygen atoms of the crown ether. By varying the length of the chain forming the crown, thus varying the size of the cavity of the cycle, different cations could be encapsulated, ranging from small alkali metal ions such as Li^+ or Na^+ to bigger species such as transition metal ions or lanthanide ions (Figure 4).[10] Interestingly, it was observed that the solubility of the metallic ions was modified when complexed to crown ethers, making them soluble in apolar solvents such as hydrocarbons.

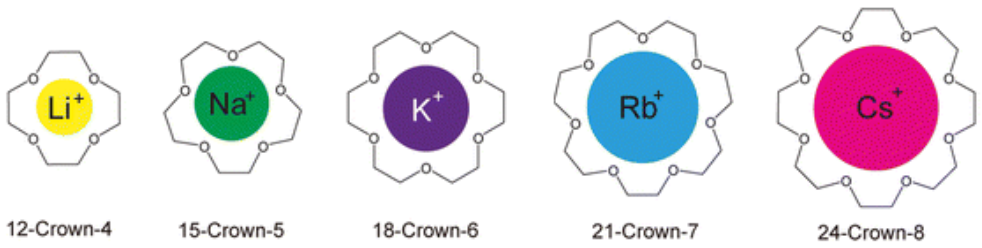

Figure 4: Schematic representation of the encapsulation of metallic cations inside crown ethers

These works on the concept of encapsulation of a "guest" molecule inside the cavity of a "host" molecule were only the beginning of what would become an essential component of supramolecular chemistry as a whole. Since then, many examples of host-guest systems have been reported in the literature. While some of them focus on organic molecules as hosts, such as cyclodextrins or calixarenes, attention was quickly given to metalla-assemblies capable of encapsulating a guest molecule. The first of this kind is a copper-based M_2L_2-type structure reported in 1984 by Maverick.[11] Because of the affinity of the metal towards nitrogen-bonding ligands, this metalla-rectangle was able to encapsulate small diamines inside its cavity. A few years later, Fujita and co-workers reported the self-assembly of a platinum-based supramolecular complex,[12] using ethylenediamine as a ligand "blocking" two cis positions of the coordination sphere of the metal, inducing the square shape of the resulting assembly in the presence of the linear linker 4,4'-bipyridine (Figure 5). As with Maverick's work, this platinum complex was able to encapsulate small aromatic molecule, this time using π-stacking effect as host-guest interaction. The strong positive charge of the assembly makes it highly soluble in water, allowing – similarly to the case of crown ethers – the solubility of the hydrophobic guest molecule in aqueous media when encapsulated.

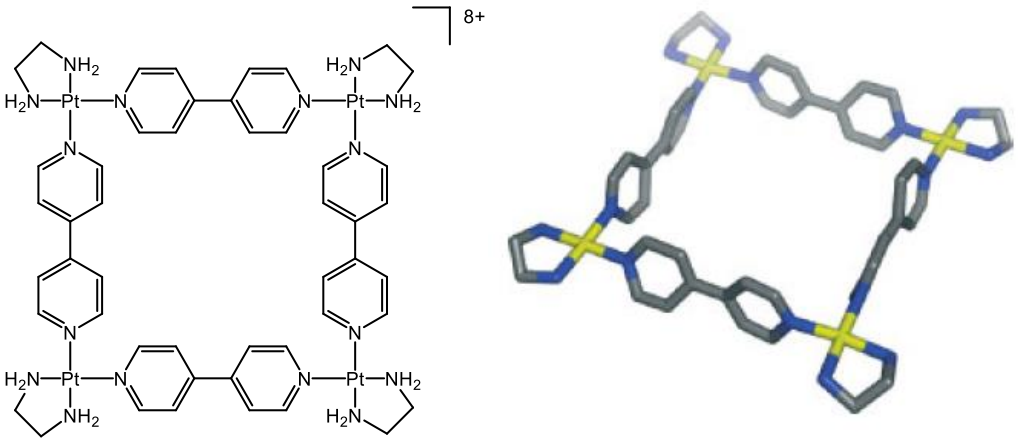

Figure 5: X-ray crystal structure of Fujita's M_4L_4 platinum square

With its number of interesting features and properties, it was just a matter of time before ruthenium was investigated as the center of such supramolecular assemblies. In particular, arene ruthenium species were considered as the main building blocks. This type of compounds was first synthesized in 1967 by Winkhaus and Singer by reducing ruthenium (III) trichloride with 1,3-cyclohexadiene, even though the polymeric structure they proposed

was eventually found to be false.[13] The right structure of the compound formed was confirmed a few years later,[14] and consists in a dinuclear ruthenium (II) species, $[(\eta^6\text{-}C_6H_6)Ru(\mu^2\text{-}Cl)Cl]_2$, where the two metal atoms are bridged together by two chlorine atoms (Scheme 1).

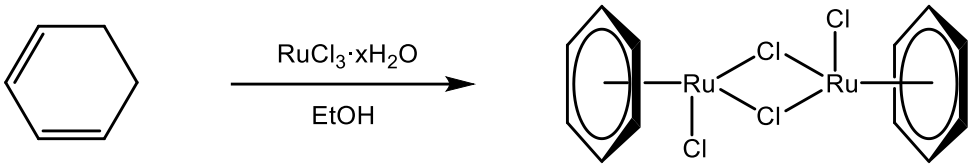

Scheme 1: Synthesis of benzene ruthenium dichloride dimer

Due to its easy synthesis and its excellent stability under atmospheric conditions, this compound became a key starting material for the synthesis of a whole library of ruthenium species suitable to make organometallic supramolecular assemblies. Indeed, the chlorine atoms of the dimer are particularly labile and easily removed, either to form monomeric, "half-sandwich" complexes; or to access other dinuclear species by using bridging tetradentate ligands such as dihydroxybenzoquinone derivatives.

The former approach has been extensively developed by several groups, with many examples of metalla-cages based on arene mono-ruthenium species existing in the literature. Especially worth mentioning is the work of Severin regarding the design of ruthenium crown ether analogues.[15] Using arene ruthenium mononuclear complexes and polydentate anionic organic ligands, neutral metalla-crowns were synthesized. Like their organic counterparts, these assemblies exhibit host-guest properties, selectively binding alkali cations depending on the size of the assembly. The results obtained were highly interesting, and represent a milestone in this area of ruthenium supramolecular chemistry.

The latter approach was mainly developed by our group, with the report of several dinuclear complexes obtained using *para*-cymene dinuclear ruthenium species $[(\eta^6\text{-}p\text{-}MeC_6H_4Pr^i)Ru(\mu^2\text{-}Cl)Cl]_2$ as starting material. Like its benzene counterpart mentioned above, this dinuclear compound is obtained easily from ruthenium trichloride hydrate and α-phellandrene,[16] and can be reacted with appropriate OO∩OO ligands to form different ruthenium dinuclear "clips",[17] which size vary according to the spacer between the two ruthenium atoms, a feature very interesting to take into account when building supramolecular assemblies (Figure 6). These compounds are usually quantitatively obtained and are very easy

to handle; as they combine the hydrophilic nature of the metal and the hydrophobic nature of the aromatic moiety, they are generally soluble in polar and apolar solvents alike, such as water or dichloromethane.

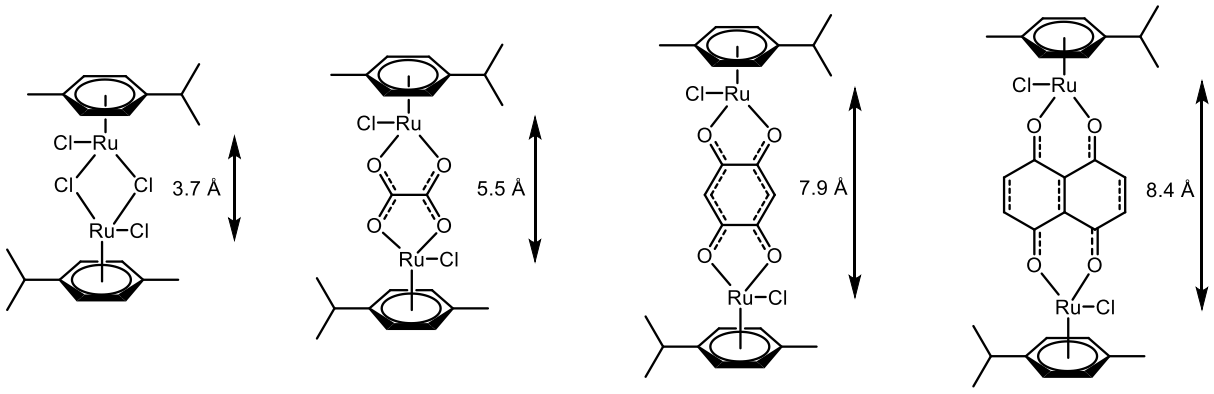

Figure 6: Ruthenium dinuclear clips with associated Ru-Ru lengths

After removal of the terminal chlorine atoms with an appropriate reagent (silver trifluoromethanesulfonate is commonly used), these clips can be reacted with a molecule that will act as the "panel" of the cage, given that this molecule possesses a group with binding affinity for ruthenium – pyridyl derivatives are an excellent example of such molecules. This way, by varying the clip and panel used, it is possible to access a whole library of ruthenium metalla-cages with different sizes and geometries: depending on the molecule used as panel, the resulting cage can be of rectangular, prismatic or even cubic shape.

This versatility is particularly interesting in a host-guest chemistry point of view, as the size of the cavity will greatly vary depending on the assembly. A lot of compounds can then be considered as guests, ranging from organic aromatic molecules such as pyrene or coronene,[18] to small metal complexes, such as the reported encapsulation of platinum and palladium complexes into a prismatic ruthenium cage (Figure 7).[19]

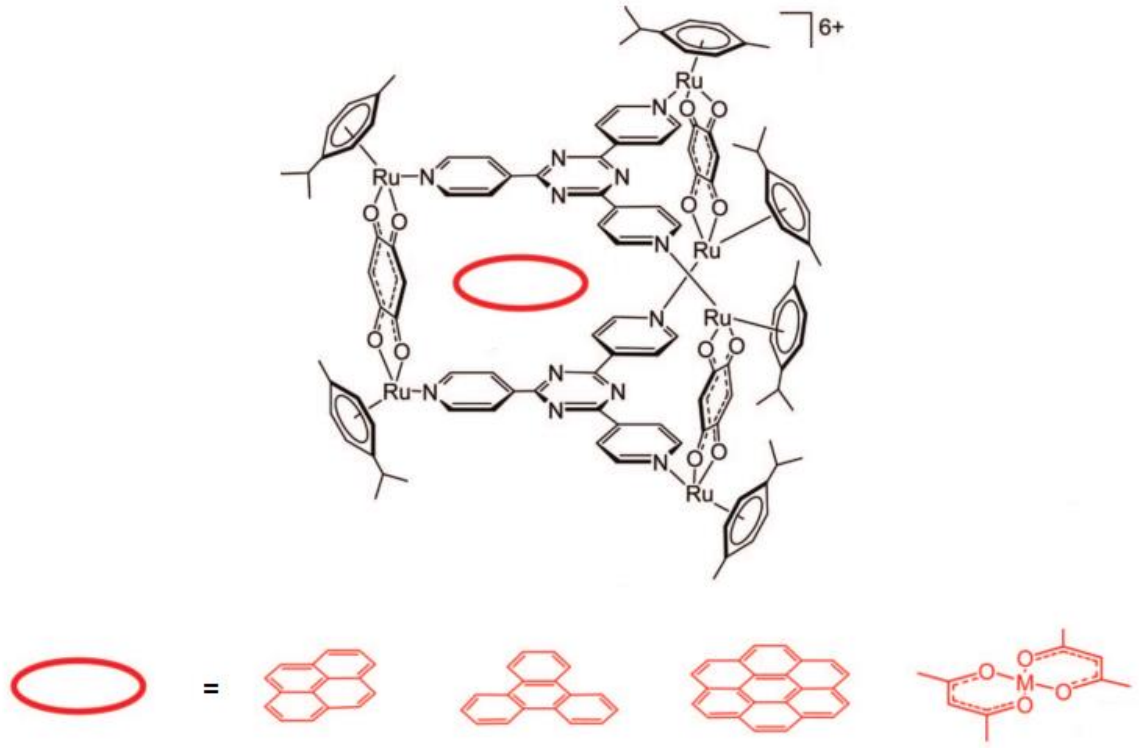

Figure 7: Typical hexanuclear ruthenium metalla-cage synthesized in our group, using 4-tpt (2,4,6-tris(4-pyridyl)triazine) as panel, and examples of guest molecules

In the last few years, this kind of supramolecular assembly was exploited in the context of medicinal chemistry. Indeed, one of the limitations when designing drugs is their solubility: since they are dispensed intravenously or orally, they need to be soluble in aqueous media, which is not always the case when molecules feature hydrophobic moieties such as aromatic rings. A way to overcome this issue is to encapsulate the target molecule inside the cavity of a metalla-assembly. As mentioned before, these ruthenium cages are mainly cationic and obtained as their trifluoromethanesulfonate salts, making them, as well as the guest molecule trapped into its hydrophobic cavity, highly soluble in water. This “Trojan horse” strategy was applied in the case of cancer treatment, where the ruthenium assembly acts as a vehicle able to transport its guest to the tumoral cells. This idea also revolves around the enhanced permeability and retention (EPR) effect. This concept states that large molecules tend to accumulate preferentially in cancerous tissue than in healthy ones. Using our ruthenium cages to transport it, the target molecule would then affect the tumor cells more selectively, leading to a better drug efficiency. This approach has been investigated in our group for the transport of photosensitizers in the case of photodynamic therapy, with very promising results.[20]

Nowadays, ruthenium is a key element when it comes to supramolecular chemistry. The accessibility of the starting materials and the diversity of compounds available make ruthenium a good building block to construct supramolecular assemblies with various sizes and shapes. While it is still a rising research topic, a large number of ruthenium assemblies have already been reported and have found applications in various fields, especially in medicinal chemistry.

1.3 Aim of this Work

The present work is divided in two parts. The first part, which is discussed in Chapter 2, focuses on the synthesis of arene ruthenium complexes containing hydrazine-thiazolo ligands, and the investigation of their properties as antitumor agents. The aim of this project is to combine the biological activity of the ruthenium moiety with that of the organic part, in order to obtain compounds with a high activity against tumoral cells. Their synthesis, characterization and biological activity will be discussed.

The second part, discussed in Chapter 3, presents the concept of light-responsive ruthenium assemblies. Organic molecules that undergo structural changes upon light irradiation are called “photoswitches”. The goal is to synthesize such molecules and include them as part of a ruthenium assembly. By doing so, it would be possible to create a structure capable of transporting a molecule inside its cavity, using host-guest interactions, and be able to trigger the light-responsive element of the assembly. This would then induce a change in the structure of the whole assembly, disrupting the host-guest interactions, thus providing a novel means to control the release of the guest molecule.

Chapter 2: Synthesis, Characterization and Anticancer Activity of Hydrazinyl-Thiazole Arene Ruthenium Complexes

2.1 Introduction

Cancer is one of the leading causes of mortality worldwide, with 14 million new cases and over 8 million cancer-related deaths reported in 2012, and it is expected that these numbers will keep rising during the next decades. Cancer is a result of an abnormal and uncontrolled cell growth, leading to the formation of tumors which can then spread throughout the body. The causes of cancer are multiple, though most of them result from environmental or lifestyle factors and tend to occur more frequently in developed countries.[21] Nowadays, several methods are used to treat cancers, the most common being surgery, radiotherapy and chemotherapy; the latter will be discussed here.

Chemotherapy is, by definition, the use of chemical compounds to treat diseases, even though its meaning is now narrowed down to the treatment of cancer only. Its emergence occurred during World War I, when the infamous mustard gas was found to be a potential suppressor of blood cells production, a property that could be used to stop the growth of tumoral cells. This led to the discovery and investigation of nitrogen mustard molecules, such as chlormethine.[22] These compounds indeed proved to be cytotoxic, and were the first alkylating agents used in chemotherapy, named after their ability to bind to DNA. Other alkylating agents were later designed (Figure 8), such as chlorambucil (marketed Leukeran), an aromatic mustard used mainly against lymphocytic leukemia, which presented less side effects and also had the advantage of being taken orally rather than intravenously.[23] Different groups of molecules were also investigated for their anticancer properties, each having their own mechanism of action. Antimetabolites, for instance, are chemicals able to interfere with DNA and RNA production, thus limiting the division of tumoral cells. Many of them are now used to treat various types of cancer, an example being gemcitabine (marketed Gemzar).[24]

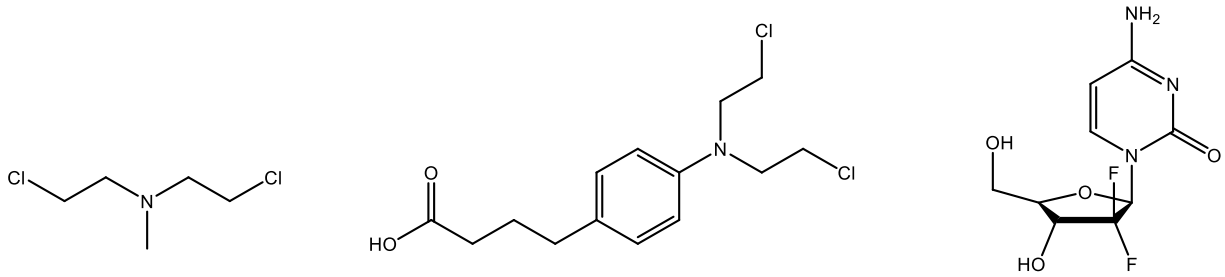

Figure 8: Alkylating agents chlormethine and chlorambucil, and antimetabolite gemcitabine

Metal based drugs have also been investigated in this field. The first metal-centered compound to be used in chemotherapy was *cis*-diamminedichloroplatinum (II), more commonly called cisplatin. This platinum complex was first discovered in the 19th century, but its anticancer properties were only found in 1965.[25] Due to its high activity against cancer cells, cisplatin was rapidly approved for clinical use. Since then, it is used against many types of cancer, such as bladder or testicular cancers, with very good cure rates for some of them. As a result, researchers have focused a lot on platinum complexes designed towards cancer treatment; besides cisplatin, two of its analogues are now used in clinics worldwide (Figure 9).

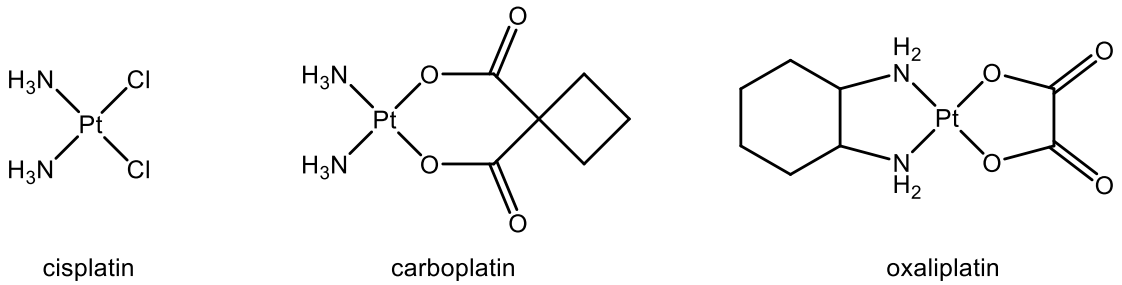

Figure 9: Clinically approved platinum complexes used in chemotherapy

Chemotherapy, while being the most widely used technique to cure cancer, has several limitations. The main one is the lack of selectivity of the drug, which also often kills healthy cells, and thus leads to undesirable side effects (hair loss, fatigue, nausea, etc.). The resistance of cancerous cells to drugs is also a major problem, as it is the case with cisplatin. Its inefficiency on platinum-resistant tumors is a huge disadvantage, which led to the search for

alternative agents to resolve this drawback. Among these candidates, ruthenium has undoubtedly stood out.

Over the last few decades, many examples of ruthenium compounds have been reported, some of which are already into clinical trials, such as the well-known complexes [imiH]*trans*-[Ru(*N*-imi)(*S*-dmso)Cl_4] (NAMI-A),[26] and [Na]*trans*-[Ru(*N*-ind)$_2Cl_4$] (NKP-1339)[27] (Figure 10). These ruthenium (III) complexes, which have shown very promising results, are in fact prodrugs: they are activated in the reductive tumor environment, generating ruthenium (II) species which appeared to be the actual antitumoral agents.

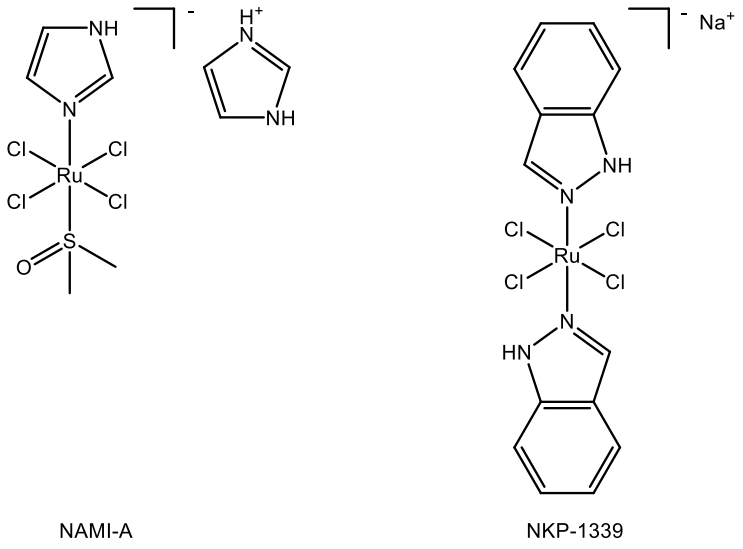

NAMI-A NKP-1339

Figure 10: Ruthenium (III) anticancer complexes NAMI-A and NKP-1339

Ever since this discovery, several groups have developed the strategy of directly using ruthenium (II) complexes when designing anticancer drugs. This led to the emergence of interesting arene ruthenium (II) compounds, such as those reported by Dyson[28] or Sadler[29] (Figure 11). Those complexes present some advantages over cisplatin, namely their activity against cisplatin-resistant cancerous cell lines, and their higher selectivity for cancerous over healthy cells, leading to reduced side effects.

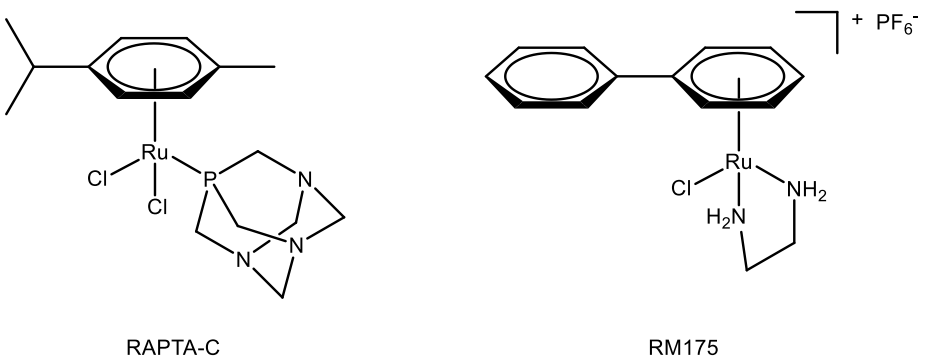

Figure 11: Arene ruthenium (II) anticancer complexes RAPTA-C and RM175

Since then, this field of research has expanded quite significantly, and the number of ruthenium complexes designed towards anticancer applications has exponentially risen over the years (Figure 12). Many researchers have also designed ruthenium-centered complexes bearing biologically active organic ligands, with the goal of taking advantage of the properties of both moieties. Hydrazinyl-thiazole compounds, for example, have received much attention in recent years due to the identification in the 1990s of several thiazole compounds showing antitumor activity.[30] These molecules can be easily synthesized and functionalized with various chemical groups, allowing a fine-tuning of the structures in order to achieve the desired biological properties,[31] and can also act as a *N*,*N*' chelating ligand towards transition metals such as ruthenium.

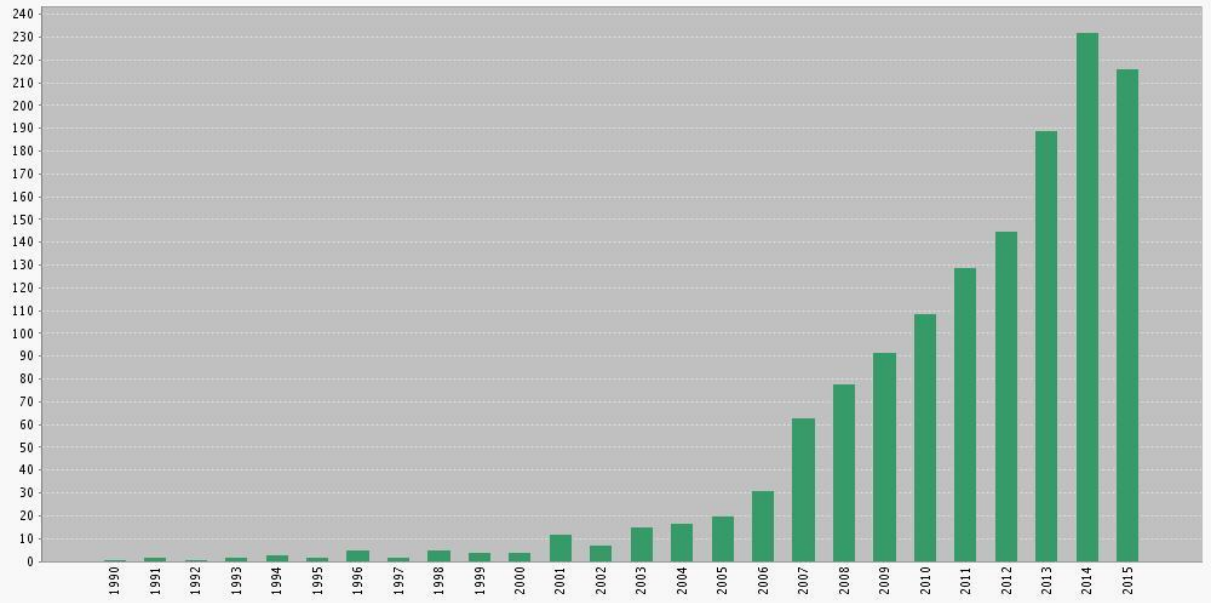

Figure 12: Number of publications per year regarding "anticancer ruthenium complexes" from 1990 to 2015

In this work, a *p*-cymene ruthenium unit and hydrazinyl-thiazole ligands were combined to generate series of organometallic compounds with significant antitumor activity, taking advantage of the synthetic versatility of thiazole derivatives and the promising biological activity of ruthenium complexes.

2.2 Phenyl Derivatives

2.2.1 General

Thiazoles and their derivatives are compounds which usually exhibit many biological properties, such as antimicrobial, antiviral or anticancerous activities. The different hydrazinyl-thiazole compounds used in this work were prepared by co-workers at the Universtiy of Cluj, Romania, using the synthetic route showed in Scheme 2.

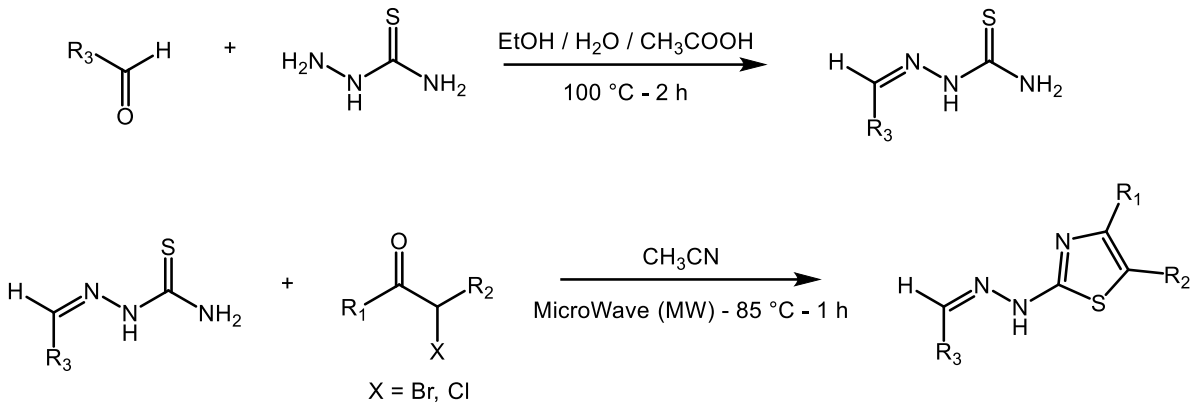

Scheme 2: Synthesis of hydrazinyl-thiazole derivatives

The first step consists in the condensation of an aromatic aldehyde with thiosemicarbazide; the desired products are then obtained thanks to a Hantzsch cyclization reaction as a second step. These reactions are fairly simple and quite efficient in terms of yield and purity, and the large choice of available aromatic aldehydes (for the first step) and *α*-halocarbonyls (for the second step) allow for a very diverse library of final compounds. The hydrazinyl-thiazole compounds obtained this way can act as bidentate ligands: both azomethine (CH=N) and thiazole nitrogen atoms are electronically available and geometrically well arranged for a coordination bond towards ruthenium (II) species. In this section, the focus is placed on phenyl-based (i.e. where R_3 is a phenyl derivative) hydrazinyl-thiazole compounds and their corresponding ruthenium complexes.

2.2.2 Results, Discussion and Structure Optimization

A series of monocationic ruthenium complexes (**1-16**) containing hydrazinyl-thiazole bidentate ligands (**L1-L16**) was prepared (Scheme 3, Table 1). The synthesis of the complexes was realized by two methods: (A) a conventional synthetic method involving one equivalent of the ruthenium dimer $(\eta^6\text{-}p\text{-cymene})_2Ru_2Cl_4$ and two equivalents of the hydrazinyl-thiazole derivatives (**L1-L16**) in methanol at room temperature for 10 hours; and (B) a microwave-assisted synthetic method, whose optimal reaction conditions were established after several experiments, varying the solvent (methanol, acetonitrile and dichloromethane), the temperature (40 °C, 60 °C, 82 °C and 100 °C) and the reaction time (0.5 h, 1 h, 1.5 h and 2 h). The best yields for the complexes were obtained after 0.5 h of microwave irradiation at 60 °C and using dichloromethane as solvent. The two alternative synthetic methods are comparable for the resulting yield (50-80%), but the microwave-assisted method demands a shorter reaction time (30 minutes versus 10 hours). In order to make it greener, the synthesis was tried using water instead of an organic solvent. Unfortunately, in water, the complexes could only be recovered in traces.

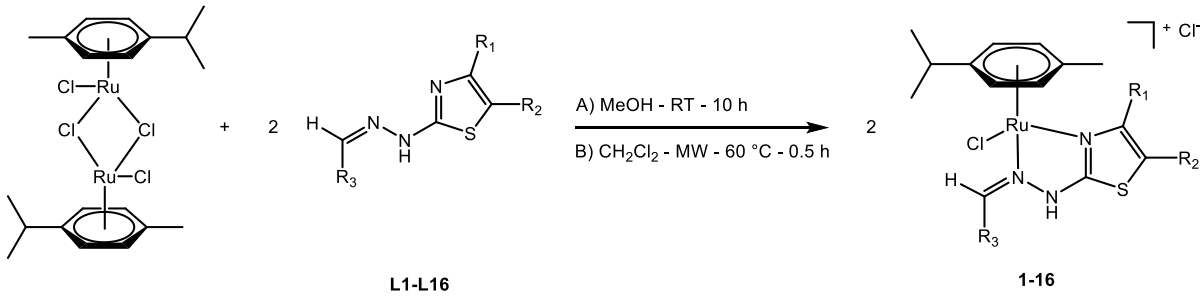

Scheme 3: Synthesis of complexes **1-16** (R_1, R_2 and R_3 functional groups are given in Table 1)

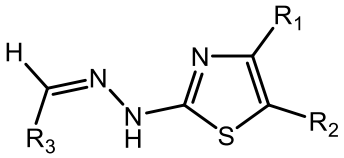

	R_1	R_2	R_3		R_1	R_2	R_3
L1	Me	H	Ph	**L9**	Me	H	4-MeO-C_6H_4
L2	Ph	H	Ph	**L10**	Ph	H	4-MeO-C_6H_4
L3	Me	COMe	Ph	**L11**	Me	COOEt	4-MeO-C_6H_4
L4	CH_2COOEt	H	2,4-Cl_2-C_6H_3	**L12**	Me	COMe	4-MeO-C_6H_4
L5	Me	COMe	2,4-Cl_2-C_6H_3	**L13**	Me	H	3-Cl-C_6H_4

L6	Me	COOEt	2,4-Cl_2-C_6H_3	**L14**	Me	COMe	3-Cl-C_6H_4
L7	Me	H	4-HO-C_6H_4	**L15**	Ph	H	3-Cl-C_6H_4
L8	Ph	H	4-HO-C_6H_4	**L16**	Me	COOEt	3-Cl-C_6H_4

Table 1: Identification of the functional groups R_1-R_3 attached to the hydrazinyl-thiazole compounds **L1-L16**

All complexes were isolated as their chloride salts, and were fully characterized by ^{1}H NMR, mass spectrometry, IR spectroscopy, elemental analysis, and for **12** by a single-crystal X-ray structure analysis. No attempt to separate the cationic enantiomers was performed, and the chiral-at-metal complexes were isolated and used as racemic mixtures. All complexes are soluble in most organic solvents; they are stable in D_2O and DMSO solutions as well as in biological media (aqueous solution containing RPMI 1640 medium with 5% fetal calf serum, glutamine, and antibiotics), showing no decomplexation of the hydrazinyl-thiazole ligands. The ^{1}H NMR spectra of all complexes show, in addition to the signals of the *p*-cymene ring, the characteristic signals of the ligand at higher chemical shifts related to its free form because of the deshielding effect produced by the arene ruthenium unit. Typical signals for the ligands after complexation are a singlet at around 9 ppm associated with the proton of the azomethine moiety (CH=N) and the proton from the hydrazine moiety (N-NH), which is the most deshielded one, appearing as a broad singlet at around 15 ppm (in some cases the signal is not observed due to the deuterium exchange). In the case of the complexes where R_2 = H, the corresponding proton of the thiazole ring is observed as a singlet at around 6.5 ppm. The mass spectra of all complexes conveniently show, in positive mode, a peak corresponding to the mass of the cation without its chloride counteranion, sometimes along with other fragment peaks (Figure 13). IR spectra of all complexes mainly show bands corresponding to the C-H bond stretch of aromatics (~2950 cm^{-1}), and more specific bands depending on R_1-R_3 groups, such as the O-H stretch of phenol derivatives (~3400 cm^{-1}) or the C=O stretch bands (~1600 cm^{-1}) when carbonyls are present in the structure.

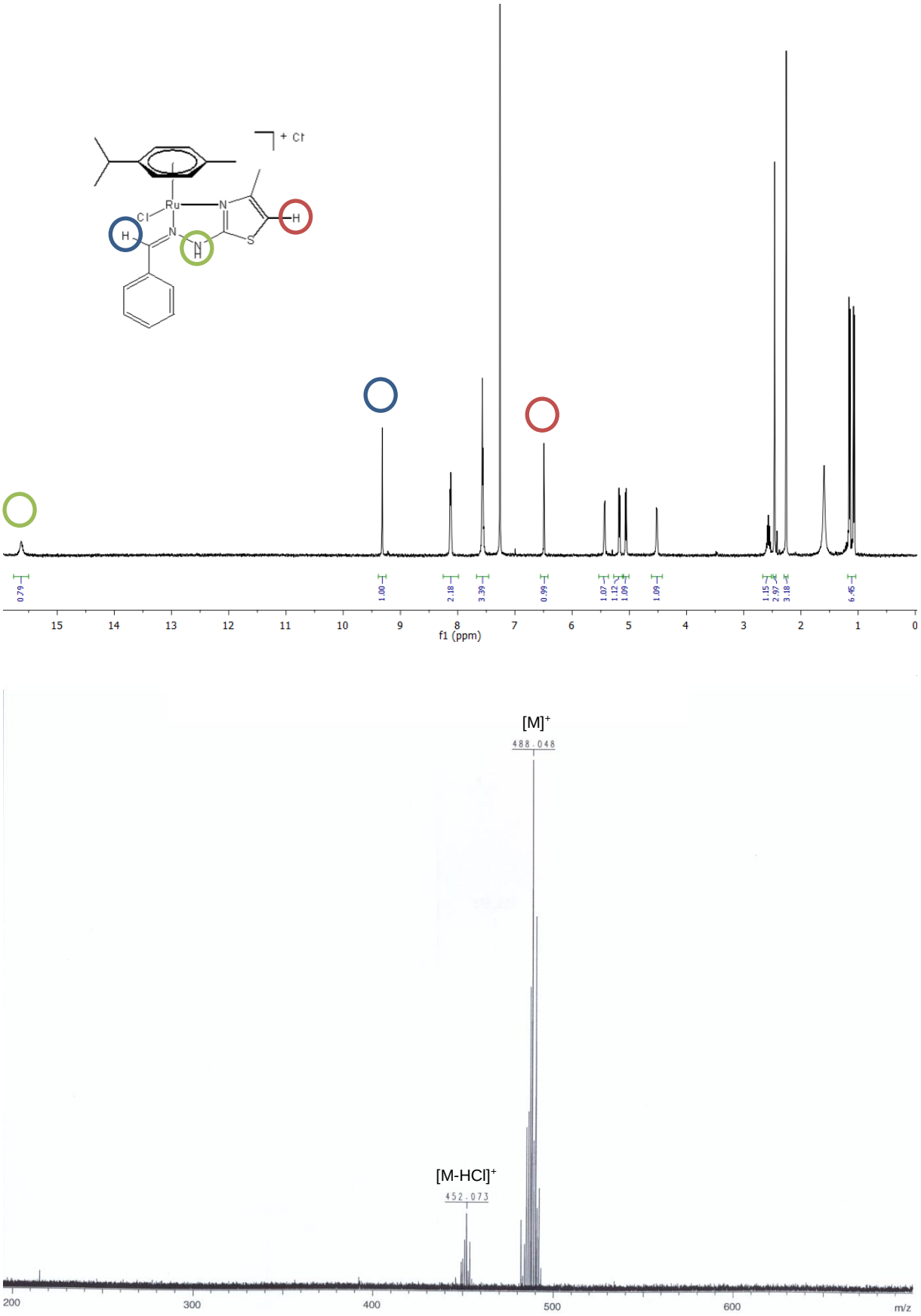

Figure 13: ^{1}H NMR spectrum of complex **1** in $CDCl_3$, with annotated characteristic signals (top); and mass spectrum of **1** with peaks attribution (bottom)

Crystals suitable for a single-crystal X-ray structure analysis were obtained for [(η^6-*p*-cymene)Ru(**L12**)Cl]Cl by slow evaporation of a solution of the complex in methanol. The molecular structure of the cation is presented in Figure 14, together with selected geometrical parameters. In complex **12**, the ruthenium center shows a typical pseudotetrahedral geometry with the hydrazinyl-thiazole ligand being *N*,*N*' coordinated. The Ru-N bond distances are 2.090(6) (thiazole) and 2.123(6) Å (hydrazine), and these values are similar to those found in analogous *N*,*N*'-coordinated pyridyl-thiazole arene ruthenium complexes.[32] In the solid state, an angle of 34.6(3)° is observed between the plane formed by the hydrazinyl-thiazole unit and the plane of the methoxyphenyl group.

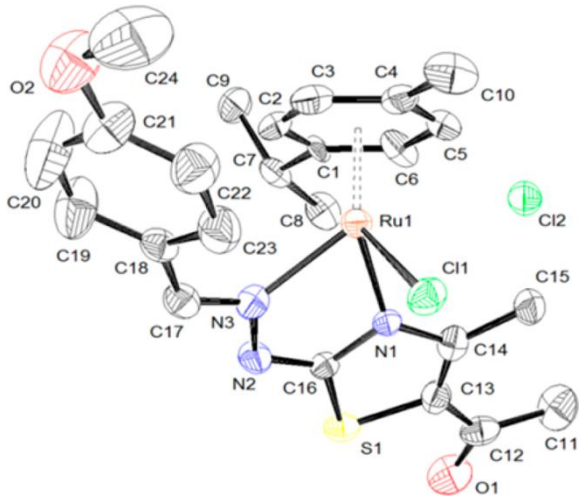

Figure 14: ORTEP drawing of complex **12** at 35% probability level, with hydrogen atoms being omitted for clarity. Selected bond lengths (Å) and angles (°): Ru(1)-Cl(1) 2.408(2), Ru(1)-N(1) 2.090(6), Ru(1)-N(3) 2.123(6), N(2)-N(3) 1.396(7), and N(3)-C(17) 1.299(8); Cl(1)-Ru(1)-N(1) 85.61(15), Cl(1)-Ru(1)-N(3) 90.04(15), N(1)-Ru(1)-N(3) 76.2(2), N(1)-C(16)-N(2) 120.5(6), C(16)-N(1)-Ru(1) 112.1(4), C(14)-N(1)-Ru(1) 133.8(5), C(17)-N(3)-Ru(1) 133.7(5), N(2)-N(3)-Ru(1) 111.1(4), N(2)-N(3)-C(17) 114.2(6), and C(13)-S(1)-C(16) 88.2(3)

Complexes **1** to **16** were tested *in vitro* for their antiproliferative activity on four cell lines: HeLa (human cervical cancer cells), A2780 (human ovarian cancer cells), A2780cisR (cisplatin-resistant human ovarian cancer cells) and HFL-1 (noncancer cells, human fibroblast). As shown in Table 2, IC_{50} values were used to determine the antiproliferative activity of the complexes. Moreover, the calculated partition coefficients (log *P*) of the hydrazinyl-thiazole compounds **L1-L16** together with their IC_{50} values on HeLa cells[31] are

presented in Table 3, thus giving an approximation of the lipophilicity and cytotoxicity of the ligands. Cisplatin and oxaliplatin were used as controls, and their IC_{50} values are also reported (Table 2).

	IC_{50} (μM)			
	HeLa	A2780	A2780cisR	HFL-1
cisplatin	20.10 ± 0.02	11.30 ± 0.02	41.13 ± 1.24	9.50 ± 0.02
oxaliplatin	12.72 ± 0.02	10.10 ± 0.03	16.57 ± 0.02	13.53 ± 0.02
1	7.42 ± 0.01	9.65 ± 0.01	12.95 ± 0.04	18.48 ± 0.02
2	2.55 ± 0.02	2.49 ± 0.02	0.93 ± 0.02	6.27 ± 0.01
3	11.42 ± 0.02	6.99 ± 0.02	2.08 ± 0.03	6.43 ± 0.02
4	3.65 ± 0.03	12.21 ± 0.03	12.62 ± 0.01	181 ± 0.89
5	7.98 ± 0.01	50.08 ± 0.03	55.58 ± 0.03	47.33 ± 0.32
6	0.84 ± 0.25	2.86 ± 0.01	6.06 ± 0.02	4.52 ± 0.01
7	19.40 ± 0.03	6.13 ± 0.25	6.19 ± 0.01	49.40 ± 0.31
8	6.87 ± 0.23	5.25 ± 0.03	4.24 ± 0.01	7.30 ± 0.03
9	7.95 ± 0.03	6.97 ± 0.33	6.80 ± 0.05	6.47 ± 0.23
10	2.26 ± 0.03	5.12 ± 0.03	1.33 ± 0.02	13.88 ± 0.03
11	5.66 ± 0.01	9.47 ± 0.03	3.14 ± 0.01	4.27 ± 0.03
12	7.88 ± 0.01	4.54 ± 0.01	2.25 ± 0.03	3.84 ± 0.01
13	11.15 ± 0.01	6.13 ± 0.02	2.14 ± 0.05	6.32 ± 0.02
14	2.69 ± 0.01	2.26 ± 0.03	2.14 ± 0.04	36.61 ± 0.48
15	6.81 ± 0.03	7.70 ± 0.12	2.77 ± 0.01	13.69 ± 0.01
16	1.72 ± 0.01	3.75 ± 0.02	3.76 ± 0.03	2.81 ± 0.03

Table 2: Cytotoxic activity of complexes **1-16** in HeLa, A2780, A2780cisR and HFL-1 cell lines

The results obtained on the three tumor cell lines (HeLa, A2780 and A2780cisR) show a promising profile for the antiproliferative activity of all complexes, most of them having a cytotoxic activity at concentrations significantly lower than that of cisplatin and oxaliplatin. Moreover, by comparing the antiproliferative effect produced by the complexes on the tumor cell lines A2780 and A2780cisR, it can be noticed that at almost the same concentrations, a similar effect is observed on both cell lines, suggesting a mode of action different from that of cisplatin. By analyzing the effect of the treatment with the complexes on the normal fibroblasts cell line HFL-1, a significant reduction of cytotoxicity can be noticed for complexes **4** (IC_{50} = 181 μM) and **14** (IC_{50} = 36.6 μM). When comparing the cytotoxic effect produced by these two complexes on all the tumor cell lines, a selectivity in favor of the noncancerous cell line can be observed, i.e. a cytotoxic effect upon normal fibroblasts 15

times lower than upon tumoral cells. Moreover, the activities of the hydrazinyl-thiazole compounds **L4** and **L14** on HeLa cells are very low (>100 μM), confirming the beneficial effect of complexation to arene ruthenium units (Tables 2 and 3).

	log *P*	IC_{50} (μM)
L1	3.1 ± 0.6	11.4 ± 0.005
L2	4.4 ± 0.6	>100
L3	2.6 ± 0.8	64.87 ± 0.005
L4	4.4 ± 0.6	>100
L5	4.0 ± 0.9	>100
L6	4.6 ± 0.9	>100
L7	2.9 ± 0.6	25.59 ± 0.010
L8	4.2 ± 0.6	20.04 ± 0.019
L9	3.3 ± 0.6	>100
L10	4.6 ± 0.6	11.1 ± 0.009
L11	3.8 ± 0.9	>100
L12	2.7 ± 0.9	>100
L13	3.9 ± 0.6	57.53 ± 0.011
L14	3.4 ± 0.9	>100
L15	5.2 ± 0.6	>100
L16	4.4 ± 0.9	>100

Table 3: Cytotoxic activity of compounds **L1-L16** in HeLa cells and calculated partition coefficients

Such variations in the activity appear to be dependent on some minor modifications in the molecular structure of the complexes, thus revealing some interesting trends. Indeed, the presence of electron-withdrawing groups (chloro and dichloro) on the phenyl ring of R_3 leads to a higher antiproliferative effect on the cancerous cell lines. The presence of a more hydrophobic substituent (phenyl) at the R_1 position of the thiazole ring also increases the antiproliferative activity, with the exception of **13** (methyl) and **15** (phenyl) which show a higher activity only on the HeLa cell line. However, the nature of the R_2 group (H, COMe and COOEt) appears to have a less predictable effect. In complexes **13**, **14** and **16** where only R_3 varied, the cytotoxicity of the complexes is comparable, while between complexes **5** and **6** the COMe derivative is significantly less cytotoxic than the COOEt analogue.

Moreover, when looking at the log *P* values of **L1**-**L16** in conjunction with their IC_{50} values on HeLa cells, it appears that the lipophilicity of the ligands does not correlate with the activity. Therefore, it can be deduced from these results that the functionalization of the

ligands can be further explored in order to optimize the biological activity of these hydrazinyl-thiazole arene ruthenium complexes.

Following these results, hydrazinyl-thiazole ruthenium complexes **17** and **18** were synthesized using the same procedure as described previously. Both include a phenyl ring as the R_1 substituent and a chlorinated phenyl ring as the R_3 substituent (Figure 15).

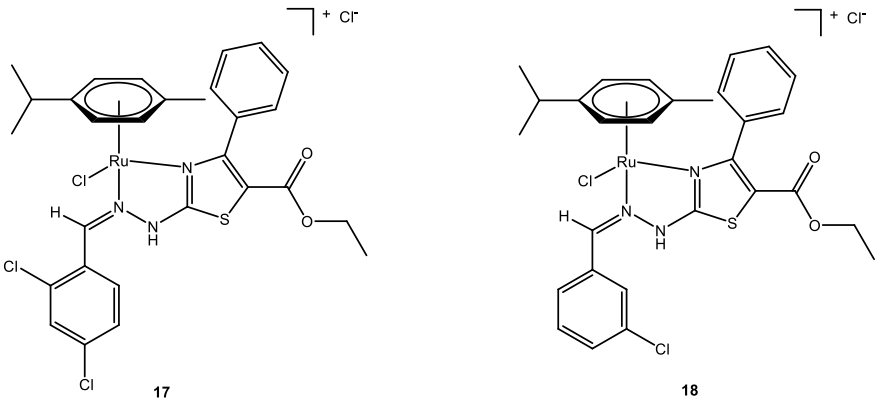

Figure 15: Complexes **17** and **18**

As for the previous series, these two complexes were isolated as their chloride salts and were successfully characterized by ^{1}H NMR spectroscopy, mass spectrometry, IR spectroscopy and elemental analysis. They share the same spectroscopic features with the other complexes, such as the typical ^{1}H NMR signals and MS peaks. Pure samples of **17** and **18** were sent to the Iuliu Hatieganu University of Medicine and Pharmacy in Cluj, Romania, for the investigation of their biological properties, and are currently undergoing cytotoxic activity tests on the same cell lines – both cancerous and healthy – as described above.

2.3 Phenothiazine Derivatives

2.3.1 General

Phenothiazine is an aromatic tricyclic compound containing both nitrogen and sulfur atoms, first synthesized in 1883 via the reaction of diphenylamine with sulfur. Phenothiazine later proved to be a parent molecule of a lot of pharmaceutically interesting compounds. One of the first and most well-known of such phenothiazine derivatives is methylene blue (Figure 16), which presents a lot of medical uses.[33]

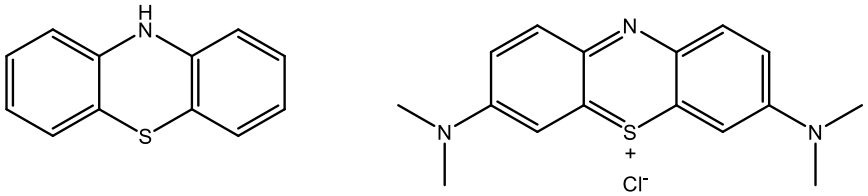

Figure 16: Phenothiazine (left) and methylene blue (right)

In recent years, some phenothiazine derivatives have been reported for their activity against human ovarian cancer cells,[34] similar to those used in the previous part of this work, while others have proved to be efficient on multidrug resistant cancerous cells,[35] making phenothiazine a promising building block in modern drug design.

In this part of this work, hydrazinyl-thiazole compounds bearing a *N*-ethyl phenothiazine ring are used as ligands for a new series of biologically active ruthenium complexes.

2.3.2 Results and Discussion

Four monocationic ruthenium complexes (**19**-**22**) containing phenothiazine-based hydrazinyl-thiazole ligands were synthesized using procedure A described previously (Figure 17).

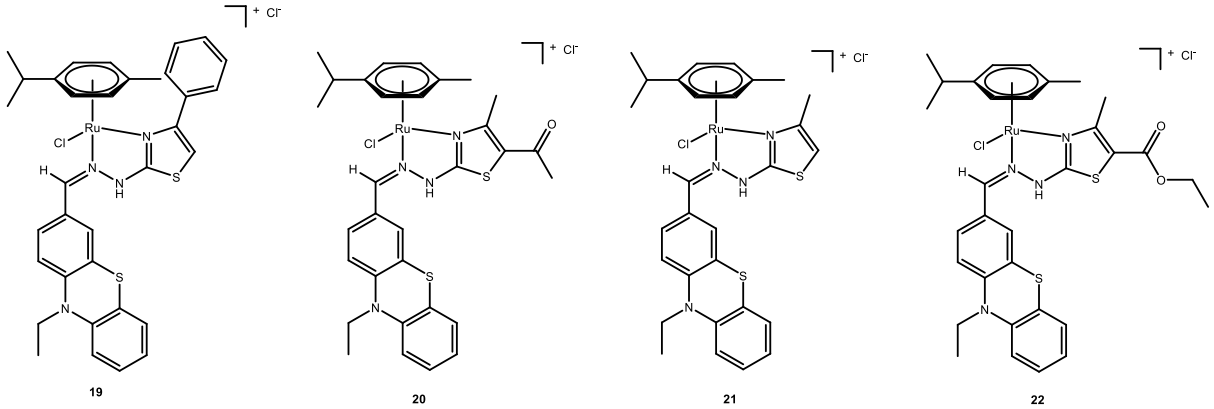

Figure 17 : Complexes **19** to **22**

These complexes were isolated as their chloride salts in good yields, comparable to those obtained for the first series of complexes. They were characterized by ^{1}H NMR spectroscopy, mass spectrometry, IR spectroscopy and elemental analysis. The proton NMR spectra show the same characteristic signals for the azomethine moiety and for the thiazole ring when R_2 = H (**19** and **21**). In addition, the typical triplet and quadruplet signals associated to the *N*-ethyl group can be observed, as emphasized in Figure 18.

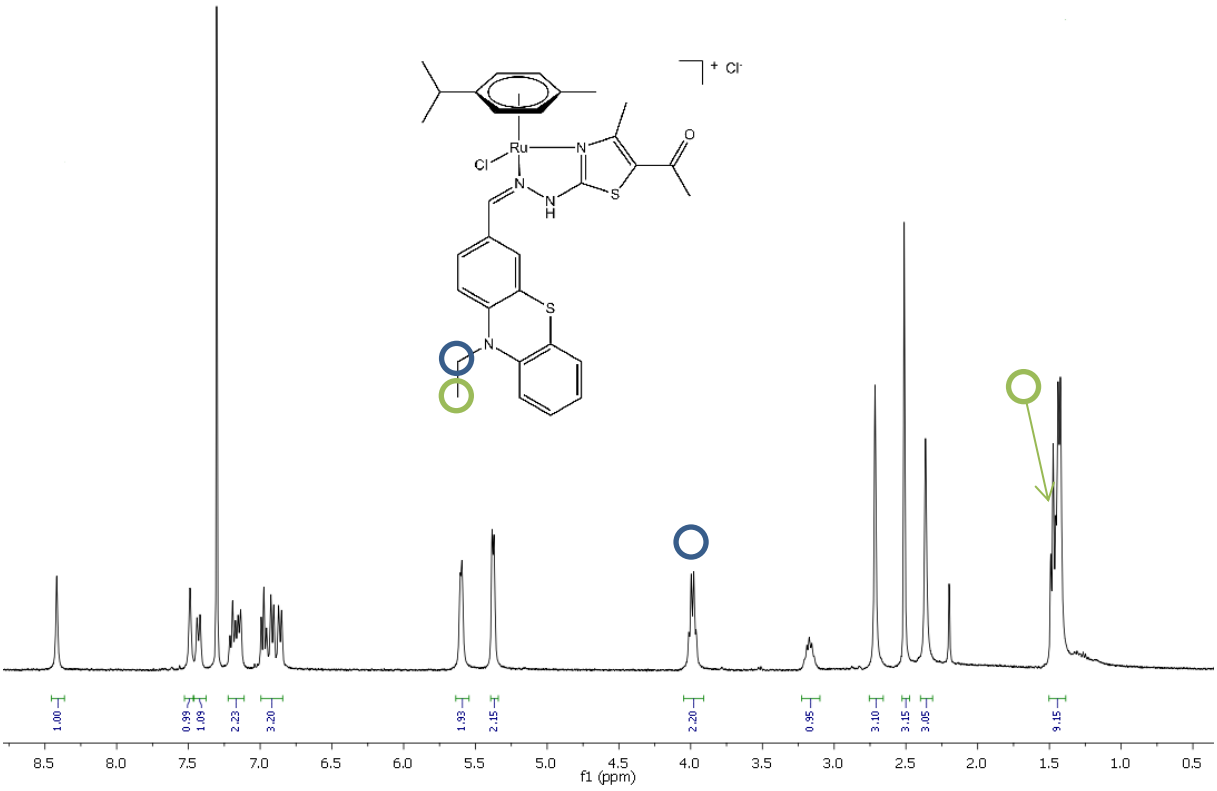

Figure 18: ^{1}H NMR spectrum of complex **20** in $CDCl_3$ with annotated characteristic signals

Since phenothiazine-type compounds are known to exhibit strong fluorescence emission,[38] experiments were conducted in order to see if this feature is still present in ruthenium-phenothiazine complexes. Emission spectra were recorded for solutions of N-ethyl-phenothiazine, ligand **L22** and complex **22** in dichloromethane ($c = 1.0 \times 10^{-6}$ mol·L^{-1}) with an excitation wavelength of 245 nm, determined by UV-visible absorption spectroscopy (Figure 19).

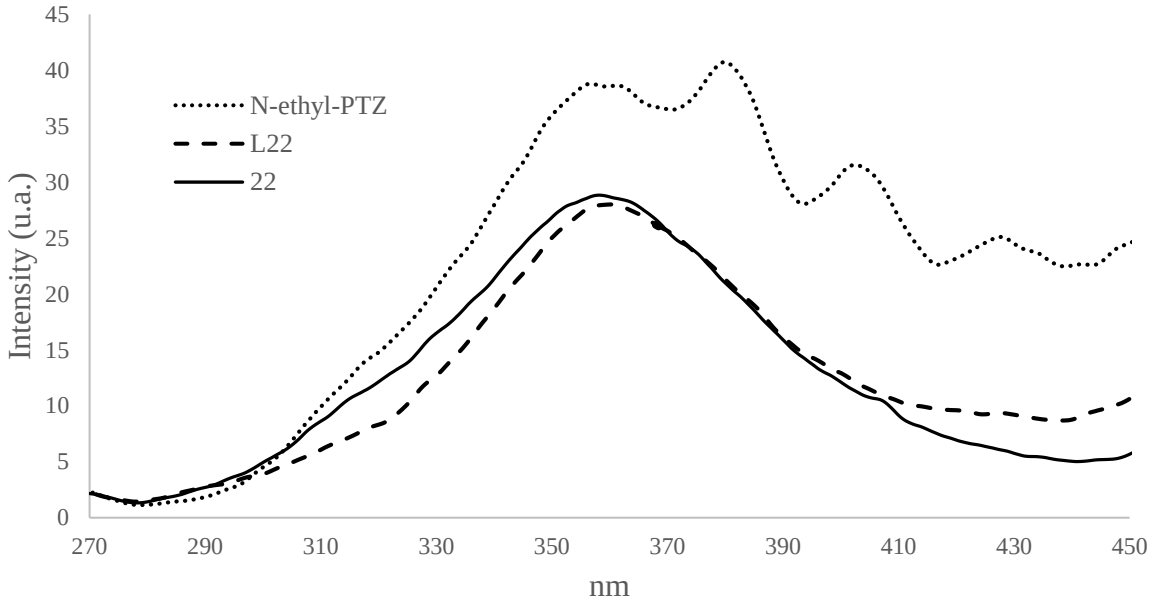

Figure 19: Fluorescence spectra of *N*-ethyl-PTZ, **L22** and **22** in CH_2Cl_2, with λ_{ex} = 245 nm

The results of this study show that both **L22** and **22** exhibit a diminution of about 25% of the emission intensity compared to free *N*-ethyl-PTZ, likely due to the presence of the hydrazinyl-thiazole moiety, disturbing the electronic environment of the phenothiazine group and thus changing its spectroscopic properties. However, ligand **L22** and ruthenium complex **22** present almost exactly the same emission spectrum, showing that the arene-ruthenium core does not hinder the fluorescence properties of the ligand. This feature is very important, as it represents an easy way to identify and track phenothiazine-containing ruthenium anticancer complexes.

Even though they bear an aromatic tricyclic moiety, all four complexes have a very similar solubility to that of the first series: they remain soluble in polar solvents, and proved to be very stable in solution. As with **17** and **18**, samples of complexes **19**-**22** were sent to the Iuliu Hatieganu University of Medicine and Pharmacy in Cluj, Romania, to perform the cytotoxicity tests on the same cell lines as previously described. These results should provide information on whether the biological properties of the phenothiazine group carry on in the complexes, and could lead – as was the case in the first series of complexes – to an optimization of the structure of the complexes in order to achieve the best possible activity.

2.4 Indole Derivatives

2.4.1 General

Indoles are aromatic bicyclic compounds, consisting of a benzene ring fused to a nitrogen-containing pyrrole ring. Indoles are natural compounds, mostly found in plants and in green vegetables. This class of molecules has been known to be phytonutrient, i.e. to present health-protecting properties. More recently, the intake of vegetables containing indoles has been associated with the reduction of the risk of several cancers.[36] Indole-3-carbinol and its dimer 3,3'-diindolylmethane, for example (Figure 20), have shown to induce apoptosis in several human cancerous cell lines.[37]

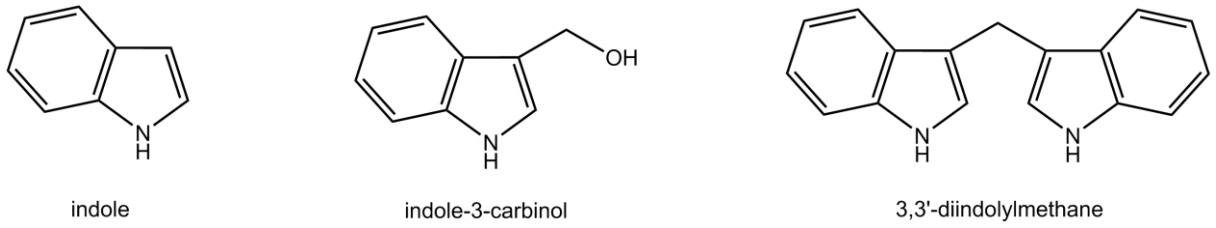

Figure 20: Indole and its derivatives indole-3-carbinol and 3,3'-diindolylmethane

In the last part of this work, hydrazinyl-thiazole ligands containing an indole moiety are used for the synthesis of ruthenium complexes, with the goal of combining the biological properties of the organic thiazole and indole groups and that of the metallic ruthenium center.

2.4.2 Results and Discussion

A series of nine ruthenium complexes (**23**-**31**) bearing indole hydrazinyl-thiazole ligands was synthesized using procedure A as described before.

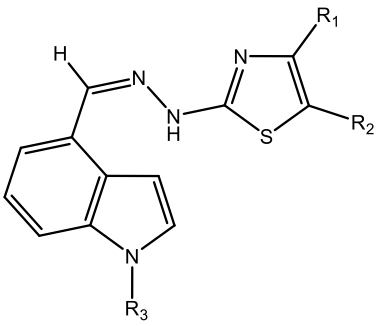

	R_1	R_2	R_3	log *P*
L23	Me	H	H	3.1 ± 0.8
L24	Me	COMe	H	2.5 ± 1.1
L25	Ph	H	H	4.4 ± 0.9
L26	CH_2COOEt	H	H	2.9 ± 0.9
L27	Me	H	COMe	3.1 ± 0.9
L28	Ph	H	COMe	4.4 ± 0.9
L29	Me	COMe	COMe	2.5 ± 1.2
L30	Me	COOEt	COMe	3.6 ± 1.2
L31	CH_2COOEt	H	COMe	2.9 ± 0.9

Table 4: Identification of the functional groups R_1-R_3 attached to the hydrazinyl-thiazole compounds **L23**-**L31** and calculated partition coefficients

Complexes **23**-**31** were isolated as their chloride salts and were characterized by ^{1}H NMR spectroscopy, mass spectrometry, IR spectroscopy and elemental analysis. In addition to the usual characteristic signals of the hydrazinyl-thiazole moiety, the *N*-acetyl group present in complexes **27** to **31** can be easily noticed both on proton NMR and IR spectra – especially in complexes **27** and **28**, where it is the only carbonyl group in the structure. All complexes, including those bearing hydrophobic substituents and thus having high partition coefficients, show good solubility in water, a crucial property when considering medicinal applications.

Compounds **23**-**31** were submitted for biological testing, still using the same human cancerous cell lines in order to evaluate their cytotoxicity, with results pending. As for the previous series of complexes, good anticancer activity is expected thanks to the combination of the ruthenium core and the indole-containing organic pharmacophore.

2.5 Conclusion

Three series of novel monocationic ruthenium complexes containing hydrazinyl-thiazole ligands were synthesized and characterized. The complexes forming the first series (**1**-**16**) – phenyl derivatives – were submitted to biological tests to investigate their anticancer properties against human ovarian and cervical cancer cells. Results were overall good, with most complexes exhibiting better cytotoxicity than clinically used compounds cisplatin and oxaliplatin. Moreover, in the case of two complexes (**4** and **14**), a selectivity in favor of cancer cells over healthy cells was observed. This later on led to the synthesis of complexes **17** and **18**, which structures were designed according to the previously obtained results, by choosing R_1-R_3 groups that seemed to contribute to both cytotoxicity and selectivity. These two complexes are currently undergoing biological tests.

Two other series of hydrazinyl-thiazole ruthenium complexes were then synthesized, using phenothiazine and indole moieties, respectively, as part of the structure of the ligands. Indeed, these classes of molecules present some biological activity on their own; the goal of this project was to exploit this feature in order to further bring out the synergy between the ruthenium core and the organic ligand. This resulted in the synthesis and characterization of thirteen new complexes which are now being tested for their antiproliferative activity.

Chapter 3: Design and Synthesis of Light Responsive Arene Ruthenium Assemblies

3.1 Introduction

Molecular switches are, by definition, molecular systems consisting of at least two different states, connected to each other through a reversible transformation activated by an external stimulus. Such systems have been the subject of much attention over the years, as they present a wide range of potential applications, from optical displays to molecular electronics. Indeed, having access to two different states in a molecule – or a molecular assembly – allows one to perform binary logic at a molecular level, which can prove very useful, in particular if each state can be isolated and "gated" behind a particular stimulus; this concept is illustrated in Scheme 4.[39]

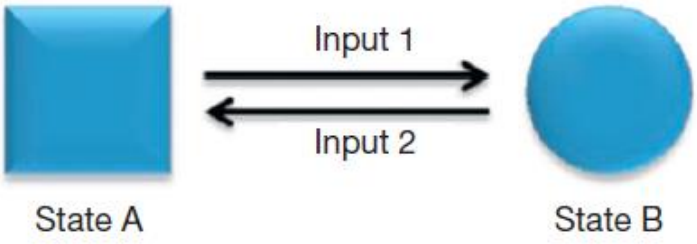

Scheme 4: Sketched concept of a molecular switch

Molecular switches can be very diverse in their mode of operation, whether regarding the type of transformation involved or the stimulus applied to perform said transformation. While staying concise, the present introduction will summarize examples of recent and popular molecular switch systems, especially in the field of organometallic chemistry.

Redox reactions have been thoroughly investigated in that matter, thanks to the large amount of different systems available and their reversible nature.[40] Moreover, electrons represent an easily accessible and relatively mild stimulus to trigger a molecular switch. Among all existing examples, the redox system reported by Yano and co-workers is a particularly interesting one (Scheme 5).[41]

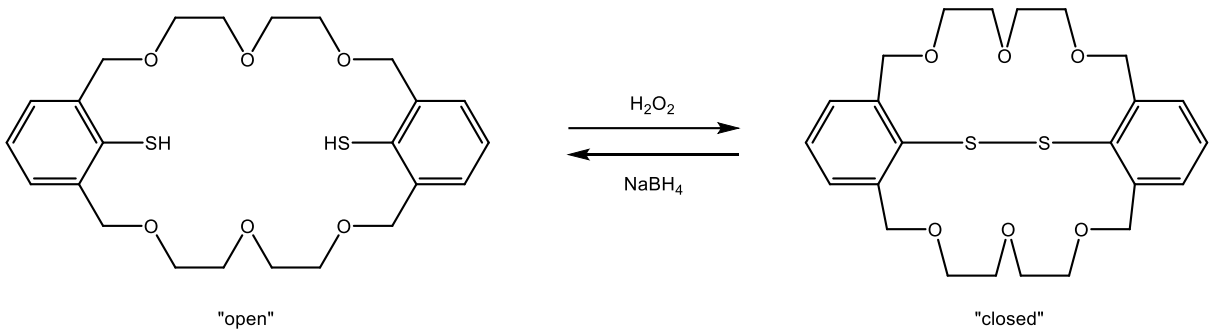

Scheme 5: Example of a redox-triggered molecular switch

The dithiol compound pictured above, which structure resembles that of crown ethers, acts as a receptor of small cations such as Ag^+ thanks to its cavity. Upon oxidation with hydrogen peroxide, a disulfide bridge is formed between the two sulfur atoms, thus blocking the cavity of the molecule and making the complexation of a cation impossible. The disulfide compound can then be reduced using sodium borohydride, reverting back to the open, crown ether-like dithiol form. This redox reaction gives access to a switchable host-guest system, a feature very interesting for many different applications, as will be discussed in this chapter.

Molecular switching does not necessarily involve structure changing, though; the difference between the two states of a switch can be about properties. Staying in the field of molecular recognition and host-guest chemistry, examples have been reported of organic compounds having their properties altered when complexed to a guest molecule. It is the case for the system shown in Scheme 6: the anthracene moiety of the molecule has its luminescence quenched due to the presence of the lone electron pair of the nearby nitrogen atoms. The luminescence is recovered either upon protonation of these nitrogen atoms, or upon complexation of a metallic ion such as Zn^{2+}, the organic molecule acting as a bidentate ligand towards the transition metal.[42] The original state can then be recovered by using a base or by removing the metal cation. This example, by combining host-guest chemistry and luminescence on-off switching, makes for a very nice chemical sensor, and is merely one of many similar systems.

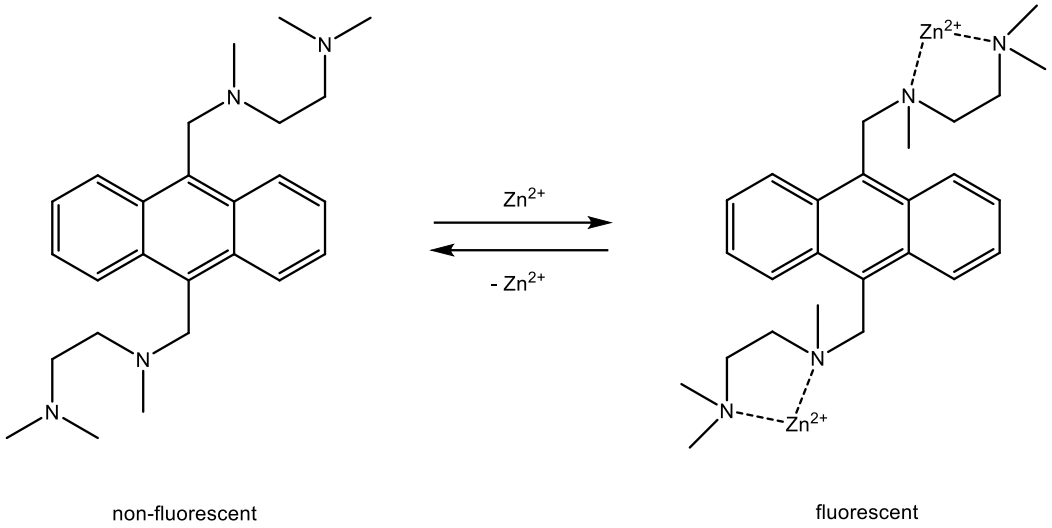

Scheme 6: Example of a complexation-triggered molecular switch

A lot of other molecular switches have recently been reported in the literature, using various stimuli to operate, such as pressure,[43] temperature,[44] or variation of the pH.[45] However, one of the most interesting and widely used type of switchable systems, and the main topic of the current chapter, is light-triggered molecular switches. Indeed, light is a convenient and powerful tool to use in such a context, especially considering the large number of functional groups that undergo structural changes when irradiated by light.

Among this huge photochemical library of compounds available, a few classes of molecules have stood out and have proved to be promising candidates for use as molecular switches. One of them is diarylethenes. These molecules, which have been extensively studied by Irie, can undergo a reversible cyclization reaction using the right wavelengths (Scheme 7).[46] Diarylethenes present some interesting features, such as the tunability of their structure (and therefore of their absorption properties), and the thermal stability of its two forms, allowing for a light-only activation of the switch under the right conditions. Numerous applications of the switchable property of diarylethenes have been reported in the last few years, including some, interestingly, in the field of host-guest chemistry.[47]

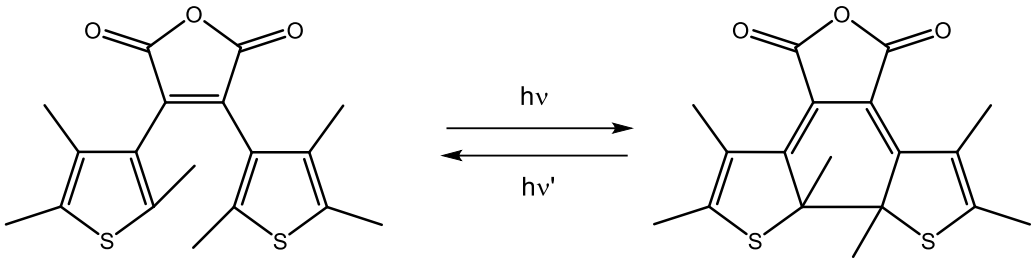

Scheme 7: Example of a diarylethene photoswitch

Many other photoswitchable molecules exist, some of which will be discussed in this chapter. Among them, azobenzenes[48] and spiropyrans,[49] for example, have seen interesting applications in organometallic chemistry, thanks to their unique photochromic properties. The goal of the present project is to use such photoswitchable moieties and include them as part of ruthenium metalla-assemblies. Since the release of guest molecules from inside the cavity of a ruthenium cage has so far mainly been controlled by varying the size of the cavity[50] or by uncontrolled breaking of the assembly,[51] the focus of our group in the last few years has been to find novel means to control the guest release. The synthesis of light-triggered assemblies would represent a step in the achievement of this purpose. This could particularly be of high interest for drug delivery systems (Scheme 8), as light has proven to be a convenient and mild tool to use for medicinal applications.

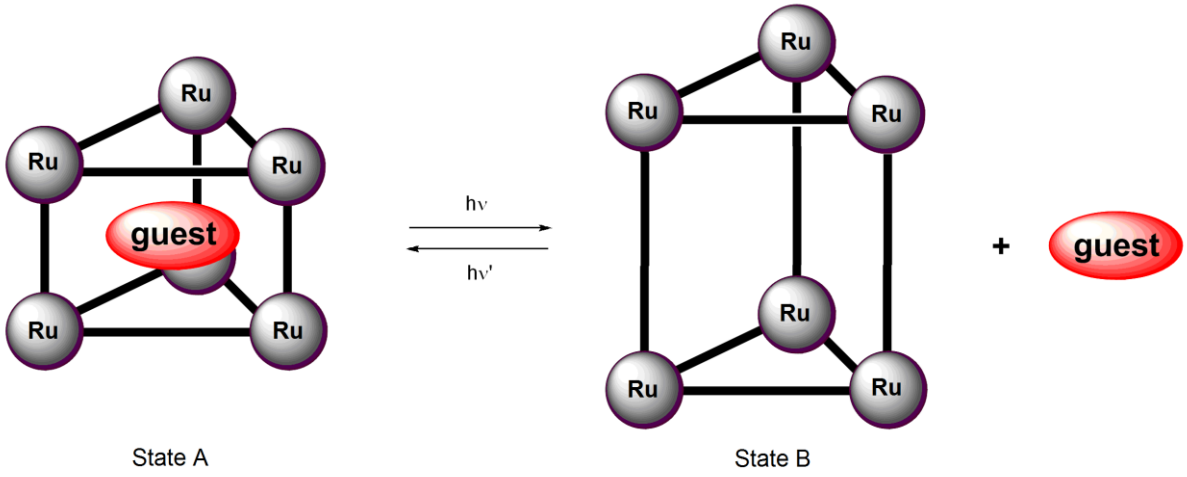

Scheme 8: Schematic representation of the concept of guest release from a light-triggered ruthenium assembly

3.2 Ruthenium-Azopyridine Assemblies

3.2.1 General

Azobenzene-type compounds are molecules consisting of a nitrogen-nitrogen double bond, each nitrogen being linked to an aryl group. Azobenzene itself was first reported in 1834 by Mitscherlich,[52] although its photochemical properties were only discovered more than a century later.[53] Azobenzene can undergo isomerization from its *trans* (*E*) form – the most stable one – to its *cis* (*Z*) form – less stable – using UV light. Although the reverse isomerization tends to occur thermally in the dark, the *trans* form can be selectively recovered using irradiation with visible blue light (Scheme 9).

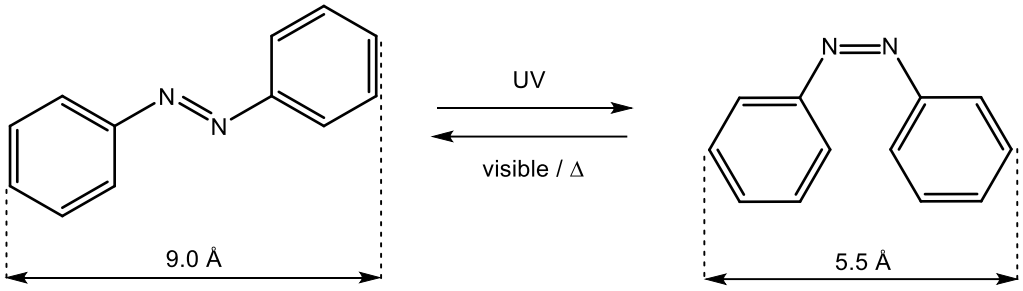

Scheme 9: Photochemical isomerization of azobenzene

This transformation induces a drastic change in the geometry of the molecule: the distance between the two atoms in position 4 of the aromatic rings decreases from 9 Å to 5.5 Å; and unlike the *trans* isomer, the *cis* one is not flat: the aromatic rings electronically repulse each other, creating an angular geometry.[54] The switching ability of azobenzenes has been exploited in many different fields over the years, for instance in biology in order to control some biological processes using irradiation.[55] Interesting examples of host-guest chemistry have also been reported,[56] taking advantage of the isomerization feature of the azo moiety to design functional switches based on molecular recognition, such as the one shown in Scheme 10.[57]

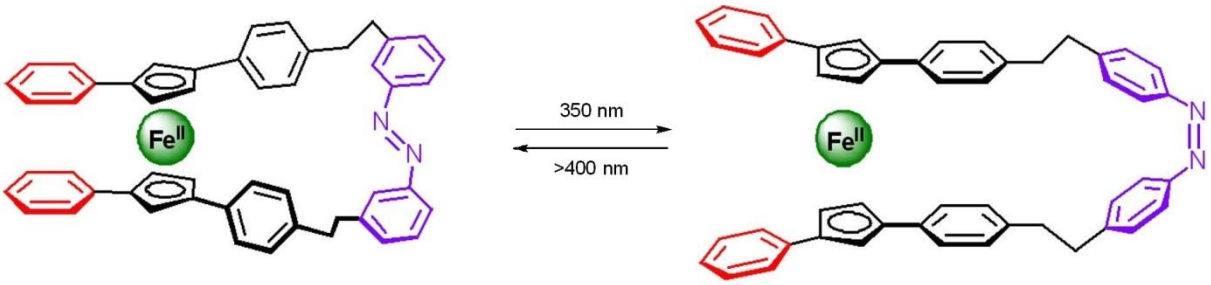

Scheme 10: "Molecular scissors" using the isomerization of azobenzene to control the encapsulation of a Fe (II) ion

In this work, azopyridine is used as an azobenzene derivative along with dinuclear ruthenium species to generate a series of organometallic assemblies. Their photochemical properties are then investigated to see if the unique features of the azo moiety remain present in the ruthenium assemblies.

3.2.2 Results and Discussion

Four cationic ruthenium-azopyridine rectangles (**32-35**) were prepared, using different ruthenium starting materials (Scheme 11). The synthesis was realized in two steps. The first one involved reacting one equivalent of ruthenium dimer with two equivalents of silver triflate in dichloromethane at room temperature for 3 hours in order to form the triflate intermediate (not isolated). The second step involved filtering the reaction mixture (in order to eliminate the silver chloride formed during the first step) into a solution of one equivalent of 4,4'-azopyridine in dichloromethane; this mixture was then refluxed for 10 hours. After isolation and purification, the tetracationic rectangles were obtained in good yields as their triflate salts.

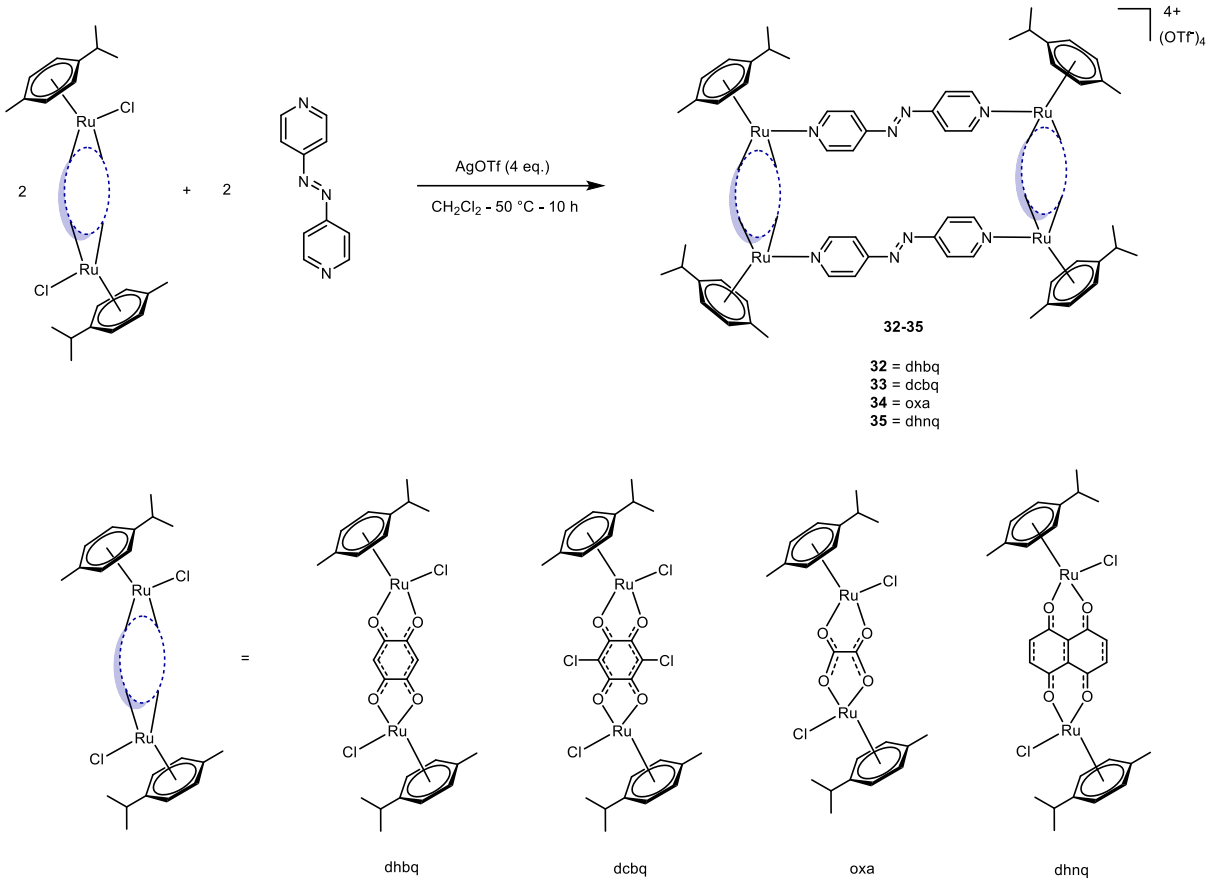

Scheme 11: Synthesis and structures of ruthenium-azopyridine rectangles **32-35**

Simultaneously to this work, Stang and co-workers reported the synthesis and characterization of several ruthenium-azopyridine rectangles in order to investigate their anticancer properties, including **32**, **34** and **35**.[58] Therefore, the focus of the discussion will be on rectangle **33**, as it was not reported before. All rectangles were characterized by ^{1}H NMR spectroscopy, and for **33** by mass spectrometry, infrared spectroscopy, and UV-visible spectroscopy. The proton NMR spectra unsurprisingly show all signals slightly shifted compared to the starting materials. The infrared spectrum only shows bands corresponding to the C-H stretch of aromatics (~2900 cm^{-1}) and the C=O stretch (~1600 cm^{-1}) of the benzoquinone moiety. The nitrogen-nitrogen double bond can unfortunately not be seen in infrared spectroscopy due to its null dipolar moment and its symmetry. **33** was found to be poorly soluble in most organic solvents except for nitromethane – though soluble enough at concentrations required to perform UV-visible spectroscopy.

In order to investigate the photochemical properties of these ruthenium-azopyridine assemblies, UV-visible absorption spectra were recorded to determine the optimal irradiation

wavelengths to use. Figure 21 presents the absorption spectra of azobenzene, azopyridine and metalla-rectangle **33**.

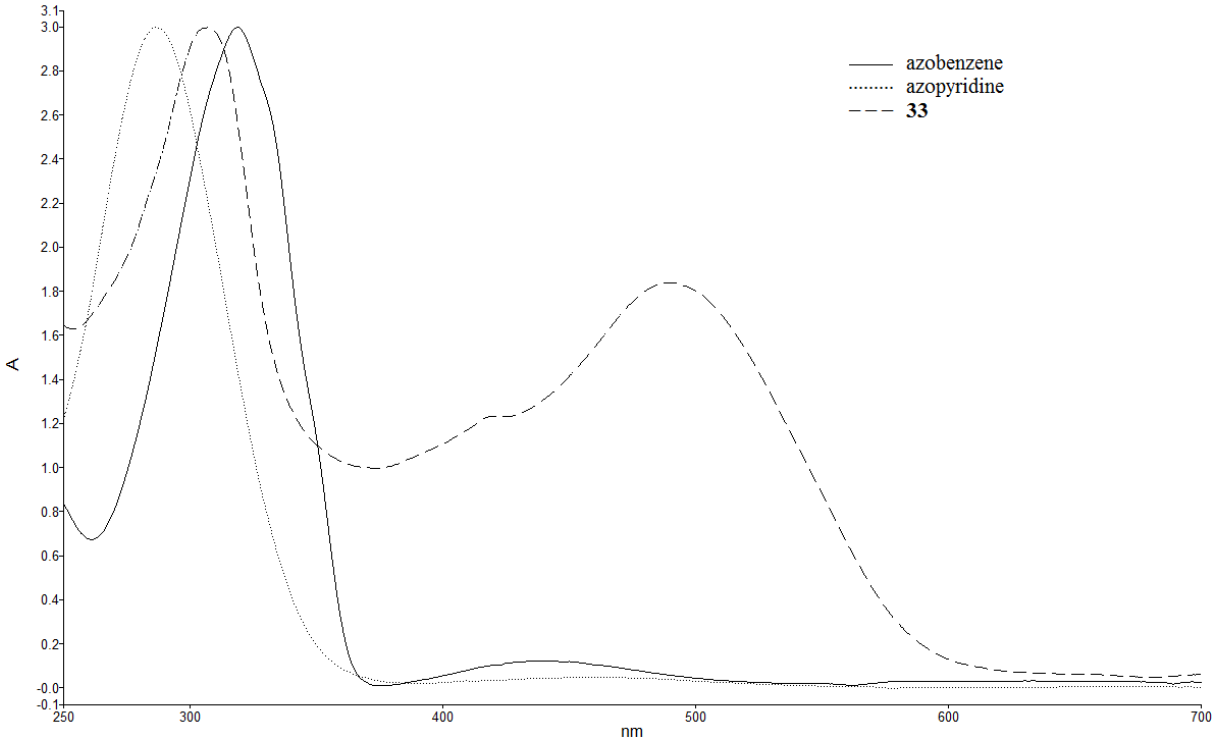

Figure 21: Normalized UV-visible absorption spectra of azobenzene, azopyridine and **33** in CH_2Cl_2

A clear difference can be observed when comparing the spectra for azobenzene and azopyridine. While azobenzene has an absorption peak located at 319 nm, and is therefore suited for an irradiation with UV-A rays (315-400 nm), azopyridine has its absorption peak located at 283 nm, making it better suited for an irradiation using UV-C (100-280 nm) rays. Rectangle **33** presents a bathochromic shift of its UV absorption compared to azopyridine alone, in addition to a visible absorption peak which is due to a metal-ligand charge transfer.

Since azopyridine has not been as extensively studied as azobenzene in the literature, irradiation experiments have been realized to investigate the isomerization of *trans*-azopyridine to its *cis* form. A solution of azopyridine in dichloromethane ($c = 1.0 \times 10^{-5}$ $mol.L^{-1}$) was introduced into a closed quartz glass tube and submitted to irradiation with UV-C rays; UV-visible spectra were recorded after certain amounts of time to monitor the isomerization process (Figure 22).

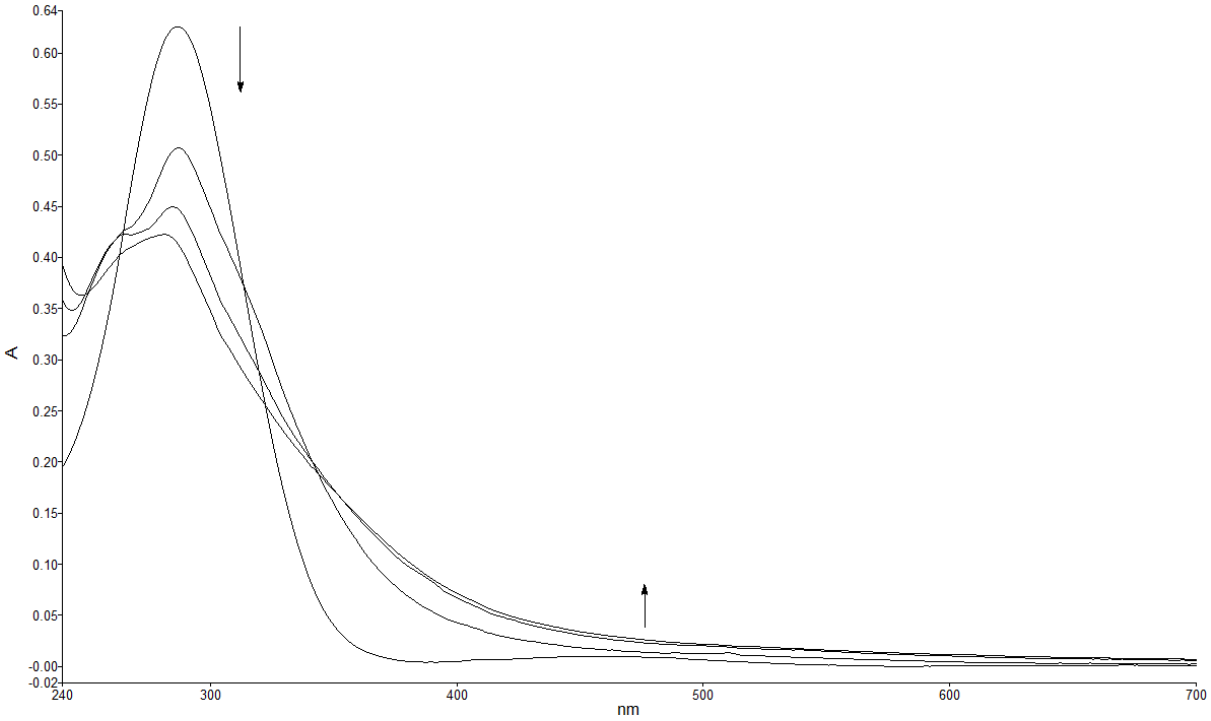

Figure 22: UV-spectra of azopyridine in CH_2Cl_2 before and after (10, 30 and 60 minutes, respectively) irradiation with UV-C rays

The results are quite similar to what can be observed in the case of azobenzene.[59] Upon irradiation, the absorption peak located in the UV region decreases in intensity by 33%, while the visible absorption slightly increases. This suggests the successful isomerization of *trans*-azopyridine to its *cis* form. No further changes of the spectrum were observed after more than one hour of irradiation. When left in the dark overnight, the solution presents a spectrum similar to the one prior to any irradiation, suggesting the successful reverted isomerization from *cis*- to *trans*-azopyridine. Since UV-visible spectroscopy does not allow for an easy quantification of the proportion of the two isomers, the same irradiation study was conducted, this time monitored by ^{1}H NMR spectroscopy. Indeed, the proton signals of *cis*-azopyridine are shifted downfield compared to the *trans* form, making it easy to distinguish between the two isomers.[60] Their proportion can then be conveniently estimated by integration of the signals. The results of this study are presented in Figure 23.

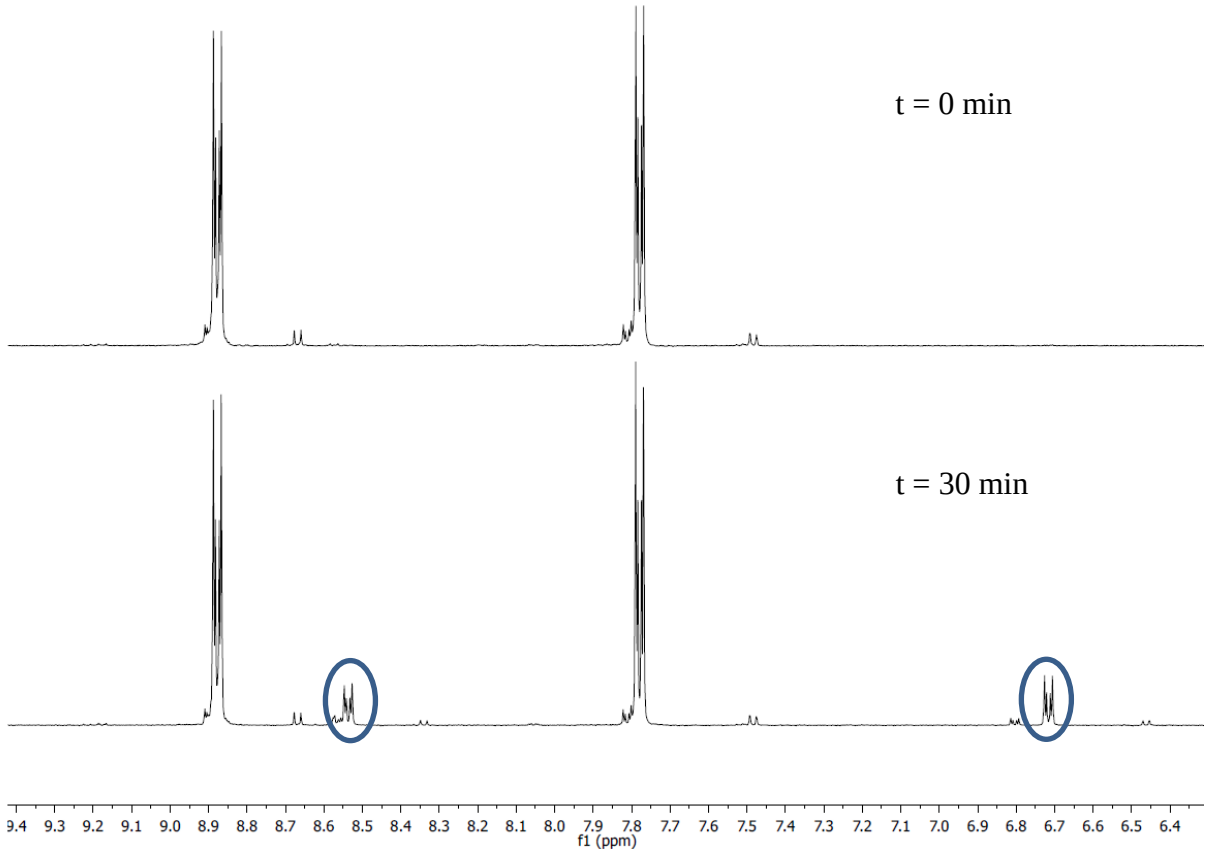

Figure 23: ^{1}H NMR spectra of *trans*-azopyridine in CD_2Cl_2 before (top) and after 30 minutes of irradiation with UV-C rays (bottom), with annotated *cis*-azopyridine peaks

Only a partial conversion of *trans*-azopyridine to *cis*-azopyridine can be observed: integration of the signals reveals that a 13% conversion is attained after 30 minutes of irradiation. No further changes were observed even after a prolonged irradiation time. As observed with UV-visible spectroscopy, disappearance of the peaks related to the *cis* isomer after leaving the solution in the dark overnight confirms the reverted isomerization. The reasons of this poor isomerization ratio compared to azobenzene are unclear; the first mention of this phenomenon was made by Kinugawa and co-workers, who came to the conclusion that the electron-withdrawing nitrogen of the pyridyl group must have some kind of influence on the isomerization of the azo moiety.[61] Several years later, Espinet and co-workers reported values in concordance with the results described above, i.e. a similar decrease in absorbance (36%) and a 85/15 *trans*/*cis* ratio determined by proton NMR spectroscopy.[60] Bandara and Burdette later performed studies on several substituted azobenzenes,[59] including some

containing electron-withdrawing groups in their structure, but observed very similar behaviors to that of azobenzene, making azopyridine a particular case in that matter.

Unfortunately, when rectangles **32-35** were submitted to irradiation with UV light (both UV-A and UV-C rays irradiations were attempted), no changes were observed either by UV-visible or NMR spectroscopy even after several days of irradiation. Several hypotheses can be formulated to explain this absence of isomerization. One is in the continuity of Kinugawa's statement: if the low electron density of the aromatic rings has a negative influence on the isomerization properties, then the ruthenium-pyridyl bond further lowering this electronic density can enhance this influence, possibly leading to a very low or non-existent isomerization. In his work, Espinet synthesized gold (I) and silver (I) azopyridine complexes and indeed observed a diminution of the *trans* to *cis* conversion ratio compared to the free ligand, giving credit to this hypothesis. However, isomerization still occurred, even at low rates, implying there may be other reasons to the absence of isomerization in rectangles **32-35**. Another hypothesis can be formed regarding the isomerization mechanism of azobenzenes. Several different mechanisms have been proposed for this transformation, mainly falling into two groups: rotation-based and inversion-based mechanisms (Scheme 12).

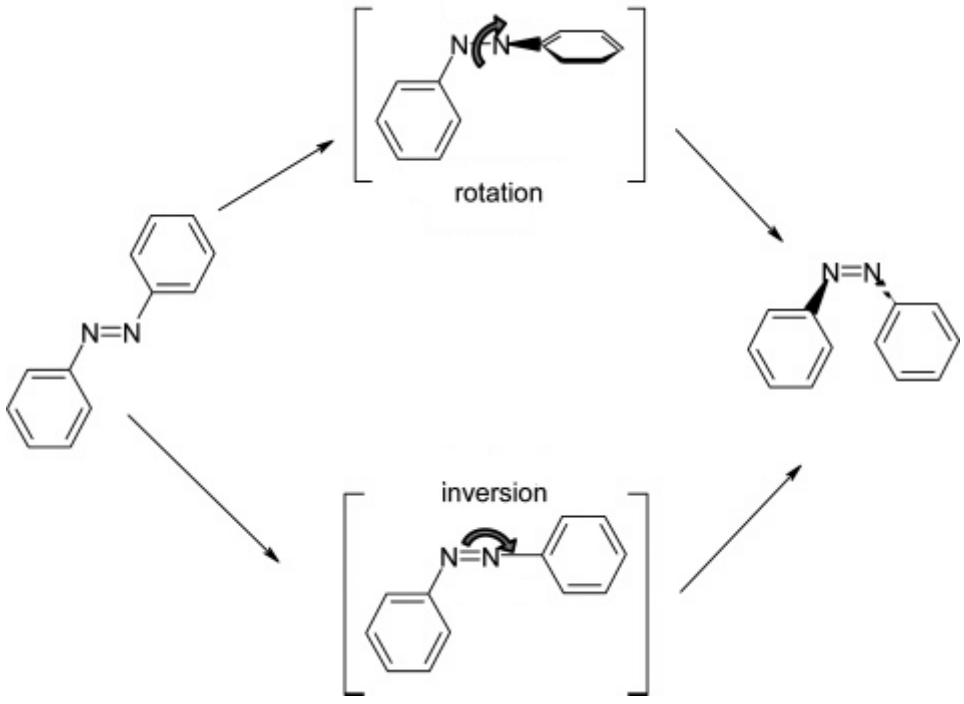

Scheme 12: Rotation and inversion pathways for the isomerization mechanism of azobenzenes

The rotation mechanism involves a transition state where the two nitrogen atoms are linked by a single bond instead of a double bond, allowing free rotation along the N-N axis. The inversion mechanism involves a transition through a linear (180°) N=N-C angle between the *trans* and *cis* isomers. While there have been evidence of both types of mechanism, and while several pathways may happen simultaneously, each azobenzene system is unique and its isomerization mechanism depends on a number of factors, such as the structure of the molecule or the excited states involved in the isomerization process.[59] Regardless, some hypotheses can be proposed in the case of ruthenium-azopyridine rectangles **32-35**. Indeed, it can be easily conceived that from a mechanical point of view, a rotation mechanism would not be feasible for a cyclic compound. In **32-35**, each azopyridine is linked to the other one *via* the ruthenium clips, making impossible the complete rotation of the N-N bond to form the *cis* isomer. Since isomerization of cyclic azobenzene compounds have successfully been reported[62] – and logically deduced as inversion-driven – assumption can be made that rectangles **32-35**, which show no *trans* to *cis* isomerization, need to operate through a rotation mechanism. The cyclic structure of these assemblies induces rigidity, thus preventing this mechanism to happen; a feature that Espinet's complexes lack, possibly explaining why these more flexible compounds exhibit the isomerization of the azo moiety.

3.2.3 Conclusion

Four cationic ruthenium-azopyridine rectangles were successfully synthesized and characterized. Irradiation studies monitored by UV-visible and ^{1}H NMR spectroscopies were performed to investigate their photochemical properties. Unfortunately, all rectangles failed to exhibit the *trans* to *cis* isomerization of the azo moiety. These results were interpreted by two hypotheses. The first one revolves around the poor isomerization activity of azopyridine itself, which could be worsened by the coordination of the pyridyl group to a metal. The second one revolves around the isomerization mechanism. The results obtained in this work point towards a rotation mechanism for these compounds, rendered impossible because of the cyclic nature of the assemblies.

3.3 Ruthenium-Anthracene Assemblies

3.3.1 General

Anthracene is a tricyclic aromatic molecule, consisting of three benzene rings arranged in a linear fashion. Anthracene is mostly obtained from coal tar, and is mainly used as the precursor of anthraquinone, which is used in the preparation of dyes such as the well-known red alizarin. Anthracene undergoes a photodimerization upon irradiation with UV light (Scheme 13).[63] The product of this [4+4] cycloaddition loses the aromaticity of the central rings, resulting in a curved structure, unlike the flat anthracene monomer. As consequences, the structural and spectral properties are greatly changed, and anthracene dimers tend to be insoluble in most common organic solvents.[64] The monomeric form can be retrieved upon heating or irradiation with a different wavelength (which depends on the absorption spectrum) of the dimer.

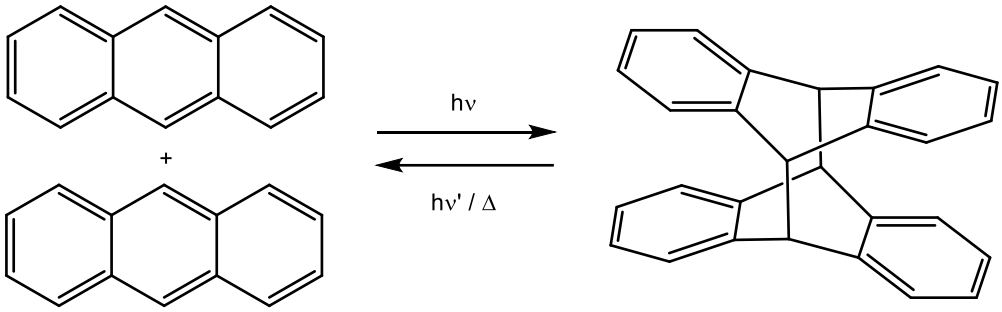

Scheme 13: Photodimerization of anthracene

Like many other aromatic molecules, anthracene is able to bind singlet oxygen through a [4+2] cycloaddition to form an endo-peroxide (Scheme 14).[65] These endo-peroxides can then be dissociated under certain conditions, releasing a singlet oxygen molecule while reverting to the anthracene starting compound. This feature has been the subject of much attention in the last years, as anthracene could in this case act as a vehicle to transport singlet oxygen; an interesting concept especially in medicinal chemistry, considering the high cytotoxicity of singlet oxygen.[66]

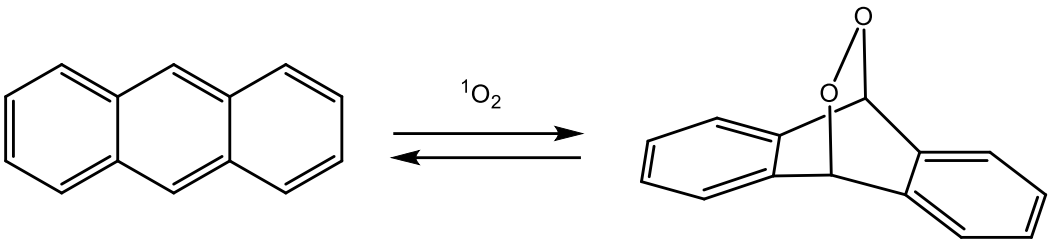

Scheme 14: Formation of an endo-peroxide *via* the reaction of anthracene with singlet oxygen

Anthracenes can be functionalized easily at multiple positions, making them interesting building blocks for the construction of supramolecular entities. Therefore, in this part of the work, anthracene is used as part of ruthenium metalla-assemblies; their synthesis, characterization, and the investigation of their photochemical properties will be discussed.

3.3.2 Results and Discussion

In order to make it a suitable ligand towards ruthenium, anthracene first needs to be functionalized. To achieve this purpose, 9,10-dibromoanthracene and 3-ethynylpyridine were submitted to a Sonogashira coupling reaction using a modified literature procedure to form ligand **L36** (Scheme 15).[67]

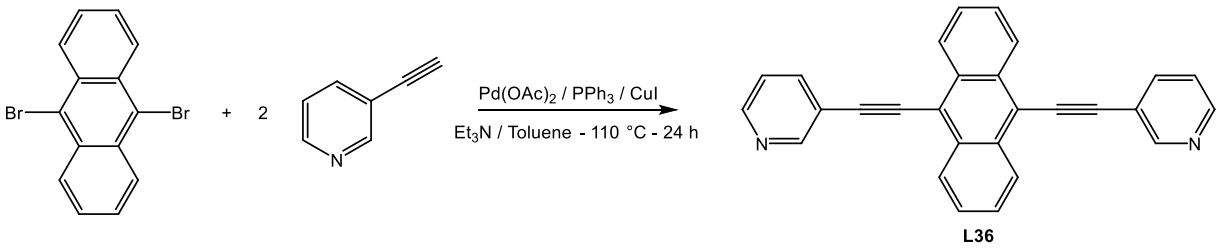

Scheme 15: Synthesis of anthracene-based ligand **L36**

After purification, **L36** was obtained as an orange solid with 28% yield, as 9-bromo-10-(3-ethynylpyridine)anthracene, the mono-substituted product, is predominant even after a prolonged reaction time. **L36** was only characterized by ^{1}H and ^{13}C NMR spectroscopy, as it was reported before, although not studied for its photodimerization properties.[68] This ligand was then used in the synthesis of metalla-rectangle **36**, using the same procedure as previously

described (Scheme 16). The oxalato-bridged ruthenium dimer was chosen for its short Ru-Ru distance, in order to favor the [4+4] cycloaddition reaction of the anthracene moiety within the rectangle.

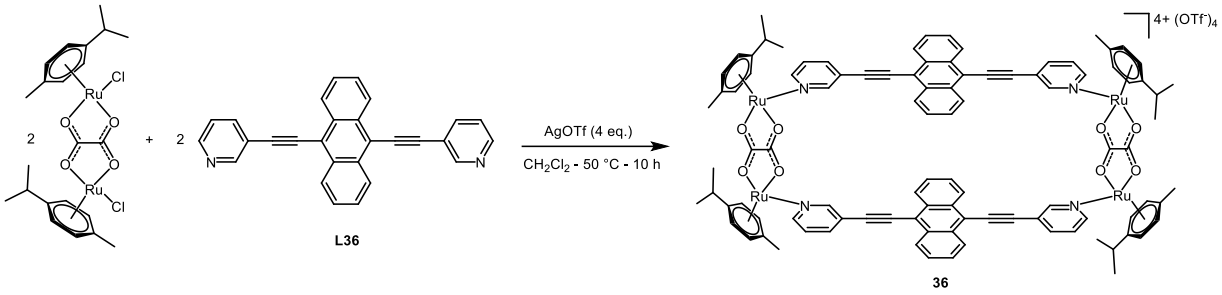

Scheme 16: Synthesis of ruthenium-anthracene rectangle **36**

Rectangle **36** was obtained as a yellow solid with 83% yield, and was characterized by ^{1}H and ^{13}C NMR spectroscopy, mass spectrometry, infrared spectroscopy, UV-visible spectroscopy and elemental analysis. Proton NMR signals present shifts compared to the starting materials, especially in the case of the pyridyl groups, more affected by the coordination to the ruthenium due to their proximity. Mass spectrometry confirms the formation of the structure pictured above with many characteristic peaks, such as $[M\text{-}2OTf]^{2+}$, $[M\text{-}3OTf]^{3+}$ and $[M\text{-}4OTf]^{4+}$. Infrared spectroscopy shows in particular the C=O stretch of the oxalato moiety (~1600 cm^{-1}) and the C ≡ C (~2200 cm^{-1}) stretch of the organic panels. Rectangle **36** is soluble in most organic solvents as well as in water, unlike hydrophobic ligand **L36**.

Irradiation experiments were conducted both on ligand **L36** and rectangle **36** in order to study the photodimerization process. First, a solution of **L36** in CH_2Cl_2 ($c = 1.0 \times 10^{-5}$ $mol \cdot L^{-1}$) was placed in a sealed quartz vessel and submitted to irradiation using UV-C rays; UV-visible spectra were recorded before and after irradiation, as shown in Figure 24.

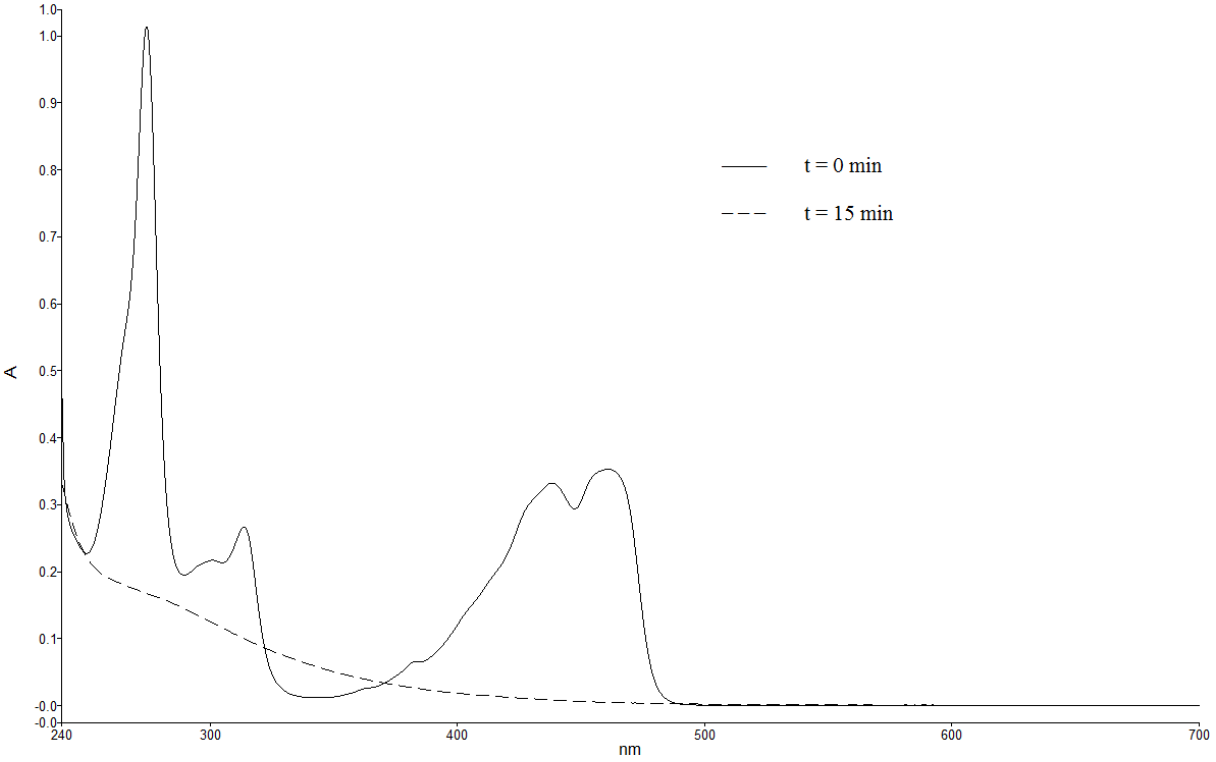

Figure 24: UV-visible spectra of **L36** in CH_2Cl_2 before and after 15 minutes of irradiation with UV-C rays

The results obtained are very similar to previously reported studies on the photodimerization of anthracene species.[64] The monomeric form (**L36**) shows a strong absorption around 250 nm due to the anthracene moiety and a visible absorption which is caused by the presence of the ethynylpyridine group. When irradiated, the UV-visible spectrum exhibits a disappearance of these absorptions, and a new absorption appears in the UV region, below 240 nm. It is worthy to mention that shorter irradiation times gave little to no changes, while irradiation times longer than 15 minutes did not induce any further change on the UV-visible spectrum. Upon irradiation, the pale yellow solution of **L36** turned colorless, but no precipitation of the supposedly less soluble dimer was observed, certainly due to the low concentration of the medium. However, when a concentrated solution of **L36** in CH_2Cl_2 was submitted to the same irradiation, white crystals appeared in the vessel. These crystals appeared to be quite poorly soluble in most solvents, but enough in $CDCl_3$ so that a ^1H NMR spectrum could be recorded (Figure 25).

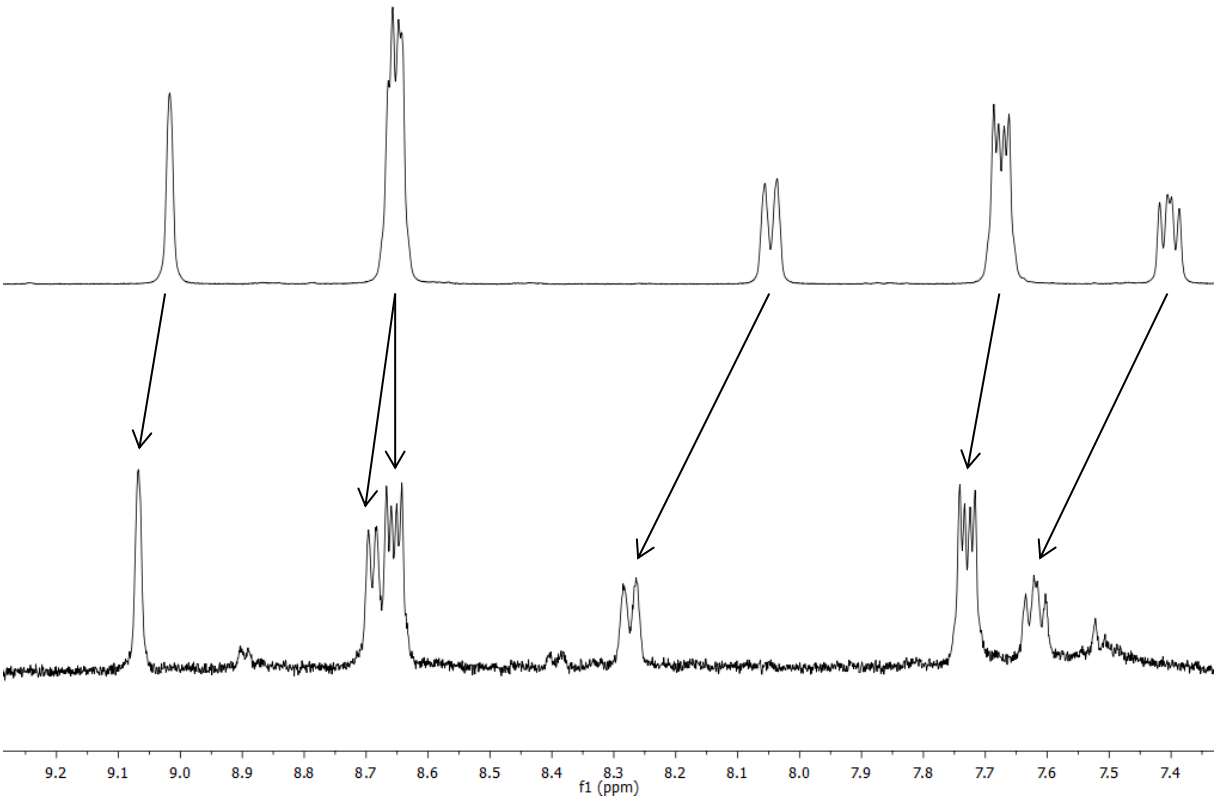

Figure 25: ^{1}H NMR spectra of **L36** in $CDCl_3$ before (top) and after 60 minutes of irradiation with UV-C rays (bottom)

Several downfield shifts can be observed after irradiation, especially regarding the signals corresponding to the pyridyl protons. Small additional peaks can also be observed on the spectrum, possibly due to a slight decomposition of the compound. Unfortunately, the concentration of the solution was not high enough to perform a well resolved ^{13}C NMR spectrum. Nevertheless, all those information tend to confirm the formation of the dimeric form of **L36**. In this system, an undesired reaction can potentially occur: the intramolecular [2+2] cycloaddition of the parallel triple bonds is indeed a photochemically activated reaction. However, an infrared spectrum of the **L36** dimer still presented the C ≡ C stretch band, and no band relative to a newly formed C=C bond – result of a potential [2+2] cycloaddition – was found. This result suggests that upon irradiation with UV-C light, the photodimerization of the anthracene moiety is favored compared to the cycloaddition of the triple bonds.

Unfortunately, no irradiation either with visible or UV light allowed to revert back to the monomeric form, possibly because of the lack of strong absorptions of the dimer. Since heat can be used to perform this transformation, thermolysis was attempted on the dimeric form of **L36**. No changes were observed when a diluted solution of the compound was heated gently (up to 100 °C, depending on the solvent), even after days (up to seven days). However, when the white crystals formed from the concentrated solution of **L36** were heated up to the melting point (> 200 °C), an insoluble black slurry formed and could not be reverted to either the monomeric or dimeric form. This led to the conclusion that the dimerization of **L36** was achieved but unfortunately irreversible.

Nevertheless, the same irradiation studies were conducted on ruthenium-anthracene rectangle **36**. A solution of **36** in CH_2Cl_2 (c = 1.0 x 10^{-5} mol·L^{-1}) placed in a sealed quartz vessel was submitted to irradiation with UV-C rays; UV-visible spectra were recorded to monitor the changes (Figure 26).

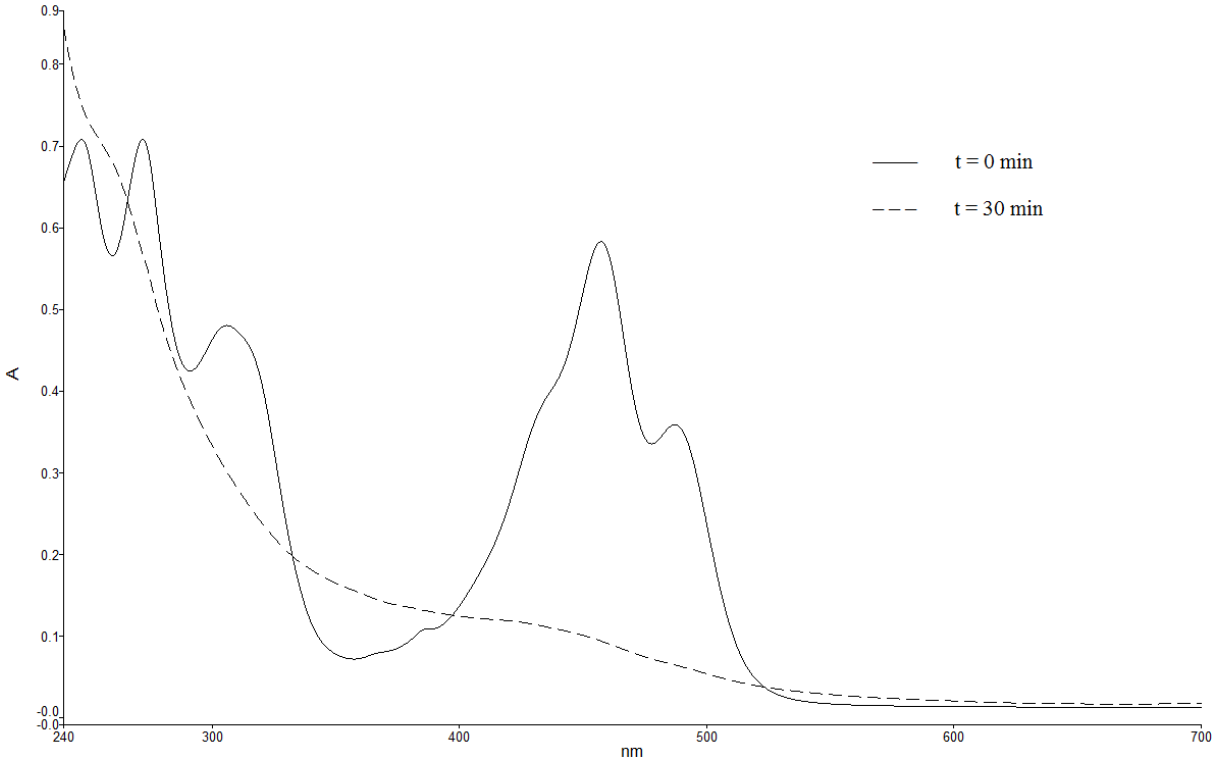

Figure 26: UV-visible spectra of **36** in CH_2Cl_2 before and after 30 minutes of irradiation with UV-C rays

Similarly to **L36**, the UV-visible spectrum of **36** drastically changed upon 30 minutes of irradiation: all absorption bands disappeared and a new band formed in the UV region below

240 nm. This absorption profile suggests the successful dimerization of the anthracene moiety within the rectangle. However, as with **L36**, a return to the original state could not be achieved either by irradiation or heating. Irradiation of a more concentrated solution of **36** for the same amount of time did not induce any changes on the ^{1}H NMR spectrum. After longer irradiation times (several hours), the solution progressively turned from yellow to black. Along with this change of aspect, the signals of the proton NMR spectrum became broader and the ratio of integrations changed, suggesting the breaking of the assembly and overall a possible decomposition of the compound. This could be explained by the fact that in more concentrated solutions, longer irradiation times are needed for the photodimerization to happen, but unfortunately also induce the breaking of the assembly.

While rectangle **36** did not prove to be a fully functional photoswitchable assembly, interesting applications can still be found for ruthenium-anthracene entities. Like with many other ruthenium metalla-assemblies synthesized in our group, encapsulation of small aromatic molecules would certainly be possible in ruthenium-anthracene rectangles, although with ruthenium spacers longer than oxalato. Indeed, anthracene-type molecules make for excellent planar panels for the construction of such assemblies; moreover, their unique UV-visible properties – both absorption and emission – make them easy and convenient to identify. Such assemblies could also be used as vehicles for the transport of singlet oxygen *via* the formation of endo-peroxides, as mentioned in the introduction. This would be of high interest particularly in medicinal chemistry, as ionic assemblies such as **36** are generally water-soluble, whereas hydrophobic anthracene-based organic molecules are not.

It is towards this perspective that collaborators at the University of Bordeaux, France, synthesized tetradentate ligand **L37**, which led to the synthesis of ruthenium metalla-assembly **37** (Scheme 17).

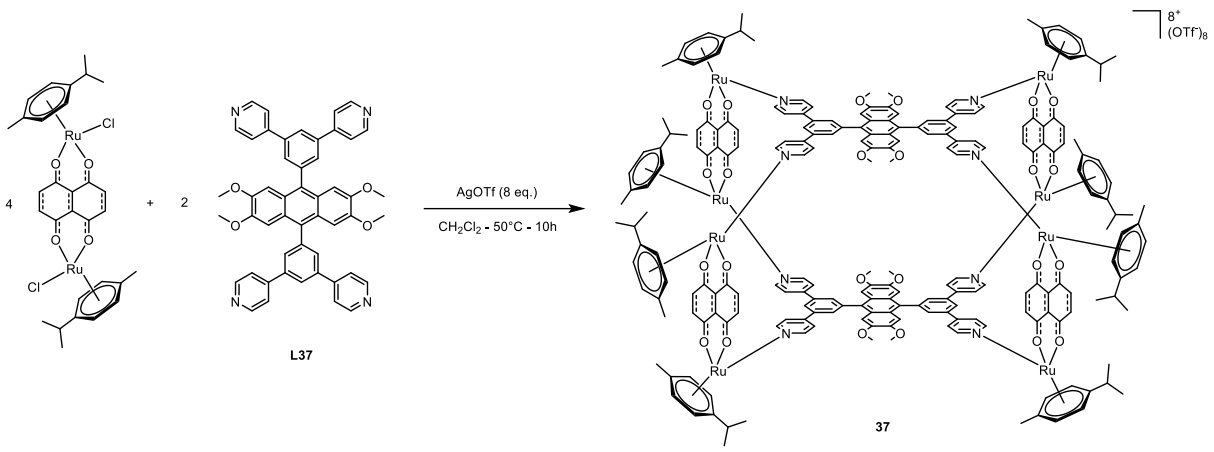

Scheme 17: Synthesis of ruthenium-anthracene cage **37**

The synthesis was carried out following the standard procedure, i.e. reacting the anthracene ligand, the ruthenium clip – in this case, the naphtoquinonato-bridged dinuclear clip – and silver triflate. The resulting polycationic cage **37** was fully characterized by ^{1}H and ^{13}C NMR spectroscopy, using HSQC and HMBC 2D experiments in order to determine the position of the carbon signals; as well as by mass spectrometry, infrared spectroscopy, UV-visible spectroscopy and elemental analysis. The proton NMR shows a duplication of most signals compared to the starting materials due to the loss of symmetry in the three dimensional structure. The mass spectrum shows the typical $[M\text{-}3OTf]^{3+}$ and $[M\text{-}4OTf]^{4+}$ signals, confirming the formation of the assembly. The most characteristic signal in the infrared spectrum is the one corresponding to the C=O stretch of the naphtoquinone moiety (~1600 cm^{-1}). Despite its highly hydrophobic panels, **37** was found to be soluble in most solvents, including water. After purification and drying, **37** was sent to the University of Bordeaux in order to study the formation of the corresponding endo-peroxide, with the goal of obtaining a functional vehicle for the transport of singlet oxygen in aqueous medium.

3.3.3 Conclusion

In this work, anthracene-based ligand **L36** and corresponding ruthenium rectangle **36** were successfully synthesized and characterized. Irradiation experiments were conducted for both compounds in order to study the photodimerization of the anthracene moiety. In the case of **L36**, it was found that the dimerization could occur but was unfortunately irreversible. In the case of **36**, results suggested that the dimerization was possible for diluted solutions, but

prolonged irradiation of more concentrated solutions resulted in the breaking and decomposition of the assembly. This led to the search of alternative applications for ruthenium-anthracene species, such as the transport of singlet oxygen through the formation of endo-peroxides. In this regard, water-soluble ruthenium cage **37** was synthesized and sent to collaborators at the University of Bordeaux, France, in order to investigate this property for potential applications in medicinal chemistry.

3.4 Ruthenium-Dihydropyrene Assemblies

3.4.1 General

Pyrene is a tetracyclic aromatic molecule consisting of four benzene rings fused into each other. Like anthracene, pyrene is usually found in coal tar and is used in the preparation of dyes. Some of its derivatives are also used as molecular probes due to strong fluorescence emission properties. Dimethyldihydropyrene (DHP) is a pyrene derivative containing two methyl groups located at the center of the structure, pointing outside of the plane in opposite directions. In 1965, Boekelhe and co-workers reported that under irradiation with visible light, DHP undergoes a ring-opening reaction to give its metacyclophane tautomer (Scheme 18).[69] This resulting cyclophanediene (CPD) is not flat like its pyrene counterpart, but rather possesses a stair-like structure. As expected, the spectral properties of the two isomers are largely different, resulting in an easy distinction between the two forms.

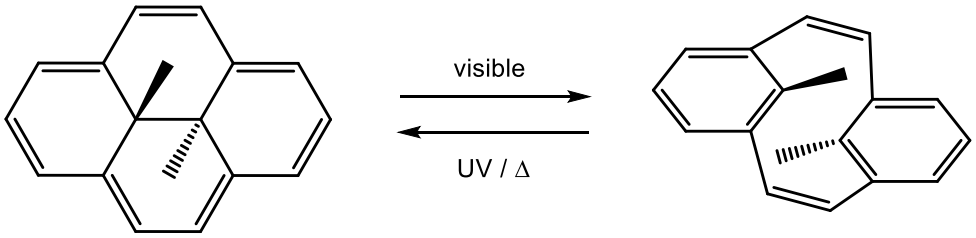

Scheme 18: Photoisomerization of dimethyldihydropyrene

The reverted cyclization reaction can be triggered by irradiation with UV light, or tends to occur thermally in the dark after a certain amount of time, the pyrene form being more stable. Many studies have been reported regarding the functionalization of dihydropyrenes and the influence of the substituents attached to their photochemical properties.[70] In most cases, dihydropyrene derivatives maintained the ability to photoisomerize. In the last part of this work, dihydropyrene is functionalized in order to become a suitable building block for the construction of ruthenium assemblies; their synthesis, characterization and properties will be discussed here.

3.4.2 Results and Discussion

Dihydropyrene precursor **DHP** was obtained through a multi-step synthesis described in Scheme 19, following procedures adapted from literature.[71]

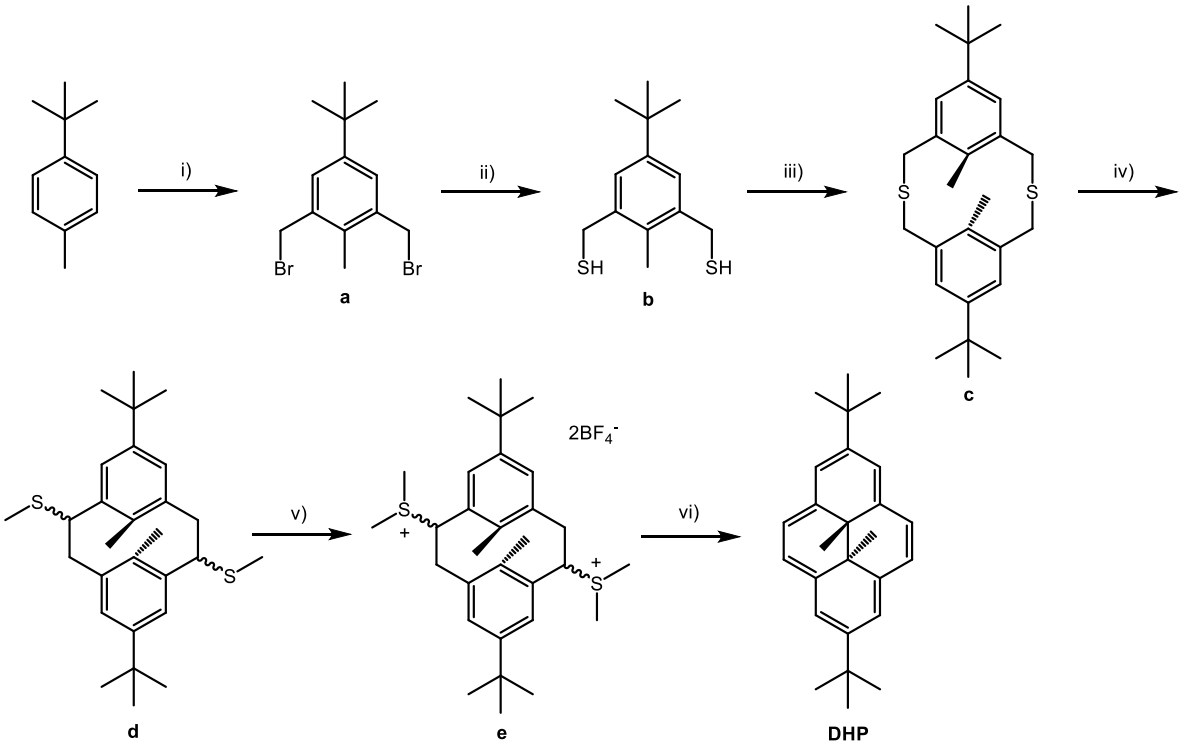

i) $ZnBr_2$, trioxane, HBr, THF, 85 °C, 4 d ; ii) thiourea, NaOH, EtOH/H_2O, 100 °C, 6 h ; iii) $NaBH_4$, KOH, EtOH/H_2O, RT, 24 h ; iv) nBuLi, MeI, THF, 0 °C, 2 h ; v) Borch reagent, CH_2Cl_2, RT, 5 h ; vi) and vii) tBuOK, THF, 70 °C, 12 h.

Scheme 19: Synthesis of dihydropyrene precursor **DHP**

This synthesis involved various chemical transformations and processes, of which the procedures are described in the Experimental Section. **DHP** was obtained successfully as a green powder with an overall yield of 42% (starting from 4-*tert*-butyltoluene) and its purity was confirmed by ^{1}H NMR spectroscopy. It was then reacted with *N*-bromosuccinimide in order to give the dibrominated compound **DHP-Br** with a 66% yield after separation from the tetrabrominated side-product. **DHP-Br** could then be involved in a Suzuki cross-coupling reaction with 4-pyridineboronic acid in order to obtain ligand **L38** (Scheme 20).

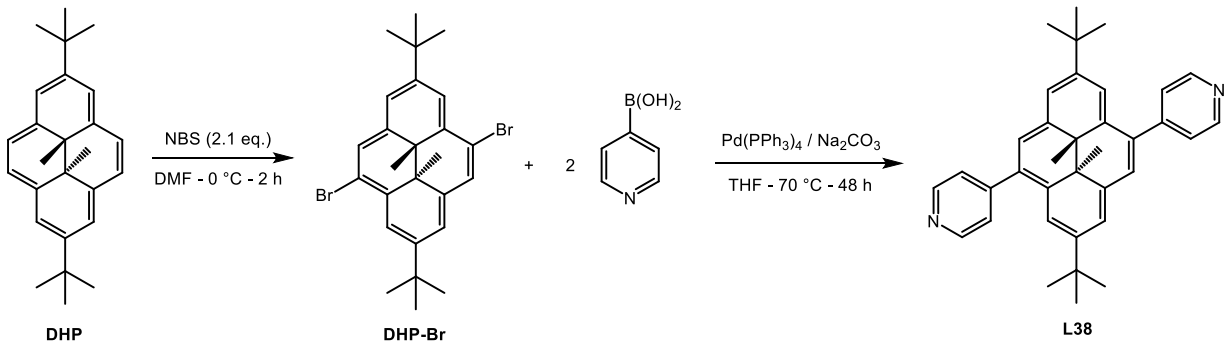

Scheme 20: Synthesis of **DHP-Br** and **L38**

L38 was obtained as a green powder with a 53% yield and was characterized by ^{1}H NMR spectroscopy, confirming the data previously reported in the literature.[72] Ligand **L38** was then engaged in a reaction with naphtoquinonato-bridged ruthenium dinuclear clip and silver triflate in order to yield ruthenium-dihydropyrene rectangle **38** as a black powder with a 38% yield (Scheme 21).

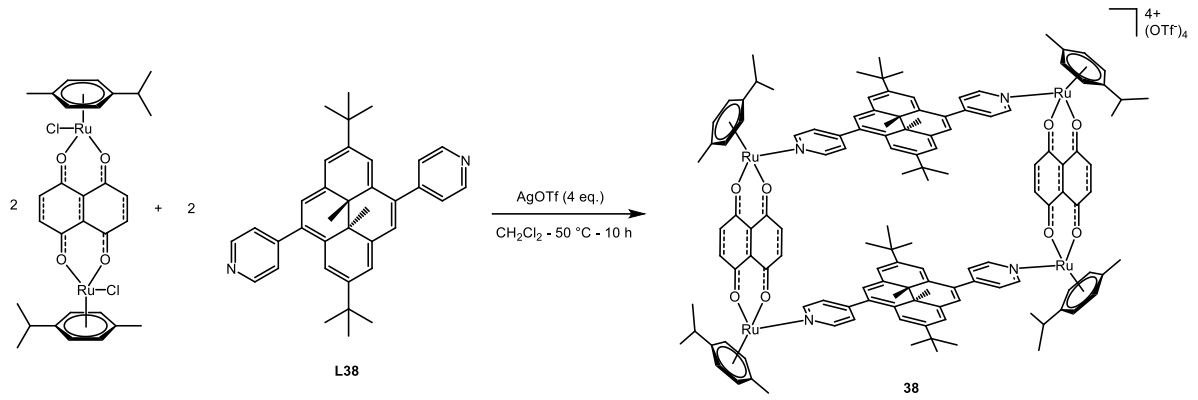

Scheme 21: Synthesis of ruthenium-dihydropyrene rectangle **38**

The structure of rectangle **38** was confirmed by ^{1}H and ^{13}C NMR spectroscopy, mass spectrometry, UV-visible spectroscopy and infrared spectroscopy. The most characteristic signals on the proton NMR spectrum are those corresponding to the naphtoquinone protons located at around 7 ppm, and those corresponding to the out of plane methyl groups on the pyrene moiety which are located at -4 ppm. The mass spectrum confirms the structure pictured above with the $[M\text{-}2OTf]^{2+}$ and $[M\text{-}3OTf]^{3+}$ characteristic peaks. The infrared spectrum unsurprisingly presents the C-H stretch of aromatics (~3000 cm^{-1}) and the C=O stretch of the naphtoquinone moiety (~1600 cm^{-1}). Rectangle **38** was found to be mildly soluble in most solvents, and unfortunately very poorly in water despite being a cationic species.

Ligand **L38** was extensively studied for its photochemical properties by Royal and co-workers.[72] It was demonstrated that **L38** could be fully converted to its open cyclophanediene (CPD) form via irradiation with visible light, and reverted to its closed form either via UV irradiation or heating. A few issues were reported though, such as the long irradiation time needed (more than 12 hours) to perform the DHP → CPD conversion, or the decomposition observed after long irradiation times with UV light for the backwards

transformation. In this work, irradiation experiments were conducted on **L38** for reference and gave essentially the same results.

UV-visible spectra were recorded both for ligand **L38** and rectangle **38** in order to determine the optimal irradiation wavelength to perform the ring-opening reaction (Figure 27).

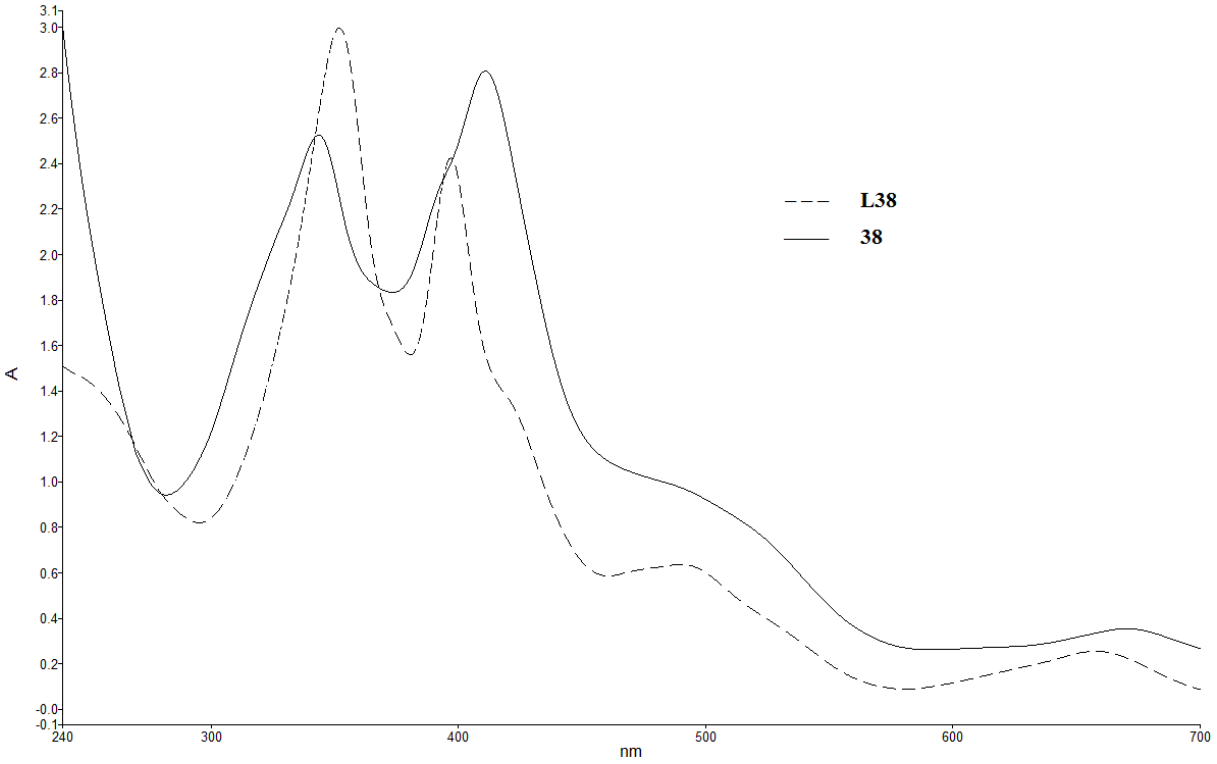

Figure 27: Normalized UV-visible spectra of ligand **L38** and rectangle **38** in CH_2Cl_2

A few differences can be observed between the ligand and the ruthenium metalla-assembly. In the rectangle, a new absorption band in the UV region (240 nm) is present due to the arene-ruthenium unit. Moreover, the two main bands corresponding to the dihydropyrene ligand (340 nm and 410 nm, respectively) are shifted in the rectangle compared to the free ligand: the former presents both a hypsochromic and a hypochromic effect, while the latter presents a bathochromic and a hyperchromic effect. These changes are however small enough that the same irradiation conditions as those used for **L38** can be applied in the case of rectangle **38**.

Following these results, a solution of **38** in CH_2Cl_2 was submitted to irradiation with visible light for up to 30 hours. The changes were monitored by UV-visible spectroscopy and are presented in Figure 28.

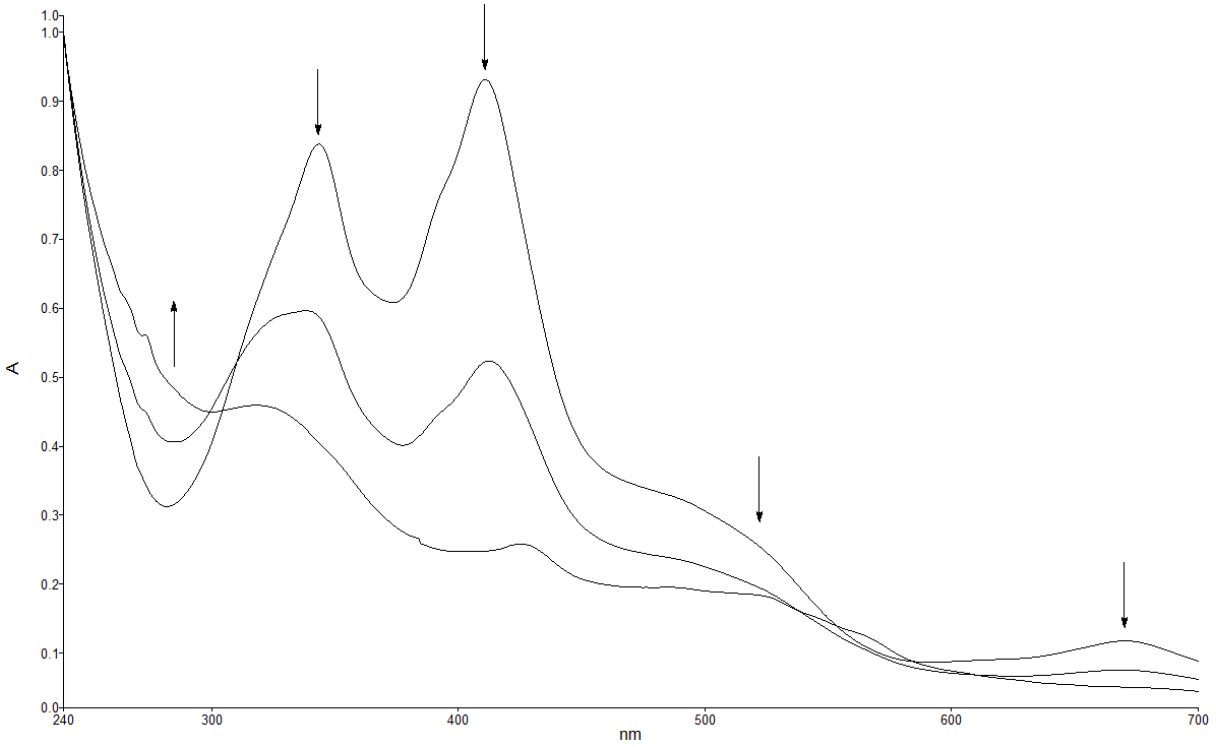

Figure 28: UV-visible spectra of **38** in CH_2Cl_2 before and after (15 and 30 hours, respectively) irradiation with visible light

After irradiation, a diminution of the intensity of the dihydropyrene-related bands can be observed, along with a rise of intensity of the shoulder band located at around 280 nm. Unsurprisingly, the band relative to the arene-ruthenium unit located at 240 nm does not exhibit any changes in intensity. These results are consistent to what was reported in the literature regarding the photochemistry of dihydropyrene compounds, and point towards the successful conversion of the dihydropyrene moiety to its cyclophanediene form within the assembly. Unfortunately, this photochemical reaction could not be monitored by NMR spectroscopy, as irradiation of a more concentrated solution of **38** did not yield any changes, even after seven days. However, it is noteworthy to mention that no signs of decomposition were observed either in the UV-visible or proton NMR spectra, even after such prolonged irradiation times.

The open form of rectangle **38** (noted ***o*-38**) was then submitted to irradiation with UV-C light in order to trigger the reverted CPD → DHP reaction. The changes were once again monitored by UV-visible spectroscopy; the results of this study are presented in Figure 29.

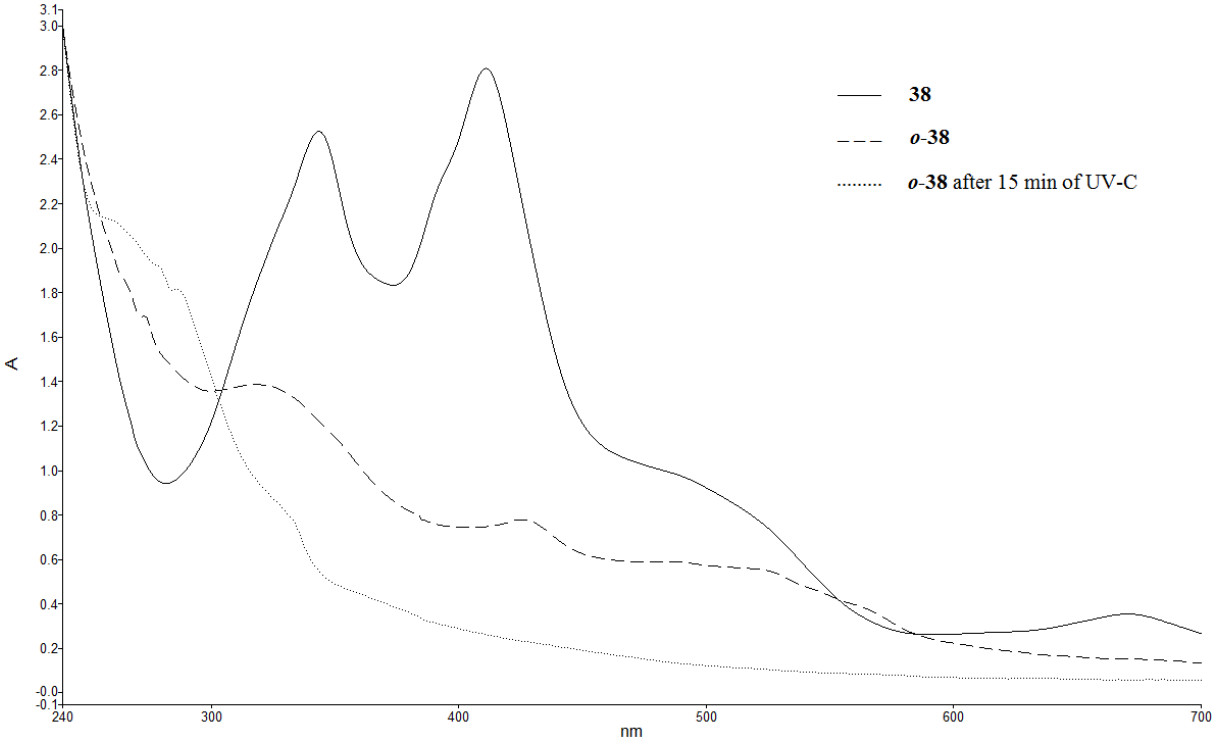

Figure 29: Normalized UV-visible spectra of **38**, ***o*-38** and ***o*-38** after 15 minutes of irradiation with UV-C rays

Changes occurred on the UV-visible spectrum after only 15 minutes of irradiation. Unfortunately, the resulting spectrum did not correspond to that of the closed form of the rectangle (**38**), as can be seen in the figure. Instead, the resulting spectrum presents a disappearance of the visible bands and a further raise of the intensity of the UV band located at around 280 nm. No further changes were observed when irradiated with UV-C light for a longer time, and the same results were obtained when the solution of ***o*-38** was submitted to irradiation with UV-A light or heating. This information, in addition to previous reports on **L38**,[72] tend to the conclusion that a decomposition of the product occurred. Moreover, changes happened in a very short time compared to what was needed in order to perform the ring-opening reaction, suggesting a drastic transformation different from a slow photochemical process. This hypothesis was further supported by the disappearance of the characteristic peaks of the metalla-assembly when the UV-irradiated solution of ***o*-38** was submitted to mass spectrometry. These results, in correlation with those obtained in the case of anthracene assemblies, also suggest that ruthenium metalla-assemblies could be subject to decomposition when exposed to strong UV irradiations.

3.4.3 Conclusion

In this work, a multi-step organic synthesis was conducted in order to obtain dihydropyrene ligand **L38** which was used to synthesize ruthenium metalla-assembly **38**. While the reversible DHP ↔ CPD photochemical transformation could not be fully achieved, ruthenium-dihydropyrene rectangle **38** proved to be a semi-functional photoswitchable assembly. The opening of the dihydropyrene moiety was indeed possible within the assembly, even if only at low concentrations. This feature, along with an optimization of the structure of ruthenium-dihydropyrene species, could potentially be used in order to release a guest molecule from inside the cavity of the assembly. Such compounds could also be used for the transport of singlet oxygen, as dihydropyrene shares this property with anthracene.[73]

Chapter 4: General Conclusion and Perspectives

The work presented in this thesis involved the design and synthesis of novel arene ruthenium species, and was divided in two sections. In the first one (Chapter 2), the synthesis of hydrazinyl-thiazole ruthenium complexes was conducted in order to test their biological properties against human cancerous cell lines. The strategy of this project was to combine the activity of the hydrazinyl-thiazole moiety – along with other organic pharmacophore groups – and that of the arene ruthenium unit. This project spawned three series of complexes, as shown in Figure 30.

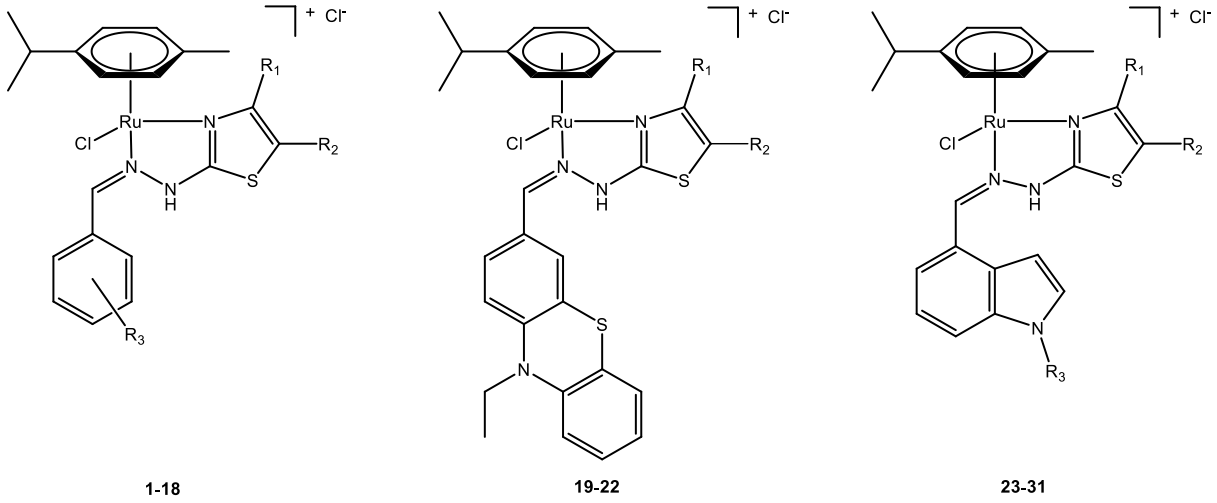

Figure 30: General structures of the three series of hydrazinyl-thiazole ruthenium complexes synthesized

The first series of complexes, composed of phenyl derivatives, was tested on cancerous and healthy cell lines and gave very satisfying results. These initial results led to an optimization of the structure of the complexes, as well as the synthesis of compounds bearing different aromatic moieties, namely phenothiazine (2nd series) and indole (3rd series). All complexes presented many interesting features, such as unique spectroscopic signatures and a good solubility in water, ideal for biological applications.

These hydrazinyl-thiazole ruthenium complexes are the first of their kind, and represent the birth of a new family of promising anticancer compounds. The strategy of combining biologically active organic and organometallic groups proved to be efficient, and many more derivatives could be explored in order to further deepen this project. Indeed, the number of

organic anticancer compounds is quite large, and functionalization of hydrazinyl-thiazole molecules was found to be relatively easy. Following these examples, other pharmacophore moieties could be included as part of the ligands in order to make the corresponding complexes. Phenyl derivatives containing alkylating groups could for instance be synthesized, in order to obtain structures resembling that of aromatic mustards. Other heterocyclic compounds such as benzofuran compounds are also known to exhibit anticancer properties[74] and could therefore be included in the structure of hydrazinyl-thiazole ligands, as pictured in Figure 31.

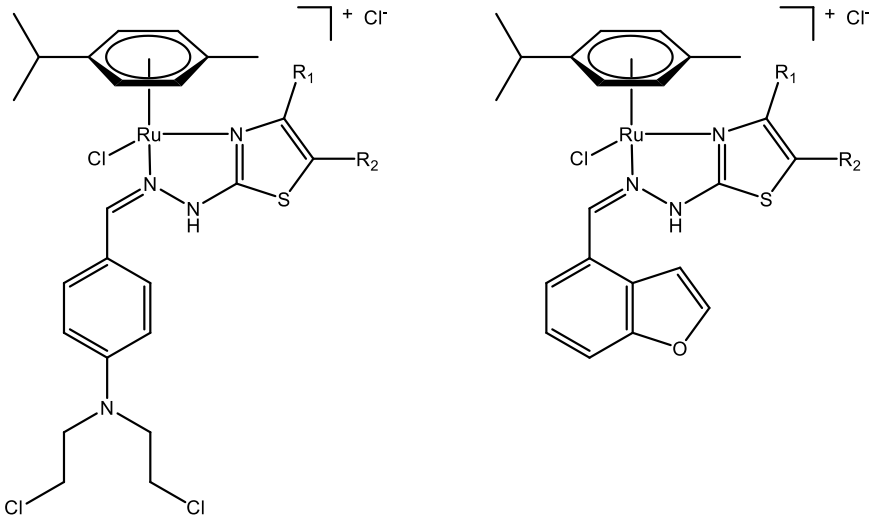

Figure 31: General structures of potential future hydrazinyl-thiazole arene ruthenium complexes, based on aromatic mustards (left) and benzofuran (right)

A large number of compounds could be synthesized this way, and optimization of the structures could be achieved thanks to the results obtained with the first three series. This would help to further expand this family of complexes, and provide advances in the search of highly active organometallic anticancer compounds.

In the second part of this work (Chapter 3), organic molecules containing a photoswitchable moiety were used in the synthesis of ruthenium metalla-assemblies. The aim of this project was to obtain structures that could be light-triggered in order to switch between two different states, thus potentially providing a novel means to control the encapsulation and release of guest molecules. Three classes of molecules were used, namely azobenzene, anthracene, and dihydropyrene derivatives (Figure 32).

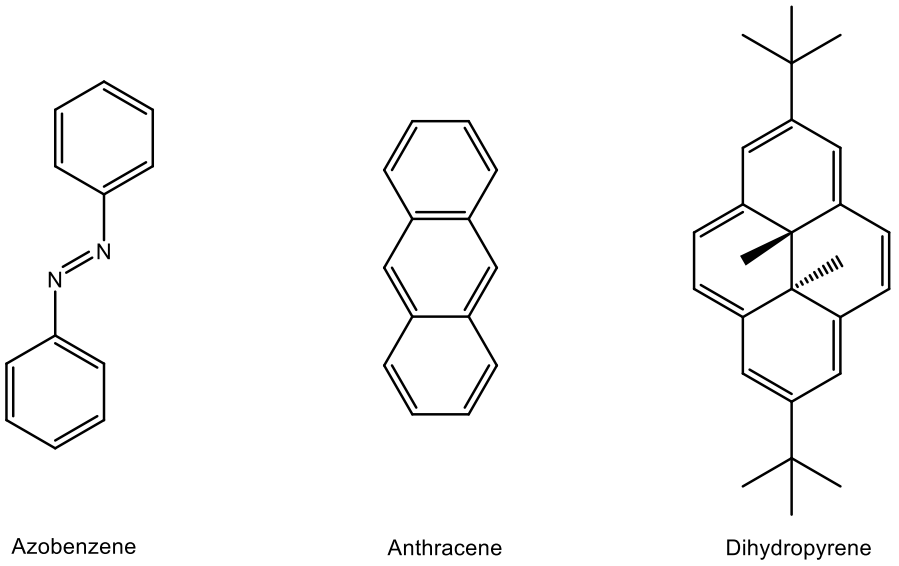

Figure 32: General structures of the three classes of photoswitchable molecules presented in Chapter 3

Each of those molecules was functionalized in order to become suitable ligands and used in the synthesis of metalla-rectangles, using various dinuclear ruthenium spacers. In the case of azobenzene derivatives, the *trans-cis* isomerization of the azo moiety could not occur in the assembly, its rigidity making the rotation around the N=N bond impossible. While the synthesized assemblies were not photoswitchable, the results gave insight on the isomerization mechanism of such compounds. In the case of both anthracene and dihydropyrene ruthenium assemblies, semi-functional photoswitchable rectangles were obtained. Indeed, the light-triggered reactions (dimerization of anthracene, ring-opening reaction of dihydropyrene) could be performed at low concentrations but unfortunately could not be reverted. Nevertheless, these assemblies hold a particular interest thanks to many relevant properties, such as their potential ability to transport singlet oxygen in aqueous media.

The synthesis and study of these compounds hopefully represents the beginning of a new field of ruthenium organometallic chemistry. Indeed, many strategies are yet to be explored in order to achieve the goal of obtaining fully functional ruthenium photoswitchable assemblies. In this project, the photoactive molecules have been included as the panels of the assemblies. An alternative to this strategy would be to include them as part of the ruthenium-ruthenium spacers. Indeed, 2,5-dihydroxy-1,4-benzoquinone, which has been used as a ruthenium-ruthenium spacer in our group for many years, can be functionalized *via* a series of

reactions.[75] This feature could be exploited in order to include a photoswitchable moiety such as anthracene on the ruthenium clip (Scheme 22).

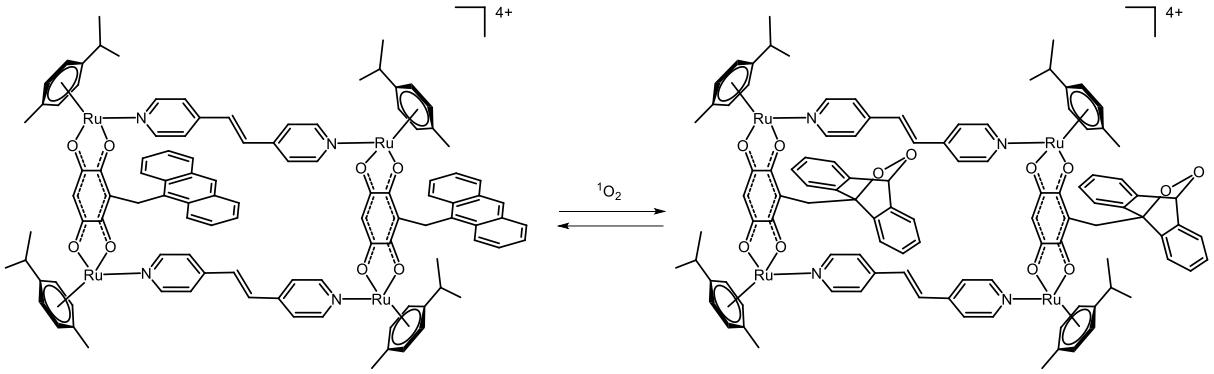

Scheme 22: Potential structure of a ruthenium assembly bearing a benzoquinone spacer functionalized with anthracene, and formation of the corresponding endo-peroxide

In this example, the size and shape of the assembly could be tuned either by changing the panel or by changing the way anthracene is connected to the benzoquinone group. This would allow to determine the optimal structure for the photodimeriazion of anthracene to block the cavity of the assembly, thus leading to an open-closed photoswitchable system. This kind of assembly could also be used for the transport of singlet oxygen, the flexibility around the anthracene moiety potentially facilitating the formation of the endo-peroxides.

Other classes of photoswitchable molecules could also be used as part of ruthenium metalla-assemblies. Among them, hemithioindigos (Scheme 23) could be promising candidates for this prospect. These molecules have indeed proven to be efficient bistable photoswitches; moreover, their asymmetrical nature makes them easy to functionalize, leading to a convenient tunability of their structure.[76] This would allow the creation of a whole new family of compounds, with potentially interesting photochemical properties.

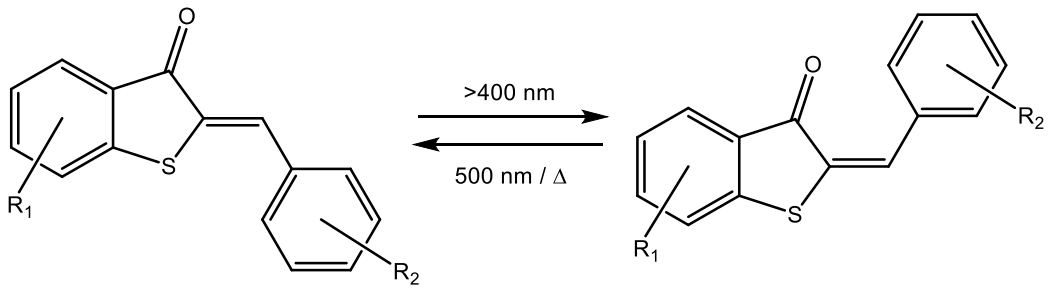

Scheme 22: Photochemical isomerization of hemithioindigos

In conclusion, this thesis represents advances in the design and synthesis of new arene ruthenium species. It confirmed the benefit of combining a ruthenium core with organic pharmacophores in order to create a family of highly cytotoxic compounds. This class of molecules could in the future be further improved and diversified, with the goal of achieving better activity and selectivity. This thesis also explored a new field of ruthenium supramolecular chemistry, with the synthesis of several assemblies bearing photoswitchable moieties. Even though the primary goal of this project – the synthesis of fully functional photoswitchable ruthenium assemblies – was not completely attained, the results provided very useful information on the photochemistry of ruthenium metalla-assemblies. This represents the ground work of a project that could hopefully be deepened by the optimization of the designed structures, in order to achieve the synthesis of light-triggered ruthenium assemblies.

Chapter 5: Experimental Section

5.1 General

Solvents of analytical grade purchased from Acros Organics, Honeywell or VWR International S.A.S were used for syntheses and not degassed or distilled prior to use, unless stated otherwise. All organic starting materials were purchased from Acros Organics, Sigma-Aldrich, Fluka, Alfa Aesar or TCI Europe and used as received. The silica gel used for column chromatography (32-64, 60 Å) was purchased from Brunschwig. The starting material $[(\eta^6\text{-}p\text{-}MeC_6H_4Pr^i)Ru(\mu^2\text{-}Cl)Cl]_2$ was prepared according to published methods.[16] The ruthenium dinuclear spacers dhbq,[19] dcbq,[18] oxa[77] and dhnq[78] used in this work were synthesized according to published methods. The hydrazinyl-thiazole derivatives (**L1-L31**) were also prepared according to the literature.[31] All other reagents were bought from commercial sources and were used without further purification.

The ^1H and ^{13}C NMR spectra were recorded on a Bruker Avance II 400 spectrometer, using the residual protonated solvent as an internal standard. Infrared spectra were recorded as KBr pellets on a PerkinElmer FTIR Spectrum One spectrometer. Elemental analyses were performed by the Mikroelementarisches Laboratorium, ETH Zürich (Zürich, Switzerland). Electrospray ionization mass spectra were recorded in positive-ion mode with a Bruker FTMS 4.7T BioAPEX II mass spectrometer (University of Fribourg, Switzerland). Microwave assisted syntheses were performed in sealed vessels using a CEM Discover LabMate instrument, ensured with online inside temperature and pressure controls. UV-visible spectra were recorded on a PerkinElmer Lambda 25 spectrophotometer. Fluorescence spectra were recorded on a PerkinElmer LS 50 B luminescence spectrophotometer. Irradiation studies were performed using a Luzchem LZC-ORG photoreactor equipped with corresponding lamps.

A crystal of complex 12 was mountd on a Stoe Image Plate Diffraction system equipped with a Φ circle goniometer, using Mo Kα graphite monochromated radiation (λ = 0.71073 Å) with Φ range 0-200°. The structure was solved by direct methods using the program SHELXS-97, while the refinement and all further calculations were carried out using SHELXL-97.[79] Figure 14 was drawn with ORTEP [80] and the structural data deposited at The Cambridge Crystallographic Data Centre: CCDC 1063589. These data can be obtained free of charge from The Cambridge Crystallographic Data Centre.

The human cervical cancer cells (HeLa), the human ovarian cancer cells (A2780), the cisplatin-resistant human ovarian cancer cells (A2780cisR) and the noncancerous cells (HFL-1) were obtained from the European Center of Cell Cultures (ECACC). These cell lines were cultivated under sterile conditions by using RPMI 1640 (Sigma-Aldrich) growth media. This medium was supplemented with fetal calf serum (FCS, Sigma-Aldrich, 5%), antibiotics (penicillin-streptomycin, Actavis Sindan Pharma, 0.1%), and glutamine (Sigma-Aldrich, 0.1%) at 37 °C and CO_2 (5%).

The cytotoxicity activity was determined using the MTT assay. The cells were seeded in 96-well plates with 100 μL of cell solution (cca. 10.000 cells/well) and incubated for 24 hours. Compounds **1**-**16** were initially dissolved in DMSO, followed by a series of successive dilutions using RPMI 1640 media, so that the final concentration of DMSO was under 0.1%. The cells were treated with complexes **1**-**16** (concentrations between 0.1 μM and 100 μM) for 24 hours, with a final volume in the well of 200 μL. After the treatment, the culture media were removed, MTT-Hanks media solution was added to each well, and the plates were incubated for a further two hours. The formazan crystals formed by the mitochondrial dehydrogenase activity of vital cells were dissolved in DMSO. The optical density, quantified by colorimetric measurements, is directly proportional to the amount of formazan crystals formed in the cells, and is an indicator of the cellular viability. The plates were measured with a multimode microplate reader (Biotek Synergy 2 Multi-Mode Microplate Reader with SQ Xenon Flash light source), and absorbance was detected at 570 nm. Cisplatin and oxaliplatin drugs were used as a positive control in the experiments, in the same concentrations as the studied compounds. All of the experiments were performed in triplicate. Values are given as the mean ± SEM. Data are represented as averages of independent experiments, performed in triplicate. The experimental data were processed with Graph Pad Prism 5 biostatistics software.

5.2 Syntheses and Characterizations

5.2.1 Hydrazinyl-Thiazole Ruthenium Complexes

General procedures for the synthesis of complexes **1**-**31**:

General procedure A: A mixture of $[(\eta^6\text{-}p\text{-}MeC_6H_4Pr^i)Ru(\mu^2\text{-}Cl)Cl]_2$ (1 equivalent) and hydrazinyl-thiazole (2 equivalents) in methanol was stirred at room temperature for 10 hours. The solvent was then completely removed under vacuum, and the residue was dissolved in dichloromethane. The product was precipitated by pouring this solution into *n*-pentane, filtering, washing multiple times with *n*-pentane, and finally drying under vacuum to afford the corresponding salts in good yields.

General procedure B: A reaction mixture containing $[(\eta^6\text{-}p\text{-}MeC_6H_4Pr^i)Ru(\mu^2\text{-}Cl)Cl]_2$ (1 equivalent) and the hydrazinyl-thiazole (2 equivalents) in dichloromethane was introduced into a quartz reaction vessel, which was sealed and then subjected to microwave irradiation for 30 minutes at an internal temperature of 60°C. The mixture was then concentrated under vacuum, and the residue was precipitated with *n*-pentane, filtered, and washed multiple times with *n*-pentane, and the solid was dried under vacuum.

1: $[(\eta^6\text{-}p\text{-}MeC_6H_4Pr^i)Ru(\mathbf{L1})Cl]Cl$. Yield: 67%. ^{1}H NMR ($CDCl_3$, 400 MHz): δ = 1.07 (d, $^3J_{H–H}$ = 7.1 Hz, 3H), 1.15 (d, $^3J_{H–H}$ = 7.1 Hz, 3H), 2.26 (s, 3H), 2.46 (s, 3H), 2.57 (sept, $^3J_{H–H}$ = 7.1 Hz, 1H), 4.52 (d, $^3J_{H–H}$ = 6.0 Hz, 1H), 5.06 (d, $^3J_{H–H}$ = 6.0 Hz, 1H), 5.18 (d, $^3J_{H–H}$ = 6.0 Hz, 1H), 5.44 (d, $^3J_{H–H}$ = 6.0 Hz, 1H), 6.49 (s, 1H), 7,55−7.57 (m, 3H), 8.12 (m, 2H), 9.32 (s, 1H), 15.63 (s, 1H) ppm. ESI-MS m/z (+): 488.1 $[M\text{-}Cl]^+$. Anal. Calcd for $C_{21}H_{25}N_3SCl_2Ru$: C, 48.18; H, 4.81; N, 8.03. Found: C, 48.18; H, 4.83; N, 7.96. IR (KBr): 2958 (m), 2919 (m), 2525 (s), 1557 (s), 1505 (s), 1387 (m), 1306 (s), 1257 (m), 1093 (m) cm^{-1}.

2: $[(\eta^6\text{-}p\text{-}MeC_6H_4Pr^i)Ru(\mathbf{L2})Cl]Cl$. Yield: 62%. ^{1}H NMR ($CDCl_3$, 400 MHz): δ = 0.96 (d, $^3J_{H–H}$ = 6.8 Hz, 3H), 1.01 (d, $^3J_{H–H}$ = 6.8 Hz, 3H), 2.14 (s, 3H), 2.36 (sept, $^3J_{H–H}$ = 6.8 Hz, 1H), 4.03 (d, $^3J_{H–H}$ = 5.4 Hz, 1H), 4.25 (d, $^3J_{H–H}$ = 5.4 Hz, 1H), 4.65−4.66 (m, 2H), 6.74 (s, 1H), 7.54− 7.56 (m, 6H), 7.90−7.91 (m, 2H), 8.12−8.13 (m, 2H), 9.30 (s, 1H), 15.88 (s, 1H) ppm. ESI-MS m/z (+): 550.1 $[M\text{-}Cl]^+$. Anal. Calcd for $C_{26}H_{27}N_3SCl_2Ru\cdot 0.5\ H_2O$: C, 52.52; H, 4.75; N, 7.07. Found: C, 52.63; H, 4.55; N, 6.90. IR (KBr): 2916 (m), 2501 (m), 1575 (s), 1500 (s), 1384 (m), 1313 (m), 1090 (s) cm^{-1}.

3: $[(\eta^6\text{-}p\text{-}MeC_6H_4Pr^i)Ru(\mathbf{L3})Cl]Cl$. Yield: 61%. ^{1}H NMR ($CDCl_3$, 400 MHz): δ = 1.08 (d, $^3J_{H–H}$ = 6.9 Hz, 3H), 1.16 (d, $^3J_{H–H}$ = 6.9 Hz, 3H), 2.28 (s, 3H), 2.45 (s, 3H), 2.56 (sept, $^3J_{H–H}$

= 6.9 Hz, 1H), 2.82 (s, 3H), 4.51 (d, $^3J_{H–H}$ = 5.8 Hz, 1H), 5.09 (d, $^3J_{H–H}$ = 5.8 Hz, 1H), 5.22 (d, $^3J_{H–H}$ = 5.8 Hz, 1H), 5.41 (d, $^3J_{H–H}$ = 5.8 Hz, 1H), 7.58−7.60 (m, 3H), 8.14 (d, $^3J_{H–H}$ = 7.1 Hz, 2H), 9.34 (s, 1H), 12.95 (s, 1H) ppm. ESI-MS m/z (+): 529.9 $[M\text{-}Cl]^+$. Anal. Calcd for $C_{23}H_{27}N_3OSCl_2Ru$: C, 48.85; H, 4.81; N, 7.43. Found: C, 48.96; H, 5.34; N, 6.87. IR (KBr): 2965 (w), 1637 (m), 1568 (s), 1475 (s), 1374 (m), 1309 (s) cm^{-1}.

4: [(η^6-*p*-$MeC_6H_4Pr^i$)Ru(**L4**)Cl]Cl. Yield: 71%. ^{1}H NMR ($CDCl_3$, 400 MHz): δ = 1.08 (d, $^3J_{H–H}$ = 6.8 Hz, 3H), 1.16 (d, $^3J_{H–H}$ = 6.8 Hz, 3H), 1.35 (t, $^3J_{H–H}$ = 7.2 Hz, 3H), 2.20 (s, 3H), 2.60 (sept, $^3J_{H–H}$ = 6.8 Hz, 1H), 3.80 (s, 2H), 4.29 (q, $^3J_{H–H}$ = 7.2 Hz, 2H), 4.37 (d, $^3J_{H–H}$ = 5.9 Hz, 1H), 5.19 (d, $^3J_{H–H}$ = 5.9 Hz, 1H), 5.24 (d, $^3J_{H–H}$ = 5.9 Hz, 1H), 5.62 (d, $^3J_{H–H}$ = 5.9 Hz, 1H), 6.83 (s, 1H), 7.47 (dd, $^3J_{H–H}$ = 8.4 Hz, $^4J_{H–H}$ = 1.9 Hz, 1H), 7.58 (d, $^4J_{H–H}$ = 1.9 Hz, 1H), 8.42 (d, $^3J_{H–H}$ = 8.4 Hz, 1H), 9.24 (s, 1H), 16.08 (s, 1H) ppm. ESI-MS m/z (+): 630.0 $[M\text{-}Cl]^+$. Anal. Calcd for $C_{24}H_{27}N_3O_2SCl_4Ru\cdot H_2O$: C, 42.24; H, 4.28; N, 6.16. Found: C, 42.43; H, 4.08; N, 6.31. IR (KBr): 2918 (m), 1732 (m), 1589 (s), 1551 (s), 1470 (s), 1384 (s), 1259 (m), 1146 (m), 1083 (m), 1056 (m) cm^{-1}.

5: [(η^6-*p*-$MeC_6H_4Pr^i$)Ru(**L5**)Cl]Cl. Yield: 51%. ^{1}H NMR ($CDCl_3$, 400 MHz): δ = 1.07 (d, $^3J_{H–H}$ = 7.1 Hz, 3H), 1.13 (d, $^3J_{H–H}$ = 7.1 Hz, 3H), 2.49 (s, 3H), 2.54 (sept, $^3J_{H–H}$ = 7.1 Hz, 1H), 2.63 (s, 3H), 2.79 (s, 3H), 5.08 (d, $^3J_{H–H}$ = 5.4 Hz, 1H), 5.35 (d, $^3J_{H–H}$ = 5.4 Hz, 1H), 5.57 (d, $^3J_{H–H}$ = 5.4 Hz, 1H), 5.65 (d, $^3J_{H–H}$ = 5.4 Hz, 1H), 7.31 (d, $^3J_{H–H}$ = 8.6 Hz, 1H), 7.42 (s, 1H), 7.98 (d, $^3J_{H–H}$ = 8.6 Hz, 1H), 8.29 (s, 1H), 12.83 (s, 1H) ppm. ESI-MS m/z (+): 599.8 $[M\text{-}Cl]^+$. Anal. Calcd for $C_{23}H_{25}N_3OSCl_4Ru\cdot H_2O$: C, 42.34; H, 4.17; N, 6.44. Found: C, 42.66; H, 3.96; N, 6.30. IR (KBr): 2975 (m), 1604 (m), 1564 (m), 1384 (s), 1328 (s), 1055 (s) cm^{-1}.

6: [(η^6-*p*-$MeC_6H_4Pr^i$)Ru(**L6**)Cl]Cl. Yield: 68%. ^{1}H NMR ($CDCl_3$, 400 MHz): δ = 1.07 (d, $^3J_{H–H}$ = 6.2 Hz, 3H), 1.15 (d, $^3J_{H–H}$ = 6.2 Hz, 3H), 1.33 (t, $^3J_{H–H}$ = 6.6 Hz, 3H), 2.21 (s, 3H), 2.62 (sept, $^3J_{H–H}$ = 6.2 Hz, 1H), 2.78 (s, 3H), 4.27 (q, $^3J_{H–H}$ = 6.6 Hz, 2H), 5.12 (d, $^3J_{H–H}$ = 5.5 Hz, 1H), 5.18 (d, $^3J_{H–H}$ = 5.5 Hz, 1H), 5.41 (d, $^3J_{H–H}$ = 5.5 Hz, 1H), 5.59 (d, $^3J_{H–H}$ = 5.5 Hz, 1H), 7.44 (d, $^3J_{H–H}$ = 8.2 Hz, 1H), 7.56 (s, 1H), 8.55 (d, $^3J_{H–H}$ = 8.2 Hz, 1H), 8.78 (s, 1H), 13.43 (s, 1H) ppm. ESIMS m/z (+): 630.0 $[M\text{-}Cl]^+$. Anal. Calcd for $C_{24}H_{27}N_3O_2SCl_4Ru$: C, 43.39; H, 4.10; N, 6.32. Found: C, 43.47; H, 4.24; N, 6.26. IR (KBr): 2965 (w), 1709 (m), 1585 (s), 1474 (s), 1373 (s), 1317 (s), 1276 (s), 1099 (s) cm^{-1}.

7: [(η^6-*p*-$MeC_6H_4Pr^i$)Ru(**L7**)Cl]Cl. Yield: 78%. ^{1}H NMR ($CDCl_3$, 400 MHz): δ = 1.07 (d, $^3J_{H–H}$ = 6.9 Hz, 3H), 1.14 (d, $^3J_{H–H}$ = 6.9 Hz, 3H), 2.27 (s, 3H), 2.46 (s, 3H), 2.54 (sept, $^3J_{H–H}$ = 6.9 Hz, 1H), 4.81 (d, $^3J_{H–H}$ = 5.7 Hz, 1H), 5.09 (d, $^3J_{H–H}$ = 5.7 Hz, 1H), 5.18 (d, $^3J_{H–H}$ = 5.7

Hz, 1H), 5.44 (d, $^3J_{H–H}$ = 5.7 Hz, 1H), 6.48 (s, 1H), 7.12 (d, $^3J_{H–H}$ = 8.4 Hz, 2H), 7.70 (d, $^3J_{H–H}$ = 8.4 Hz, 2H), 8.76 (s, 1H), 14.23 (s, 1H) ppm. ESI-MS m/z (+): 504.1 $[M\text{-}Cl]^+$. Anal. Calcd for $C_{21}H_{25}N_3OSCl_2Ru \cdot 0.5\ H_2O$: C, 45.99; H, 4.78; N, 7.66. Found: C, 45.90; H, 4.98; N, 7.12. IR (KBr): 2965 (m), 1607 (s), 1552 (m), 1509 (s), 1383 (m), 1284 (m), 1254 (m), 1174 (m) cm^{-1}.

8: [(η^6-*p*-$MeC_6H_4Pr^i$)Ru(**L8**)Cl]Cl. Yield: 69%. ^{1}H NMR ($CDCl_3$, 400 MHz): δ = 0.96 (d, $^3J_{H–H}$ = 6.3 Hz, 3H), 1.01 (d, $^3J_{H–H}$ = 6.3 Hz, 3H), 2.16 (s, 3H), 2.32 (sept, $^3J_{H–H}$ = 6.3 Hz, 1H), 3.95 (d, $^3J_{H–H}$ = 5.7 Hz, 1H), 4.60 (d, $^3J_{H–H}$ = 5.7 Hz, 1H), 4.71−4.73 (m, 2H), 6.73 (s, 1H), 7.15− 7.18 (m, 2H), 7.54−7.55 (m, 3H), 7.75−7.77 (m, 2H), 7.90−7.92 (m, 2H), 8.77 (s, 1H), 14.25 (s, 1H) ppm. ESI-MS m/z (+): 565.9 $[M\text{-}Cl]^+$. Anal. Calcd for $C_{26}H_{27}N_3OSCl_2Ru \cdot H_2O$: C, 50.40; H, 4.72; N, 6.78. Found: C, 50.17; H, 4.61; N, 6.32. IR (KBr): 2969 (s), 1605 (s), 1572 (s), 1508 (s), 1278 (m), 1174 (m) cm^{-1}.

9: [(η^6-*p*-$MeC_6H_4Pr^i$)Ru(**L9**)Cl]Cl. Yield: 73%. ^{1}H NMR ($CDCl_3$, 400 MHz): δ = 1.13 (d, $^3J_{H–H}$ = 6.8 Hz, 3H), 1.20 (d, $^3J_{H–H}$ = 6.8 Hz, 3H), 2.33 (s, 3H), 2.50 (s, 3H), 2.63 (sept, $^3J_{H–H}$ = 6.8 Hz, 1H), 3.96 (s, 3H), 4.83 (d, $^3J_{H–H}$ = 5.8 Hz, 1H), 5.15 (d, $^3J_{H–H}$ = 5.8 Hz, 1H), 5.26 (d, $^3J_{H–H}$ = 5.8 Hz, 1H), 5.50 (d, $^3J_{H–H}$ = 5.8 Hz, 1H), 6.51 (s, 1H), 7.10 (d, $^3J_{H–H}$ = 8.8 Hz, 2H), 8.18 (d, $^3J_{H–H}$ = 8.8 Hz, 2H), 9.25 (s, 1H), 15.36 (s, 1H) ppm. ESI-MS m/z (+): 517.9 $[M\text{-}Cl]^+$. Anal. Calcd for $C_{22}H_{27}N_3OSCl_2Ru$: C, 47.74; H, 4.92; N, 7.59. Found: C, 47.52; H, 4.94; N, 7.40. IR (KBr): 2966 (w), 2481 (w), 1604 (s), 1554 (m), 1509 (s), 1378 (w), 1306 (m), 1266 (s), 1180 (m), 1087 (w) cm^{-1}.

10: [(η^6-*p*-$MeC_6H_4Pr^i$)Ru(**L10**)Cl]Cl. Yield: 75%. ^{1}H NMR ($CDCl_3$, 400 MHz): δ = 0.98 (d, $^3J_{H–H}$ = 6.8 Hz, 3H), 1.02 (d, $^3J_{H–H}$ = 6.8 Hz, 3H), 2.17 (s, 3H), 2.38 (sept, $^3J_{H–H}$ = 6.8 Hz, 1H), 4.00 (d, $^3J_{H–H}$ = 6.1 Hz, 1H), 4.53 (d, $^3J_{H–H}$ = 6.1 Hz, 1H), 4.70 (d, $^3J_{H–H}$ = 6.1 Hz, 1H), 4.74 (d, $^3J_{H–H}$ = 6.1 Hz, 1H), 6.72 (s, 1H), 7.06 (d, $^3J_{H–H}$ = 8.7 Hz, 2H), 7.55 (m, 3H), 7.91 (m, 2H), 8.15 (d, $^3J_{H–H}$ = 8.7 Hz, 2H), 9.20 (s, 1H), 15.67 (s, 1H) ppm. ESI-MS m/z (+): 580.1 $[M\text{-}Cl]^+$. Anal. Calcd for $C_{27}H_{29}N_3OSCl_2Ru \cdot H_2O$: C, 51.18; H, 4.93; N, 6.63. Found: C, 51.36; H, 4.78; N, 6.49. IR (KBr): 2966 (w), 1604 (s), 1574 (m), 1509 (s), 1309 (m), 1271 (s), 1178 (m), 1085 (m) cm^{-1}.

11: [(η^6-*p*-$MeC_6H_4Pr^i$)Ru(**L11**)Cl]Cl. Yield: 72%. ^{1}H NMR ($CDCl_3$, 400 MHz): δ = 1.10 (d, $^3J_{H–H}$ = 6.9 Hz, 3H), 1.16 (d, $^3J_{H–H}$ = 6.9 Hz, 3H), 1.33 (t, $^3J_{H–H}$ = 7.1 Hz, 3H), 2.32 (s, 3H), 2.57 (sept, $^3J_{H–H}$ = 6.9 Hz, 1H), 2.82 (s, 3H), 3.93 (s, 3H), 4.30 (q, $^3J_{H–H}$ = 7.1 Hz, 2H), 4.78 (d, $^3J_{H–H}$ = 5.9 Hz, 1H), 5.13 (d, $^3J_{H–H}$ = 5.9 Hz, 1H), 5.26 (d, $^3J_{H–H}$ = 5.9 Hz, 1H), 5.45 (d,

$^{3}J_{H–H}$ = 5.9 Hz, 1H), 7.07 (d, $^{3}J_{H–H}$ = 8.7 Hz, 2H), 8.15 (d, $^{3}J_{H–H}$ = 8.7 Hz, 2H), 9.20 (s, 1H), 16.01 (s, 1H) ppm. ESI-MS m/z (+): 589.9 $[M\text{-}Cl]^{+}$. Anal. Calcd for $C_{25}H_{31}N_3O_3SCl_2Ru\cdot CH_2Cl_2$: C, 43.95; H, 4.68; Found: C, 43.67; H, 4.75. IR (KBr): 2966 (w), 1710 (m), 1604 (s), 1575 (s), 1509 (s), 1477 (m), 1372 (m), 1314 (s), 1268 (s), 1178 (m), 1099 (s) cm^{-1}.

12: [(η^6-*p*-$MeC_6H_4Pr^i$)Ru(**L12**)Cl]Cl. Yield: 70%. ^{1}H NMR ($CDCl_3$, 400 MHz): δ = 1.13 (d, $^{3}J_{H–H}$ = 6.4 Hz, 3H), 1.20 (d, $^{3}J_{H–H}$ = 6.4 Hz, 3H), 2.35 (s, 3H), 2.47 (s, 3H), 2.62 (sept, $^{3}J_{H–H}$ = 6.4 Hz, 1H), 2.86 (s, 3H), 3.96 (s, 3H), 4.81 (d, $^{3}J_{H–H}$ = 4.8 Hz, 1H), 5.16 (d, $^{3}J_{H–H}$ = 4.8 Hz, 1H), 5.29 (d, $^{3}J_{H–H}$ = 4.8 Hz, 1H), 5.46 (d, $^{3}J_{H–H}$ = 4.8 Hz, 1H), 7.10 (d, $^{3}J_{H–H}$ = 8.0 Hz, 2H), 8.20 (d, $^{3}J_{H–H}$ = 8.0 Hz, 2H), 9.18 (s, 1H), 12.46 (s, 1H) ppm. ESI-MS m/z (+): 560.1 $[M\text{-}Cl]^{+}$. Anal. Calcd for $C_{24}H_{29}N_3O_2SCl_2Ru\cdot H_2O$: C, 46.98; H, 5.09; N, 6.85. Found: C, 46.94; H, 4.91; N, 6.77. IR (KBr): 2963 (w), 1638 (m), 1604 (s), 1574 (m), 1510 (s), 1475 (m), 1374 (m), 1307 (s), 1262 (s), 1179 (m) cm^{-1}. Crystal data: Monoclinic space group $P2_1/c$ (No. 14), cell parameters a = 16.2513(19), b = 15.1904(12), and c = 13.3986(13) Å, β = 107.817(8), V = 3149.0(5) $Å^3$, T = 173(2) K, Z = 4, D_c = 1.256 g cm^{-3}, F(000) 1216, λ (Mo Kα) = 0.71073 Å, 8557 reflections measured, and 2494 unique (R_{int} = 0.2499), which were used in all calculations. The non-hydrogen atoms were refined anisotropically, using weighted full-matrix least-squares on F^2 with 304 parameters. R_1 = 0.0515 (I > 2σ(I)) and wR_2 = 0.0975, GOF = 0.629; max/min residual density 0.447/−0.729 e$Å^{-3}$.

13: [(η^6-*p*-$MeC_6H_4Pr^i$)Ru(**L13**)Cl]Cl. Yield: 70%. ^{1}H NMR ($CDCl_3$, 400 MHz): δ = 1.06 (d, $^{3}J_{H–H}$ = 6.8 Hz, 3H), 1.15 (d, $^{3}J_{H–H}$ = 6.8 Hz, 3H), 2.30 (s, 3H), 2.45 (s, 3H), 2.59 (sept, $^{3}J_{H–H}$ = 6.8 Hz, 1H), 4.63 (d, $^{3}J_{H–H}$ = 5.6 Hz, 1H), 5.11 (d, $^{3}J_{H–H}$ = 5.6 Hz, 1H), 5.17 (d, $^{3}J_{H–H}$ = 5.6 Hz, 1H), 5.46 (d, $^{3}J_{H–H}$ = 5.6 Hz, 1H), 6.44 (s, 1H), 7.51 (m, 2H), 7.91 (d, $^{3}J_{H–H}$ = 7.1 Hz, 1H), 9.24 (s, 1H), 13.95 (s, 1H) ppm. ESI-MS m/z (+): 524.1 $[M\text{-}Cl]^{+}$. Anal. Calcd for $C_{21}H_{24}N_3SCl_3Ru\cdot CH_2Cl_2$: C, 41.10; H, 4.08; N, 6.54; Found: C, 41.40; H, 4.08; N, 6.33. IR (KBr): 2966 (w), 1604 (s), 1509 (s), 1375 (m), 1309 (s), 1261 (m), 1178 (m) cm^{-1}.

14: [(η^6-*p*-$MeC_6H_4Pr^i$)Ru(**L15**)Cl]Cl. Yield: 61%. ^{1}H NMR ($CDCl_3$, 400 MHz): δ = 1.11 (d, $^{3}J_{H–H}$ = 6.8 Hz, 3H), 1.28 (d, $^{3}J_{H–H}$ = 6.8 Hz, 3H), 2.16 (s, 3H), 2.37 (s, 3H), 2.80 (s, 3H), 2.92 (sept, $^{3}J_{H–H}$ = 6.8 Hz, 1H), 4.50 (d, $^{3}J_{H–H}$ = 5.9 Hz, 1H), 5.03 (d, $^{3}J_{H–H}$ = 5.9 Hz, 1H), 5.18 (d, $^{3}J_{H–H}$ = 5.9 Hz, 1H), 5.48 (d, $^{3}J_{H–H}$ = 5.9 Hz, 1H), 7.37 (m, 2H), 7.52 (d, $^{3}J_{H–H}$ = 7.4 Hz, 1H), 7.70 (s, 1H), 8.34 (s, 1H), 12.69 (s, 1H) ppm. ESI-MS m/z (+): 564.0 $[M\text{-}Cl]^{+}$. Anal. Calcd for

$C_{23}H_{26}N_3OSCl_3Ru$: C, 46.05; H, 4.37; N, 7.00. Found: C, 45.89; H, 4.32; N, 6.98. IR (KBr): 2963 (w), 1638 (m), 1560 (s), 1475 (m), 1374 (m), 1308 (s), 1079 (w) cm^{-1}.

15: [(η^6-*p*-$MeC_6H_4Pr^i$)Ru(**L14**)Cl]Cl. Yield: 81%. ^{1}H NMR ($CDCl_3$, 400 MHz): δ = 0.98 (d, $^3J_{H–H}$ = 6.8 Hz, 3H), 1.03 (d, $^3J_{H–H}$ = 6.8 Hz, 3H), 2.18 (s, 3H), 2.40 (sept, $^3J_{H–H}$ = 6.8 Hz, 1H), 4.02 (d, $^3J_{H–H}$ = 5.9 Hz, 1H), 4.42 (d, $^3J_{H–H}$ = 5.9 Hz, 1H), 4.69 (d, $^3J_{H–H}$ = 5.9 Hz, 1H), 4.78 (d, $^3J_{H–H}$ = 5.9 Hz, 1H), 6.77 (s, 1H), 7.54 (m, 5H), 7.90 (m, 3H), 8.50 (s, 1H), 9.27 (s, 1H), 16.05 (s, 1H) ppm. ESI-MS m/z (+): 584.0 $[M\text{-}Cl]^+$. Anal. Calcd for $C_{26}H_{26}N_3SCl_3Ru \cdot 1.5\ H_2O$: C, 48.27; H, 4.52; N, 6.49. Found: C, 48.23; H, 4.01; N, 6.32. IR (KBr): 2969 (w), 2478 (m), 1578 (s), 1499 (m), 1379 (w), 1325 (w), 1257 (w), 1088 (m) cm^{-1}.

16: [(η^6-*p*-$MeC_6H_4Pr^i$)Ru(**L16**)Cl]Cl. Yield: 72%. ^{1}H NMR ($CDCl_3$, 400 MHz): δ = 1.08 (d, $^3J_{H–H}$ = 6.2 Hz, 3H), 1.17 (d, $^3J_{H–H}$ = 6.2 Hz, 3H), 1.34 (t, $^3J_{H–H}$ = 7.2 Hz, 3H), 2.32 (s, 3H), 2.60 (sept, $^3J_{H–H}$ = 6.2 Hz, 1H) 2.82 (s, 3H), 4.31 (q, $^3J_{H–H}$ = 7.2 Hz, 2H), 4.61 (d, $^3J_{H–H}$ = 5.3 Hz, 1H), 5.15 (d, $^3J_{H–H}$ = 5.3 Hz, 1H), 5.24 (d, $^3J_{H–H}$ = 5.3 Hz, 1H), 5.47 (d, $^3J_{H–H}$ = 5.3 Hz, 1H), 7.56 (m, 2H), 7.93 (m, 1H), 8.46 (s, 1H), 9.32 (s, 1H), 12.68 (s, 1H) ppm. ESI-MS m/z (+): 593.9 $[M\text{-}Cl]^+$. Anal. Calcd for $C_{24}H_{28}N_3O_2SCl_3Ru \cdot 1.5\ H_2O$: C, 43.88; H, 4.76; N, 6.40. Found: C, 43.76; H, 4.46; N, 5.88. IR (KBr): 2965 (w), 1711 (m), 1574 (s), 1475 (s), 1372 (m), 1316 (s), 1276 (s), 1100 (s) cm^{-1}.

17: [(η^6-*p*-$MeC_6H_4Pr^i$)Ru(**L17**)Cl]Cl. Yield: 63%. ^{1}H NMR ($CDCl_3$, 400 MHz): δ = 1.31 (d, $^3J_{H–H}$ = 6.8 Hz, 6H), 1.33 (t, $^3J_{H–H}$ = 7.0 Hz, 3H), 2.19 (s, 3H), 2.96 (sept, $^3J_{H–H}$ = 6.8 Hz, 1H), 4.30 (q, $^3J_{H–H}$ = 7.0 Hz, 2H), 5.38 (d, $^3J_{H–H}$ = 5.8 Hz, 2H), 5.52 (d, $^3J_{H–H}$ = 5.8 Hz, 2H), 7.43 (m, 4H), 7.55 (s, 1H), 7.80 (d, $^3J_{H–H}$ = 7.2 Hz, 2H), 7.92 (d, $^3J_{H–H}$ = 8.4 Hz, 1H), 8.22 (s, 1H), 11.28 (s, 1H) ppm. ESI-MS m/z (+): 690.0 $[M\text{-}Cl]^+$. Anal. Calcd for $C_{29}H_{29}N_3O_2SCl_4Ru \cdot 0.5CH_2Cl_2$: C, 46.08; H, 3.93; N, 5.46. Found: C, 45.67; H, 3.75; N, 5.59. IR (KBr): 2969 (m), 1703 (m), 1675 (m), 1538 (m), 1488 (s), 1336 (s), 1300 (m), 1145 (s), 1078 (m), 1014 (m), 754 (w) cm^{-1}.

18: [(η^6-*p*-$MeC_6H_4Pr^i$)Ru(**L18**)Cl]Cl. Yield: 54%. ^{1}H NMR ($CDCl_3$, 400 MHz): δ = 1.30 (t, $^3J_{H–H}$ = 7.2 Hz, 3H), 1.35 (d, $^3J_{H–H}$ = 6.9 Hz, 6H), 2.32 (s, 3H), 3.11 (sept, $^3J_{H–H}$ = 6.9 Hz, 1H), 4.29 (q, $^3J_{H–H}$ = 7.2 Hz, 2H), 5.32 (d, $^3J_{H–H}$ = 5.8 Hz, 2H), 5.52 (d, $^3J_{H–H}$ = 5.8 Hz, 2H), 7.36 (t, $^3J_{H–H}$ = 7.6 Hz, 1H), 7.47 (m, 5H), 7.73 (s, 1H), 7.79 (d, $^3J_{H–H}$ = 7.6 Hz, 2H), 8.74 (s, 1H), 12.58 (s, 1H) ppm. ESI-MS m/z (+): 656.1 $[M\text{-}Cl]^+$. Anal. Calcd for $C_{29}H_{30}N_3O_2SCl_3Ru \cdot 0.5CH_2Cl_2$: C, 48.24; H, 4.25; N, 5.72. Found: C, 48.01; H, 4.24; N, 5.34.

IR (KBr): 2968 (m), 1698 (m), 1538 (m), 1486 (s), 1336 (s), 1300 (m), 1147 (m), 1079 (m), 755 (w) cm^{-1}.

19: [(η^6-*p*-$MeC_6H_4Pr^i$)Ru(**L19**)Cl]Cl. Yield: 75%. ^1H NMR ($CDCl_3$, 400 MHz): δ = 1.02 (d, $^3J_{H–H}$ = 6.6 Hz, 3H), 1.07 (d, $^3J_{H–H}$ = 6.6 Hz, 3H), 1.52 (t, $^3J_{H–H}$ = 7.0 Hz, 3H), 2.25 (s, 3H), 2.50 (sept, $^3J_{H–H}$ = 6.6 Hz, 1H), 4.03 (q, $^3J_{H–H}$ = 7.0 Hz, 2H), 4.05 (d, $^3J_{H–H}$ = 5.7 Hz, 1H), 4.75 (d, $^3J_{H–H}$ = 5.7 Hz, 1H), 4.82 (d, $^3J_{H–H}$ = 5.7 Hz, 1H), 4.86 (d, $^3J_{H–H}$ = 5.7 Hz, 1H), 6.76 (s, 1H), 6.98 (m, 3H), 7.20 (m, 2H), 7.58 (m, 3H), 7.83 (m, 1H), 7.97 (m, 2H), 8.32 (s, 1H), 9.14 (s, 1H), 15.35 (s, 1H) ppm. ESI-MS m/z (+): 699.1 $[M\text{-}Cl]^+$. Anal. Calcd for $C_{34}H_{34}N_4S_2Cl_2Ru·0.5CH_2Cl_2$: C, 53.32; H, 4.54; N, 7.21. Found: C, 53.35; H, 4.57; N, 6.54. IR (KBr): 2918 (m), 1575 (m), 1466 (s), 1384 (m), 1243 (m), 1053 (w), 752 (w) cm^{-1}.

20: [(η^6-*p*-$MeC_6H_4Pr^i$)Ru(**L20**)Cl]Cl. Yield: 77%. ^1H NMR ($CDCl_3$, 400 MHz): δ = 1.12 (d, $^3J_{H–H}$ = 6.7 Hz, 3H), 1.21 (d, $^3J_{H–H}$ = 6.7 Hz, 3H), 1.52 (t, $^3J_{H–H}$ = 6.8 Hz, 3H), 2.35 (s, 3H), 2.46 (s, 3H), 2.86 (s, 3H), 3.18 (sept, $^3J_{H–H}$ = 6.7 Hz, 1H), 4.03 (q, $^3J_{H–H}$ = 6.8 Hz, 2H), 4.94 (d, $^3J_{H–H}$ = 5.9 Hz, 1H), 5.27 (d, $^3J_{H–H}$ = 5.9 Hz, 1H), 5.47 (d, $^3J_{H–H}$ = 5.9 Hz, 1H), 5.58 (d, $^3J_{H–H}$ = 5.9 Hz, 1H), 6.97 (m, 4H), 7.18 (m, 3H), 7.86 (s, 1H), 8.25 (s, 1H), 9.06 (s, 1H), 14.69 (s, 1H) ppm. ESI-MS m/z (+): 679.1 $[M\text{-}Cl]^+$. Anal. Calcd for $C_{31}H_{34}N_4OS_2Cl_2Ru·CH_2Cl_2$: C, 48.06; H, 4.54; N, 7.01. Found: C, 47.29; H, 4.56; N, 6.95. IR (KBr): 2921 (m), 1624 (s), 1468 (s), 1245 (m), 1110 (m), 751 (m) cm^{-1}.

21: [(η^6-*p*-$MeC_6H_4Pr^i$)Ru(**L21**)Cl]Cl. Yield: 68%. ^1H NMR ($CDCl_3$, 400 MHz): δ = 1.08 (d, $^3J_{H–H}$ = 6.5 Hz, 3H), 1.18 (d, $^3J_{H–H}$ = 6.5 Hz, 3H), 1.48 (t, $^3J_{H–H}$ = 6.7 Hz, 3H), 2.34 (s, 3H), 2.46 (s, 3H), 2.65 (sept, $^3J_{H–H}$ = 6.5 Hz, 1H), 3.99 (q, $^3J_{H–H}$ = 6.7, 2H), 4.93 (d, $^3J_{H–H}$ = 5.6 Hz, 1H), 5.22 (m, 2H), 5.47 (d, $^3J_{H–H}$ = 5.6 Hz, 1H), 6.46 (s, 1H), 6.95 (m, 3H), 7.16 (m, 2H), 7.78 (m, 1H), 8.25 (s, 1H), 9.11 (s, 1H), 15.02 (s, 1H) ppm. ESI-MS m/z (+): 637.1 $[M\text{-}Cl]^+$. Anal. Calcd for $C_{29}H_{32}N_4S_2Cl_2Ru·0.5CH_2Cl_2$: C, 49.54; H, 4.65; N, 7.83. Found: C, 48.92; H, 4.76; N, 8.17. IR (KBr): 2921 (m), 1623 (s), 1466 (s), 1242 (m), 1136 (m), 753 (m) cm^{-1}.

22: [(η^6-*p*-$MeC_6H_4Pr^i$)Ru(**L22**)Cl]Cl. Yield: 82%. ^1H NMR ($CDCl_3$, 400 MHz): δ = 1.09 (d, $^3J_{H–H}$ = 6.7 Hz, 3H), 1.18 (d, $^3J_{H–H}$ = 6.7 Hz, 3H), 1.33 (t, $^3J_{H–H}$ = 7.1 Hz, 3H), 1.49 (t, $^3J_{H–H}$ = 6.9 Hz, 3H), 2.37 (s, 3H), 2.62 (sept, $^3J_{H–H}$ = 6.7 Hz, 1H), 2.82 (s, 3H), 4.00 (q, $^3J_{H–H}$ = 6.9 Hz, 2H), 4.30 (q, $^3J_{H–H}$ = 7.1 Hz, 2H), 4.93 (d, $^3J_{H–H}$ = 5.6 Hz, 1H), 5.24 (m, 2H), 5.47 (d, $^3J_{H–H}$ = 5.6 Hz, 1H), 6.96 (m, 3H), 7.14 (d, $^3J_{H–H}$ = 7.4 Hz, 1H), 7.19 (t, $^3J_{H–H}$ = 7.4 Hz, 1H), 7.76 (m, 1H), 8.25 (s, 1H), 9.08 (s, 1H), 15.92 (s, 1H) ppm. ESI-MS m/z (+): 709.1 $[M\text{-}Cl]^+$. Anal.

Calcd for $C_{32}H_{36}N_4O_2S_2Cl_2Ru \cdot CH_2Cl_2$: C, 47.77; H, 4.62; N, 6.75. Found: C, 48.41; H, 4.87; N, 7.19. IR (KBr): 2969 (m), 1599 (s), 1465 (s), 1372 (m), 1271 (m), 1098 (s), 753 (m) cm^{-1}.

23: [(η^6-*p*-$MeC_6H_4Pr^i$)Ru(**L23**)Cl]Cl. Yield: 70%. ^{1}H NMR ($CDCl_3$, 400 MHz): δ = 1.03 (d, $^3J_{H–H}$ = 6.7 Hz, 3H), 1.09 (d, $^3J_{H–H}$ = 6.7 Hz, 3H), 2.21 (s, 3H), 2.46 (s, 3H), 2.51 (sept, $^3J_{H–H}$ = 6.7 Hz, 1H), 4.59 (d, $^3J_{H–H}$ = 5.3 Hz, 1H), 4.97 (d, $^3J_{H–H}$ = 5.3 Hz, 1H), 5.10 (d, $^3J_{H–H}$ = 5.3 Hz, 1H), 5.37 (d, $^3J_{H–H}$ = 5.3 Hz, 1H), 6.45 (s, 1H), 6.54 (d, $^3J_{H–H}$ = 2.7 Hz, 1H), 7.35 (d, $^3J_{H–H}$ = 2.7 Hz, 1H), 7.50 (m, 2H), 8.07 (m, 1H), 8.92 (s, 1H), 10.25 (s, 1H) ppm. ESI-MS m/z (+): 527.1 $[M\text{-}Cl]^+$. Anal. Calcd for $C_{23}H_{26}N_4SCl_2Ru \cdot 1.5CH_2Cl_2$: C, 42.65; H, 4.24; N, 8.12. Found: C, 42.94; H, 4.23; N, 8.30. IR (KBr): 3421 (s), 2928 (m), 1617 (m), 1384 (m), 1060 (m), 736 (m) cm^{-1}.

24: [(η^6-*p*-$MeC_6H_4Pr^i$)Ru(**L24**)Cl]Cl. Yield: 64%. ^{1}H NMR ($CDCl_3$, 400 MHz): δ = 1.11 (d, $^3J_{H–H}$ = 6.9 Hz, 3H), 1.16 (d, $^3J_{H–H}$ = 6.9 Hz, 3H), 2.31 (s, 3H), 2.46 (s, 3H), 2.56 (sept, $^3J_{H–H}$ = 6.9 Hz, 1H), 2.87 (s, 3H), 4.58 (d, $^3J_{H–H}$ = 6.0 Hz, 1H), 5.07 (d, $^3J_{H–H}$ = 6.0 Hz, 1H), 5.20 (d, $^3J_{H–H}$ = 6.0 Hz, 1H), 5.40 (d, $^3J_{H–H}$ = 6.0 Hz, 1H), 6.71 (d, $^3J_{H–H}$ = 2.8 Hz, 1H), 7.39 (t, $^3J_{H–H}$ = 2.8 Hz, 1H), 7.57 (d, $^3J_{H–H}$ = 2.8 Hz, 1H), 7.84 (d, J = 2.8 Hz, 1H), 8.42 (s, 1H), 9.08 (s, 1H) ppm. ESI-MS m/z (+): 569.1 $[M\text{-}Cl]^+$. Anal. Calcd for $C_{25}H_{28}N_4OSCl_2Ru \cdot H_2O$: C, 48.23; H, 4.86; N, 9.00. Found: C, 48.62; H, 4.80; N, 8.44. IR (KBr): 3430 (s), 2927 (m), 1614 (m), 1571 (s), 1511 (s), 1375 (m), 1312 (s), 734 (m) cm^{-1}.

25: [(η^6-*p*-$MeC_6H_4Pr^i$)Ru(**L25**)Cl]Cl. Yield: 71%. ^{1}H NMR ($CDCl_3$, 400 MHz): δ = 1.47 (d, $^3J_{H–H}$ = 6.9 Hz, 6H), 2.41 (s, 3H), 3.25 (sept, $^3J_{H–H}$ = 6.9 Hz, 1H), 5.40 (d, $^3J_{H–H}$ = 5.6 Hz, 2H), 5.63 (d, $^3J_{H–H}$ = 5.6 Hz, 2H), 6.67 (s, 1H), 7.46-7.52 (m, 7H), 7.68 (d, $^3J_{H–H}$ = 8.5 Hz, 1H), 7.81 (d, $^3J_{H–H}$ = 7.1 Hz, 2H), 7.96 (s, 1H), 8.41 (s, 1H) ppm. ESI-MS m/z (+): 589.1 $[M\text{-}Cl]^+$. Anal. Calcd for $C_{28}H_{28}N_4SCl_2Ru \cdot 2CH_2Cl_2$: C, 45.36; H, 4.06; N, 7.05. Found: C, 45.84; H, 3.85; N, 7.63. IR (KBr): 2923 (m), 1623 (s), 1384 (m), 1349 (m), 1297 (w), 1124 (w), 729 (m) cm^{-1}.

26: [(η^6-*p*-$MeC_6H_4Pr^i$)Ru(**L26**)Cl]Cl. Yield: 62%. ^{1}H NMR ($CDCl_3$, 400 MHz): δ = 1.05 (d, $^3J_{H–H}$ = 6.8 Hz, 3H), 1.10 (d, $^3J_{H–H}$ = 6.8 Hz, 3H), 1.37 (t, $^3J_{H–H}$ = 7.1 Hz, 3H), 2.22 (s, 3H), 2.55 (sept, $^3J_{H–H}$ = 6.8 Hz, 1H), 3.86 (d, $^2J_{H–H}$ = -13.4 Hz, 2H), 4.30 (q, $^3J_{H–H}$ = 7.1 Hz, 2H), 4.67 (d, $^3J_{H–H}$ = 5.8 Hz, 1H), 5.02 (d, $^3J_{H–H}$ = 5.8 Hz, 1H), 5.15 (d, $^3J_{H–H}$ = 5.8 Hz, 1H), 5.51 (d, $^3J_{H–H}$ = 5.8 Hz, 1H), 6.55 (d, $^3J_{H–H}$ = 2.8 Hz, 1H), 6.77 (s, 1H), 7.34 (d, $^3J_{H–H}$ = 2.8 Hz, 1H), 7.50 (m, 2H), 8.08 (s, 1H), 8.94 (s, 1H), 10.04 (s, 1H) ppm. ESI-MS m/z (+): 599.1 $[M\text{-}Cl]^+$. Anal. Calcd for $C_{26}H_{30}N_4O_2SCl_2Ru \cdot CH_2Cl_2$: C, 45.07; H, 4.48; N, 7.79. Found: C,

45.12; H, 4.46; N, 7.79. IR (KBr): 2926 (m), 1731 (m), 1615 (s), 1579 (m), 1384 (m), 1350 (m), 1255 (m), 1133 (m), 735 (m) cm^{-1}.

27: [(η^6-*p*-$MeC_6H_4Pr^i$)Ru(**L27**)Cl]Cl. Yield: 76%. ^1H NMR ($CDCl_3$, 400 MHz): δ = 1.40 (d, $^3J_{H–H}$ = 7.0 Hz, 6H), 2.34 (s, 3H), 2.67 (s, 3H), 2.78 (s, 3H), 3.16 (sept, $^3J_{H–H}$ = 7.0 Hz, 1H), 5.34 (d, $^3J_{H–H}$ = 5.9 Hz, 2H), 5.57 (d, $^3J_{H–H}$ = 5.9 Hz, 2H), 6.14 (s, 1H), 7.73 (s, 1H), 8.14 (d, $^3J_{H–H}$ = 7.8 Hz, 1H), 8.45 (d, $^3J_{H–H}$ = 7.8 Hz, 1H), 8.51 (d, $^3J_{H–H}$ = 7.8 Hz, 1H), 8.67 (s, 1H), 8.99 (s, 1H), 9.44 (s, 1H) ppm. ESI-MS m/z (+): 569.1 $[M\text{-}Cl]^+$. Anal. Calcd for $C_{25}H_{28}N_4OSCl_2Ru·0.5CH_2Cl_2$: C, 47.34; H, 4.52; N, 8.66. Found: C, 46.79; H, 4.68; N, 8.44. IR (KBr): 2924 (m), 1711 (m), 1631 (s), 1448 (m), 1377 (m), 1217 (s), 746 (m) cm^{-1}.

28: [(η^6-*p*-$MeC_6H_4Pr^i$)Ru(**L28**)Cl]Cl. Yield: 66%. ^1H NMR ($CDCl_3$, 400 MHz): δ = 1.01 (d, $^3J_{H–H}$ = 7.0 Hz, 3H), 1.06 (d, $^3J_{H–H}$ = 7.0 Hz, 3H), 2.16 (s, 3H), 2.45 (sept, $^3J_{H–H}$ = 7.0 Hz, 1H), 2.84 (s, 3H), 5.39 (d, $^3J_{H–H}$ = 5.9 Hz, 1H), 5.41 (d, $^3J_{H–H}$ = 5.9 Hz, 1H), 5.52 (d, $^3J_{H–H}$ = 5.9 Hz, 1H), 5.62 (d, $^3J_{H–H}$ = 5.9 Hz, 1H), 6.82 (s, 1H), 7.69 (s, 1H), 7.84 (d, $^3J_{H–H}$ = 7.5 Hz, 2H), 7.99 (m, 2H), 8.29 (d, $^3J_{H–H}$ = 7.5 Hz, 2H), 8.49-8.57 (m, 4H), 9.12 (s, 1H) ppm. ESI-MS m/z (+): 631.1 $[M\text{-}Cl]^+$. Anal. Calcd for $C_{30}H_{30}N_4OSCl_2Ru·H_2O$: C, 52.63; H, 4.71; N, 8.18. Found: C, 53.01; H, 4.45; N, 8.19. IR (KBr): 2926 (m), 1717 (s), 1623 (s), 1567 (s), 1450 (s), 1219 (s), 753 (m) cm^{-1}.

29: [(η^6-*p*-$MeC_6H_4Pr^i$)Ru(**L29**)Cl]Cl. Yield: 70%. ^1H NMR ($CDCl_3$, 400 MHz): δ = 1.32 (d, $^3J_{H–H}$ = 7.0 Hz, 6H), 2.20 (s, 3H), 2.56 (s, 3H), 2.71 (s, 3H), 2.72 (s, 3H), 2.97 (sept, $^3J_{H–H}$ = 7.0 Hz, 1H), 5.39 (d, $^3J_{H–H}$ = 6.0 Hz, 2H), 5.52 (d, $^3J_{H–H}$ = 6.0 Hz, 2H), 7.50 (m, 2H), 7.75 (s, 1H), 8.28 (t, $^3J_{H–H}$ = 5.1 Hz, 1H), 8.40 (s, 1H), 8.48 (t, $^3J_{H–H}$ = 5.1 Hz, 1H) ppm. ESI-MS m/z (+): 611.1 [M-Cl]+. Anal. Calcd for $C_{27}H_{30}N_4O_2SCl_2Ru·0.5CH_2Cl_2$: C, 47.94; H, 4.53; N, 8.13. Found: C, 48.45; H, 4.68; N, 7.79. IR (KBr): 2929 (m), 1718 (m), 1624 (s), 1567 (m), 1450 (s), 1371 (s), 1327 (m), 1218 (s), 1033 (m), 752 (m) cm^{-1}.

30: [(η^6-*p*-$MeC_6H_4Pr^i$)Ru(**L30**)Cl]Cl. Yield: 79%. ^1H NMR ($CDCl_3$, 400 MHz): δ = 1.28 (d, $^3J_{H–H}$ = 7.1 Hz, 3H), 1.33 (d, $^3J_{H–H}$ = 7.1 Hz, 3H), 1.40 (t, $^3J_{H–H}$ = 7.1 Hz, 3H), 2.35 (s, 3H), 2.68 (s, 3H), 2.79 (s, 3H), 3.14 (sept, $^3J_{H–H}$ = 7.1 Hz, 1H), 4.35 (q, $^3J_{H–H}$ = 7.1 Hz, 2H), 5.36 (d, $^3J_{H–H}$ = 6.3 Hz, 2H), 5.59 (d, $^3J_{H–H}$ = 6.3 Hz, 2H), 7.45 (m, 2H), 7.71 (s, 1H), 8.22 (m, 1H), 8.45 (m, 2H), 9.71 (s, 1H) ppm. ESI-MS m/z (+): 641.1 $[M\text{-}Cl]^+$. Anal. Calcd for $C_{28}H_{32}N_4O_3SCl_2Ru·0.5CH_2Cl_2$: C, 47.60; H, 4.63; N, 7.79. Found: C, 47.64; H, 4.53; N, 8.31. IR (KBr): 2930 (m), 1700 (s), 1616 (m), 1560 (s), 1450 (s), 1372 (s), 1218 (s), 1092 (s), 757 (m) cm^{-1}.

31: [(η^6-*p*-$MeC_6H_4Pr^i$)Ru(**L31**)Cl]Cl. Yield: 82%. ^{1}H NMR ($CDCl_3$, 400 MHz): δ = 1.12 (d, $^3J_{H–H}$ = 6.8 Hz, 3H), 1.23 (d, $^3J_{H–H}$ = 6.8 Hz, 3H), 1.41 (t, $^3J_{H–H}$ = 7.2 Hz, 3H), 2.31 (s, 3H), 2.69 (sept, $^3J_{H–H}$ = 6.8 Hz, 1H), 2.83 (s, 3H), 3.91 (d, $^2J_{H–H}$ = -13.7 Hz, 2H), 4.35 (q, $^3J_{H–H}$ = 7.2 Hz, 2H), 4.84 (d, $^3J_{H–H}$ = 5.8 Hz, 1H), 5.33 (d, $^3J_{H–H}$ = 5.8 Hz, 1H), 5.37 (d, $^3J_{H–H}$ = 5.8 Hz, 1H), 5.65 (d, $^3J_{H–H}$ = 5.8 Hz, 1H), 6.84 (s, 1H), 7.49-7.56 (m, 3H), 7.92 (m, 1H), 8.57 (d, $^3J_{H–H}$ = 8.0 Hz, 1H), 9.07 (s, 1H), 9.40 (s, 1H) ppm. ESI-MS m/z (+): 641.1 [M-Cl]+. Anal. Calcd for $C_{28}H_{32}N_4O_3SCl_2Ru$: C, 49.70; H, 4.77; N, 8.28. Found: C, 49.97; H, 5.12; N, 8.47. IR (KBr): 2929 (m), 1722 (s), 1617 (m), 1576 (m), 1547 (m), 1451 (s), 1379 (s), 1217 (s), 754 (m) cm^{-1}.

5.2.2 Light-Responsive Ruthenium Assemblies

Synthesis of ruthenium-azopyridine rectangles **32-35**: A mixture of the dinuclear ruthenium spacer (1 equivalent) and silver trifluoromethanesulfonate (2 equivalents) in dichloromethane was stirred at room temperature for 3 hours. The resulting mixture was filtrated in order to eliminate the silver chloride formed, and the solution was added to a solution of 4,4'-azopyridine (1 equivalent) in dichloromethane. The mixture was then refluxed overnight, and consequently concentrated under vacuum. The residue was dissolved in a few milliliters of dichloromethane, and slow addition of diethyl ether induced the precipitation of the rectangles, which were then filtered and dried under vacuum.

33: Yield: 61%. ^{1}H NMR (CD_3NO_2, 400 MHz): δ = 1.44 (d, $^3J_{H–H}$ = 7.1 Hz, 24H), 2.33 (s, 12H), 2.99 (sept, $^3J_{H–H}$ = 7.1 Hz, 4H), 5.90 (d, $^3J_{H–H}$ = 6.3 Hz, 8H), 6.07 (d, $^3J_{H–H}$ = 6.3 Hz, 8H), 7.85 (d, $^3J_{H–H}$ = 6.8 Hz, 8H), 8.63 (d, $^3J_{H–H}$ = 6.8 Hz, 8H) ppm. ESI-MS m/z (+): 1009.8 $[M-2OTf]^{2+}$. IR (KBr): 2969 (m), 1606 (m), 1505 (s), 1374 (s), 1260 (s), 1159 (s), 1030 (s), 866 (m), 638 (s) cm^{-1}. UV-visible (CH_2Cl_2, C = 6.0 x 10^{-6} mol·L^{-1}): λ_{max} = 307 nm (ε = 3.50 x 10^5 L·mol^{-1}·cm^{-1}), 489 nm (ε = 2.15 x 10^5 L·mol^{-1}·cm^{-1}).

Synthesis of anthracene-based ligand **L36**: A mixture of 9,10-dibromoanthracene (1 equivalent) and 3-ethynylpyridine (2.2 equivalents) was dissolved in a 1:1 triethylamine-toluene solution under nitrogen. A mixture of palladium (II) acetate (0.02 equivalent), copper (I) iodide (0.025 equivalent) and triphenylphosphine (0.055 equivalent) was then added. The reaction medium was refluxed for 24 hours; the solvent was then removed under vacuum and the residue was stirred in water for two hours in order to eliminate the triethylammonium salt.

The solid was filtered and dried under vacuum, and finally recrystallized in toluene to yield **L36** as an orange powder.

L36: Yield: 57%. ^{1}H NMR ($CDCl_3$, 400 MHz): δ = 7.41 (m, 2H), 7.68 (dd, $^{3}J_{H–H}$ = 6.6 Hz, $^{4}J_{H–H}$ = 3.3 Hz, 4H), 8.05 (d, $^{3}J_{H–H}$ = 7.7 Hz, 2H), 8.66 (m, 6H), 9.02 (s, 2H) ppm.

Synthesis of ruthenium-anthracene rectangle **36**: A mixture of [(η^6-*p*-$MeC_6H_4Pr^i$)$_2$$Ru_2(oxa)Cl_2$] (1 equivalent) and silver trifluoromethanesulfonate (2 equivalents) in dichloromethane was stirred at room temperature for 3 hours. The resulting mixture was filtrated in order to eliminate the silver chloride formed, and the solution was added to a solution of **L36** (1 equivalent) in dichloromethane. The mixture was then refluxed overnight, and consequently concentrated under vacuum. The residue was dissolved in a few milliliters of dichloromethane, and slow addition of diethyl ether induced the precipitation of **36** as a yellow powder, which was then filtered and dried under vacuum.

36: Yield: 83%. ^{1}H NMR (Acetone-d_6, 400 MHz): δ = 1.44 (d, $^{3}J_{H–H}$ = 7.0 Hz, 12H), 1.47 (d, $^{3}J_{H–H}$ = 7.0 Hz, 12H), 2.38 (s, 12H), 3.05 (sept, $^{3}J_{H–H}$ = 7.0 Hz, 4H), 6.05 (d, $^{3}J_{H–H}$ = 6.1 Hz, 4H), 6.08 (d, $^{3}J_{H–H}$ = 6.1 Hz, 4H), 6.20 (d, $^{3}J_{H–H}$ = 6.1 Hz, 4H), 6.23 (d, $^{3}J_{H–H}$ = 6.1 Hz, 4H), 7.36 (m, 8H), 7.66 (t, $^{3}J_{H–H}$ = 6.8 Hz, 4H), 8.18 (m, 12H), 8.65 (m, 8H) ppm. ^{13}C NMR (Acetone-d_6, 400 MHz): δ = 17.26, 21.40, 21.74, 31.01, 81.39, 82.20, 91.95, 96.46, 97.99, 102.54, 116.94, 119.97, 122.84, 123.17, 126.24, 126.70, 127.20, 130.89, 142.83, 151.62, 153.70, 171.10, 171.23 ppm. ESI-MS m/z (+): 469.6 $[M\text{-}4OTf]^{4+}$, 675.7 $[M\text{-}3OTf]^{3+}$, 1088.8 $[M\text{-}2OTf]^{2+}$. Anal. Calcd for $C_{104}H_{88}N_4O_{20}S_4F_{12}Ru_4$: C, 50.48; H, 3.58; N, 2.26. Found: C, 50.64; H, 3.84; N, 2.17. IR (KBr): 2927 (w), 2208 (w), 1624 (s), 1417 (m), 1262 (s), 1195 (m), 1149 (m), 1058 (s), 1030 (s), 883 (w), 769 (m) cm^{-1}. UV-visible (CH_2Cl_2, C = 1.0 x 10^{-5} $mol \cdot L^{-1}$): λ_{max} = 247 nm (ε = 7.88 x 10^5 $L \cdot mol^{-1} \cdot cm^{-1}$), 272 nm (ε = 7.94 x 10^5 $L \cdot mol^{-1} \cdot cm^{-1}$), 306 nm (ε = 5.45 x 10^5 $L \cdot mol^{-1} \cdot cm^{-1}$), 457 nm (ε = 6.43 x 10^5 $L \cdot mol^{-1} \cdot cm^{-1}$), 488 nm (ε = 3.90 x 10^5 $L \cdot mol^{-1} \cdot cm^{-1}$).

Synthesis of ruthenium-anthracene cage **37**: A mixture of [(η^6-*p*-$MeC_6H_4Pr^i$)$_2$$Ru_2$(dhnq)$Cl_2$] (2 equivalents) and silver trifluoromethanesulfonate (4 equivalents) in dichloromethane was stirred at room temperature for 3 hours. The resulting mixture was filtrated in order to eliminate the silver chloride formed, and the solution was added to a solution of **L37** (1 equivalent) in dichloromethane. The mixture was then refluxed overnight, and consequently concentrated under vacuum. The residue was dissolved in a few milliliters of dichloromethane,

and slow addition of diethyl ether induced the precipitation of **37** as a green powder, which was then filtered and dried under vacuum.

37: Yield: 73%. ^{1}H NMR (Acetone-d_6, 400 MHz): δ = 1.37 (d, $^{3}J_{H–H}$ = 6.9 Hz, 24H), 1.43 (d, $^{3}J_{H–H}$ = 6.9 Hz, 24H), 2.21 (s, 12H), 2.24 (s, 12H), 2.31 (s, 12H), 2.96 (sept, $^{3}J_{H–H}$ = 6.9 Hz, 8H), 3.65 (s, 12H), 5.83 (d, $^{3}J_{H–H}$ = 5.6 Hz, 16H), 6.04 (d, $^{3}J_{H–H}$ = 5.6 Hz, 16H), 6.14 (s, 4H), 6.91 (s, 4H), 7.28 (d, $^{3}J_{H–H}$ = 2.1 Hz, 8H), 7.39 (d, $^{3}J_{H–H}$ = 2.1 Hz, 8H), 7.94 (s, 4H), 8.12 (d, $^{3}J_{H–H}$ = 6.1 Hz, 8H), 8.13 (s, 4H), 8.30 (d, $^{3}J_{H–H}$ = 6.1 Hz, 8H), 8.60 (d, $^{3}J_{H–H}$ = 6.1 Hz, 8H), 8.68 (s, 4H), 8.70 (d, $^{3}J_{H–H}$ = 6.1 Hz, 8H) ppm. ^{13}C NMR (Acetone-d_6, 400 MHz): δ = 16.88, 21.95, 31.09, 54.10, 55.35, 83.45, 85.02, 100.22, 103.12, 103.73, 104.30, 123.65, 124.93, 125.97, 131.92, 132.21, 136.50, 138.13, 148.73, 150.14, 153.18, 171.39 ppm. ESI-MS m/z (+): 1187.64 $[M\text{-}4OTf]^{4+}$, 1633.25 $[M\text{-}3OTf]^{3+}$. Anal. Calcd for $C_{228}H_{204}N_8O_{48}S_8F_{24}Ru_8 \cdot 2\ CH_2Cl_2$: C, 50.09; H, 3.80; N, 2.03. Found: C, 49.73; H, 3.93; N, 1.77. IR (KBr): 2929 (w), 1611 (w), 1538 (s), 1274 (s), 1031 (m) cm^{-1}. UV-visible (CH_2Cl_2, C = 4.7 x 10^{-7} $mol \cdot L^{-1}$): λ_{max} = 279 nm (ε = 1.11 x 10^6 $L \cdot mol^{-1} \cdot cm^{-1}$), 303 nm (ε = 4.88 x 10^5 $L \cdot mol^{-1} \cdot cm^{-1}$), 377 nm (ε = 2.01 x 10^5 $L \cdot mol^{-1} \cdot cm^{-1}$).

Multi-step synthesis of dihydropyrene precursor **DHP**:

Step i): synthesis of **a**: A mixture of 4-*tert*-butyltoluene (1 equivalent), 1,3,5-trioxane (0.9 equivalent), zinc (II) bromide (0.1 equivalent) in hydrobromic acid (33% in acetic acid) and acetic anhydride was stirred at 85 °C for five days. Once back at room temperature, the mixture was poured onto ice. The resulting yellow precipitate was filtered, washed with water and a saturated solution of $NaHCO_3$, and dried under vacuum. It was finally recrystallized in hexane in order to yield a white powder.

Step ii): synthesis of **b**: Product **a** (1 equivalent) was added to a 40 °C solution of thiourea (2 equivalents) in ethanol; the resulting mixture was refluxed for two hours. A solution of sodium hydroxide was then added under nitrogen and the refluxed was resumed for three more hours. The mixture was cooled in an ice bath, and cold concentrated sulfuric acid was gently added. The product was then extracted with diethyl ether, washed with water, and the solvent was removed under vacuum. Recrystallization of the crude product in hexane gave **b** as a white powder.

Step iii): synthesis of **c**: A solution of **a** (1 equivalent) and **b** (1 equivalent) in dry benzene was added dropwise under nitrogen to a solution of potassium hydroxide and sodium

borohydride in ethanol. The drop rate was adjusted so that the addition lasted 24 hours. The solvents were then removed under vacuum, and the residue was dissolved in dichloromethane and washed with water. After removal of the solvent, the crude product was recrystallized in toluene to yield **c** as a white powder.

Step iv): synthesis of **d**: To an ice-cooled solution of **c** (1 equivalent) in THF was slowly added *n*-butyllithium (3.9 equivalents) under nitrogen. After one hour of stirring at room temperature, methyl iodide (4 equivalents) was added, and the stirring was resumed for another 30 minutes. The mixture was then poured onto ice and the product was extracted with dichloromethane, washed with water, and the solvent was removed under vacuum to yield **d** as a yellow oil.

Step v): synthesis of **e**: A solution of trimethyl orthoformate (3 equivalents) in dry dichloromethane was colled to -30 °C, after what boron trifluoride (3 equivalents) was added. The mixture was stirred at 0 °C for 30 minutes, cooled back to -30 °C, and washed with dichloromethane. To the resulting oily Borch reagent[81] was added a solution of **d** (1 equivalent) in dichloromethane, at -30 °C and under nitrogen. The mixture was then stirred at room temperature for three hours, and washed with ethyl acetate for a further two hours. The product was then filtered and dried under vacuum to give **e** as a white powder.

Step vi): synthesis of **DHP**: Potassium tert-butylate (2.7 equivalents) was added to a suspension of **e** (1 equivalent) in dry THF, and the mixture was refluxed for 12 hours under nitrogen. An aqueous solution of hydrochloric acid was added, and the product was extracted with dichloromethane and washed with water. After removal of the solvent under vacuum, the green residue was chromatographed over silica gel using hexane as eluent to yield **DHP** as a green powder.

DHP: Yield (from *tert*-butyltoluene): 42%. ^{1}H NMR ($CDCl_3$, 400 MHz): δ = -4.04 (s, 6H), 1.70 (s, 18H), 8.46 (s, 4H), 8.54 (s, 4H) ppm.

Synthesis of brominated dihydropyrene intermediate **DHP-Br**: To an ice-cooled solution of **DHP** (1 equivalent) in dry DMF was added an ice-cooled solution of *N*-bromosuccinimide (2.1 equivalents). The mixture was stirred at 0 °C for two hours and was then poured onto ice. The product was extracted with hexane, washed with water, and the solvent was removed under vacuum. The crude product was then chromatographed over silica gel using hexane as eluent to yield **DHP-Br** as a green powder.

DHP-Br: Yield: 66%. ^{1}H NMR ($CDCl_3$, 400 MHz): δ = -3.83 (s, 6H), 1.68 (s, 18H), 8.48 (s, 2H), 8.64 (s, 2H), 8.81 (s, 2H) ppm.

Synthesis of dihydropyrene-based ligand **L38**: A solution of **DHP-Br** (1 equivalent) and 4-pyridineboronic acid (2.2 equivalents) in THF was added to a solution of $Pd(PPh_3)_4$ (0.2 equivalent) and Na_2CO_3 (4.75 equivalents) in water. The mixture was refluxed for 48 hours, after what the solvent was removed under vacuum. The residue was dissolved in water and the product was extracted with dichloromethane, then concentrated under vacuum. Slow addition of diethyl ether precipitated **L38**, which was filtered, dried under vacuum and isolated as a green powder.

L38: Yield: 53%. ^{1}H NMR ($CDCl_3$, 400 MHz): δ = -3.68 (s, 6H), 1.61 (s, 18H), 7.78 (m, 4H), 8.48 (s, 2H), 8.60 (s, 2H), 8.65 (s, 2H), 8.86 (m, 4H) ppm.

Synthesis of ruthenium-dihydropyrene rectangle **38**: A mixture of $[(\eta^6\text{-}p\text{-}MeC_6H_4Pr^i)_2Ru_2(dhnq)Cl_2]$ (1 equivalent) and silver trifluoromethanesulfonate (2 equivalents) in dichloromethane was stirred at room temperature for 3 hours. The resulting mixture was filtrated in order to eliminate the silver chloride formed, and the solution was added to a solution of **L38** (1 equivalent) in dichloromethane. The mixture was then refluxed overnight, and consequently concentrated under vacuum. The residue was dissolved in a few milliliters of dichloromethane, and slow addition of diethyl ether induced the precipitation of **38** as a brown powder, which was then filtered and dried under vacuum.

38: Yield: 38%. ^{1}H NMR (Acetone-d_6, 400 MHz): δ = -3.98 (s, 3H), -3.92 (s, 6H), -3.74 (s, 3H), 1.17 (s, 18H), 1.20 (s, 9H), 1.33 (d, $^{3}J_{H-H}$ = 7.0 Hz, 12H), 1.37 (d, $^{3}J_{H-H}$ = 7.0 Hz, 12H), 1.54 (s, 9H), 2.32 (s, 12H), 3.03 (sept, $^{3}J_{H-H}$ = 7.0 Hz, 4H), 5.93 (d, $^{3}J_{H-H}$ = 5.8 Hz, 8H), 6.12 (d, $^{3}J_{H-H}$ = 5.8 Hz, 8H), 7.22 (s, 4H), 7.44 (s, 4H), 7.45 (s, 4H), 7.99 (d, $^{3}J_{H-H}$ = 6.3 Hz, 8H), 8.33 (s, 4H), 8.40 (s, 4H), 8.92 (d, $^{3}J_{H-H}$ = 6.3 Hz, 8H) ppm. ^{13}C NMR (Acetone-d_6, 400 MHz): δ = 14.66, 17.10, 22.00, 30.14, 31.12, 31.39, 36.28, 83.26, 84.94, 100.31, 103.89, 119.91, 123.04, 124.63, 128.48, 130.57, 133.52, 138.01, 152.41, 170.88, 172.11 ppm. ESI-MS m/z (+): 1306.9 $[M\text{-}2OTf]^{2+}$. IR (KBr): 2964 (m), 1611 (m), 1536 (s), 1422 (m), 1275 (s), 1159 (m), 1031 (s), 638 (m) cm^{-1}. UV-visible (CH_2Cl_2, C = 1.0 x 10^{-5} mol·L^{-1}): λ_{max} = 344 nm (ε = 8.39 x 10^5 L·mol^{-1}·cm^{-1}), 411 nm (ε = 9.32 x 10^5 L·mol^{-1}·cm^{-1}), 489 nm (ε = 3.25 x 10^5 L·mol^{-1}·cm^{-1}).

References

[1] Pitchkov V.N., *Platinum Metals Reviews*, **1996**, *40*, 181-188.

[2] Greenwood N.N., Earnshaw, A., *Chemistry of the Elements*, Pergamon Press, **1984**, 1242-1286.

[3] Gulliver, D.J., Levason, W., *Coordination Chemistry Reviews*, **1982**, *46*, 1-127.

[4] Murahashi, S.-I., *Ruthenium in Organic Synthesis*, Wiley-VCH, **2004**, 398 pages.

[5] Ikariya, T., Ishii, Y., Kawano, H., Arai, T., Saburi, M., Yoshikawa, S., Akutagawa, S., *Journal of the Chemical Society, Chemical Communications*, **1985**, 922-924.

[6] Nguyen, S.T., Johnson, L.K., Grubbs, R.H., Ziller, J.W., *Journal of the American Chemical Society*, **1992**, *114*, 3974-3975.

[7] Kalyanasundaram, K., Grätzel, M., *Material Matters*, **2009**, 4.4, 88.

[8] Lehn, J.-M., *Science*, **1993**, *260*, 1762-1763.

[9] Pedersen, C.J., *Journal of the American Chemical Society*, **1967**, *89*, 7017-7036.

[10] Ogoshi, T., Yamagishi, T., *Pillararenes*, Royal Society of Chemistry, **2015**, 1-22.

[11] Maverick, A.W., Klavetter, F.E., *Inorganic Chemistry*, **1984**, *23*, 4129-4130.

[12] Fujita, M., Yazaki, J., Ogura, K., *Journal of the American Chemical Society*, **1990**, *112*, 5647-5648.

[13] Winkhaus, G., Singer, H., *Journal of Organometallic Chemistry*, **1967**, *7*, 487-491.

[14] Bennett, M.A., Smith, A.K., *Journal of the Chemical Society, Dalton Transactions*, **1974**, 233-241.

[15] Severin, K., *Coordination Chemistry Reviews*, **2003**, *245*, 3-10.

[16] Bennett, M.A., Huang, T.-N., Matheson, T.W., Smith, A.K., *Inorganic Syntheses*, **1982**, *21*, 74-78.

[17] Barry, N., Furrer, J., Therrien, B., *Helvetica Chimica Acta*, **2010**, *93*, 1313-1328.

[18] Mattsson, J., Govindaswamy, P., Furrer, J., Sei, Y., Yamaguchi, K., Süss-Fink, G., Therrien, B., *Organometallics*, **2008**, *27*, 4346-4356.

[19] Therrien, B., Süss-Fink, G., Govindaswamy, P., Renfrew, A.K., Dyson, P.J., *Angewandte Chemie International Edition*, **2008**, *47*, 3773-3776.

[20] Schmitt, F., Freudenreich, J., Barry, N.P.E., Juillerat-Jeanneret, L., Süss-Fink, G., Therrien, B., *Journal of the American Chemical Society*, **2012**, *134*, 754-757.

[21] Stewart, B.W., Wild, C.P., *World Cancer Report 2014*, Lyon: International Agency for Research on Cancer, **2014**, 630 pages.

[22] Weisse, A.B., *Medical Odysseys*, Rutgers University Press, **1991**, 250 pages.

[23] Faguet, G.B., *Journal of Clinical Oncology*, **1994**, *12*, 1974-1990.

[24] Aapro, M.S., Martin, C., Hatty, S., *Anticancer Drugs*, **1998**, *9*, 191-201.

[25] Rosenberg, B., VanCamp, L., Krigas, T., *Nature*, **1965**, *205*, 698-699.

[26] Rademaker-Lakhai, J.M., Bongard, D., Pluim, D., Beijnen, J.H., Schellens, J.H., *Clinical Cancer Research*, **2004**, *10*, 3717-3727.

[27] Trondl, R., Heffeter, P., Kowol, C.R., Jakupec, M.A., Berger, W., Keppler, B.K., *Chemical Science*, **2014**, *5*, 2925-2932.

[28] Allardyce, C.S., Dyson, P.J., Ellis, D.J., Heath, S.L., *Chemical Communications*, **2001**, 1396-1397.

[29] Morris, R.E., Aird, R.E., Murdoch, P.D., Chen, H.M., Cummings, J., Hughes, N.D., Parsons, S., Parkin, A., Boyd, G., Jodrell, D.I., Sadler, P.J., *Journal of Medicinal Chemistry*, **2005**, *48*, 4161-4171.

[30] El-Subbagh, H.I., Al-Obaid, A.M., *European Journal of Medicinal Chemistry*, **1996**, *31*, 1017-1021.

[31] Grozav, A., Gaina, L.I., Pileczki, V., Crisan, O., Silaghi-Dumitrescu, L., Therrien, B., Zaharia, V., Berindan-Neagoe, I., *International Journal of Molecular Sciences*, **2014**, *15*, 22059-22072.

[32] Gras, M., Therrien, B., Süss-Fink, G., Casini, A., Edafe, F., Dyson, P.J., *Journal of Organometallic Chemistry*, **2010**, *695*, 1119-1125.

[33] Mitchell, S.C., *Current Drug Targets*, **2006**, *7*, 1181-1189.

[34] Barbieri, F., Alama, A., Tasso, B., Boido, V., Bruzzo, C., Sparatore, F., *Investigational New Drugs*, **2003**, *21*, 413-420.

[35] Bisi, A., Meli, M., Gobbi, S., Rampa, A., Tolomeo, M., Dusonchet, L., *Bioorganic & Medicinal Chemistry*, **2008**, *16*, 6474-6482.

[36] El Sayed, M.T., Hamdy, N.A., Osman, D.A., Ahmed, K.M., *Advances in Modern Oncology Research*, **2015**, *1*, 20-35.

[37] Ahmad, A., Sakr, W.A., Rahman, K.M., *Cancers*, **2011**, *3*, 2955-2974.

[38] Kawanishi, Y., Kitamura, N., Tazuke, S., *Journal of Physical Chemistry*, **1986**, *90*, 2469-2475.

[39] Bianchi, A., Delgado-Pinar, E., Garcia-España, E., Pina, F., *Comprehensive Inorganic Chemistry II*, **2013**, *8*, 969-1037.

[40] Canary, J.W., *Chemical Society Reviews*, **2009**, *38*, 747-756.

[41] Nabeshima, T., Furusawa, H., Yano, Y., *Angewandte Chemie International Edition in English*, **1994**, *33*, 1750-1751.

[42] Huston, M.E., Haider, K.W., Czarnik, A.W., *Journal of the American Chemical Society*, **1988**, *110*, 4460-4462.

[43] Nagata, Y., Takeda, R., Suginome, M., *Chemical Communications*, **2015**, *51*, 11182-11185.

[44] Kudernac, T., Kobayashi, T., Uyama, A., Uchida, K., Nakamura, S., Feringa, B.L., *The Journal of Physical Chemistry A*, **2013**, *117*, 8222-8229.

[45] Grunder, S., McGrier, P.L., Whalley, A.C., Boyle, M.M., Stern, C., Stoddart, J.F., *Journal of the American Chemical Society*, **2013**, *135*, 17691-17694.

[46] Irie, M., *Chemical Reviews*, **2000**, *100*, 1685-1716.

[47] Han, M., Michel, R., He, B., Chen, Y.-S., Stalke, D., John, M., Clever, G.H., *Angewandte Chemie International Edition*, **2013**, *52*, 1319-1323.

[48] Deo, C., Bogliotti, N., Métivier, R., Retailleau, P., Xie, J., *Organometallics*, **2015**, *34*, 5775-5784.

[49] Collins, G.E., Choi, L.-S., Ewing, K.J., Michelet, V., Bowen, C.M., Winkler, J.D., *Chemical Communications*, **1999**, *4*, 321-322.

[50] Barry, N., Zava, O., Dyson, P.J., Therrien, B., *Chemistry A European Journal*, **2011**, *17*, 9669-9677.

[51] Paul, L.E.H., Therrien, B., Furrer, J., *Inorganic Chemistry*, **2012**, *51*, 1057-1067.

[52] Mitscherlich, E., *Annalen der Pharmacie*, **1834**, *12*, 311-314.

[53] Hartley, G.S., *Nature*, **1937**, *140*, 281-282.

[54] Rau, H., *Photochemistry and Photophysics*, **1990**, *2*, 119-142.

[55] Banghart, M., Borges, K., Isacoff, E., Trauner, D., Kramer, R.H., *Nature Neuroscience*, **2004**, *7*, 1381-1386.

[56] Shinkai, S., Minami, T., Kusano, Y., Manabe, O., *Journal of the American Chemical Society*, **1983**, *105*, 1851-1856.

[57] Muraoka, T., Kinbara, K., Kobayashi, Y., Aida, T., *Journal of the American Chemical Society*, **2003**, *125*, 5612-5613.

[58] Vajpayee, V., Lee, S., Kim, S.-H., Kang, S.C., Cook, T.R., Kim, H., Kim, D.W., Verma, S., Lah, M.S., Kim, I.S., Wang, M., Stang, P.J., Chi, K.-W., *Dalton Transactions*, **2013**, *42*, 466-475.

[59] Bandara, H.M.D., Burdette, S.C., *Chemical Society Reviews*, **2012**, *41*, 1809-1825.

[60] Bardají, M., Barrio, M., Espinet, P., *Dalton Transactions*, **2011**, *40*, 2570-2577.

[61] Yamada, S., Nagata, S., Kinugawa, C., *Journal of the Japan Society of Colour Material*, **2005**, *78*, 461-467.

[62] Rau, H., Luddecke, E., *Journal of the American Chemical Society*, **1982**, *104*, 1616-1620.

[63] Greene, F.D., Misrock, S.L., Wolfe, Jr, J.R., *Journal of the American Chemical Society*, **1955**, *77*, 3852-3855.

[64] Breton, G.W., Vang, X., *Journal of Chemical Education*, **1998**, *75*, 81-82.

[65] Aubry, J.-M., Pierlot, C., Rigaudy, J., Schmidt, R., *Accounts of Chemical Research*, **2003**, *36*, 668-675.

[66] Kochevar, I.E., Lynch, M.C., Zhuang, S., Lambert, C.R., *Photochemistry and Photobiology*, **2000**, *72*, 548-553.

[67] Winter, S., Weber, E., Eriksson, L., Csoregh, I., *New Journal of Chemistry*, **2006**, *30*, 1808-1819.

[68] Ciesielski, A., Piot, L., Samori, P., Jouaiti, A., Hosseini, M.W., *Advanced Materials*, **2009**, *21*, 1131-1136.

[69] Blattman, H., Meuche, D., Heilbron, E., Molyneux, R.J., Boekelhe, V., *Journal of the American Chemical Society*, **1965**, *87*, 130-131.

[70] Mitchell, R.H., *European Journal of Organic Chemistry*, **1999**, *11*, 2695-2703.

[71] Mitchell, R.H., Ward, T.R., Chen, Y.S., Wang, Y., Weerawarna, S.A., Dibble, P.W., Marsella, M.J., Almutairi, A., Wang, Z.Q., *Journal of the American Chemical Society*, **2003**, *125*, 2974-2988.

[72] Roldan, D., Cobo, S., Lafolet, F., Vila, N., Bochot, C., Bucher, C., Saint-Aman, E., Boggio-Pasqua, M., Garavelli, M., Royal, G., *Chemistry A European Journal*, **2015**, *21*, 455-467.

[73] Cobo, S., Lafolet, F., Saint-Aman, E., Philouze, C., Bucher, C., Silvi, S., Credi, A., Royal, G., Chemical Communications, 2015, 51, 13886-13889.

[74] Khanam, H.S., *European Journal of Medicinal Chemistry*, **2014**, *97*, 483-504.

[75] Viault, G., Grée, D., Das, S., Yadav, J.S., Grée, R., *European Journal of Organic Chemistry*, **2011**, *7*, 1233-1241.

[76] Wiedbrauk, S., Dube, H., *Tetrahedron Letters*, **2015**, *56*, 4266-4274.

[77] Yan, H., Süss-Fink, G., Neels, A., Stoeckli-Evans, H., *Dalton Transactions*, **1997**, 4345-4350.

[78] Barry, N., Therrien, B., *European Journal of Inorganic Chemistry*, **2009**, 4695-4700.

[79] Sheldrick, G.M., *Acta Crystallographica Section A*, **2008**, *64*, 112-122.

[80] Farrugia, L., *Journal of Applied Crystallography*, **1997**, *30*, 565.

[81] Borch, R.F., *Journal of Organic Chemistry*, **1969**, *34*, 627-629.

List of Structures

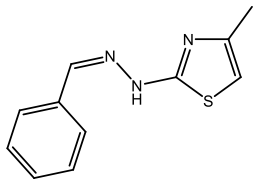

L1

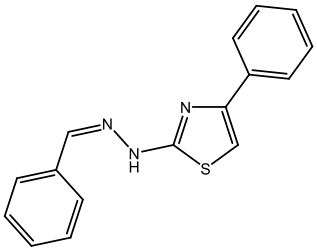

L2

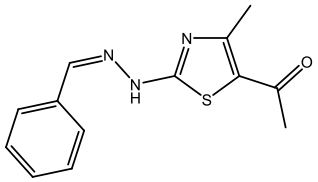

L3

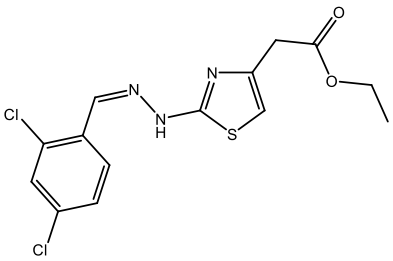

L4

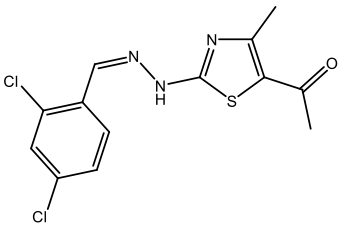

L5

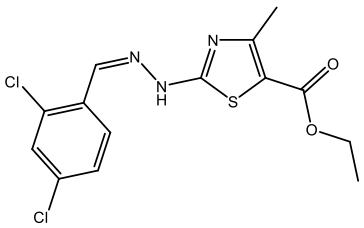

L6

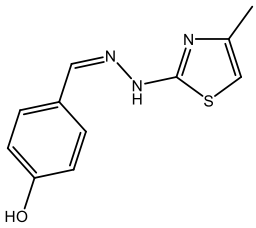

L7

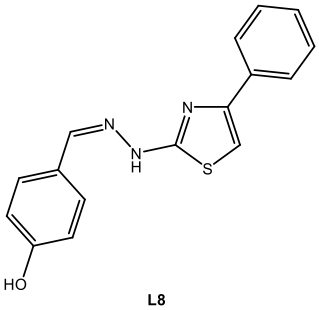

L8

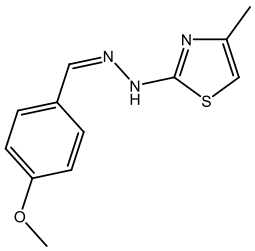

L9

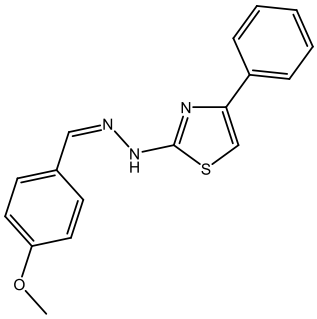

L10

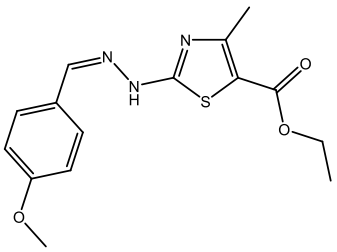

L11

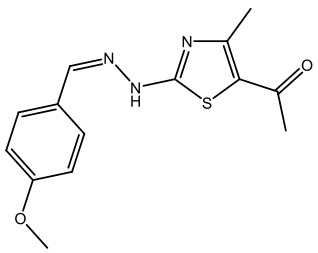

L12

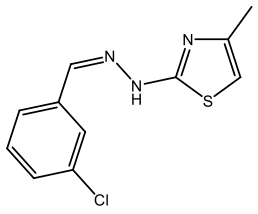

L13

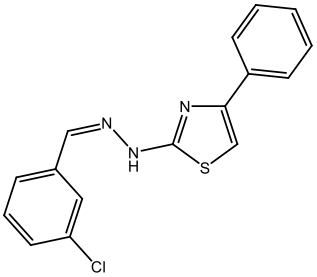

L14

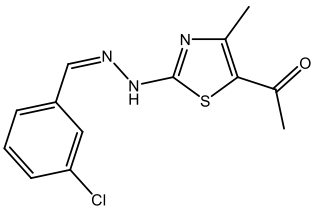

L15

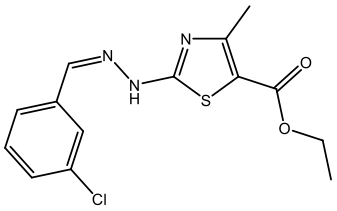

L16

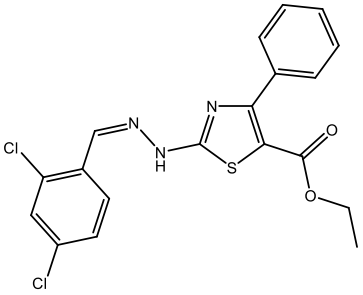

L17

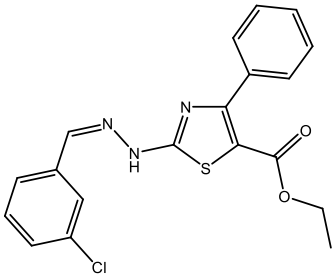

L18

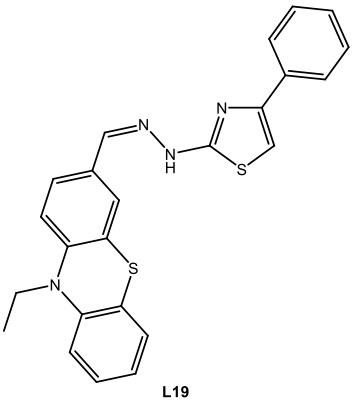

L19

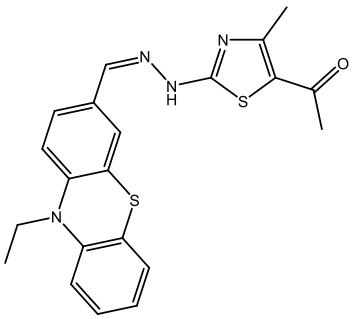

L20

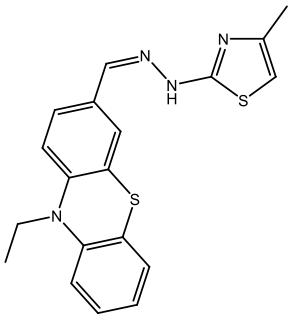

L21

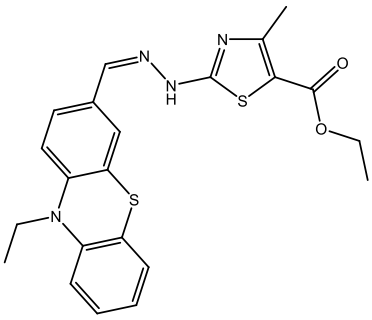

L22

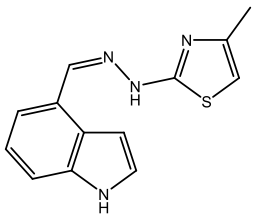

L23

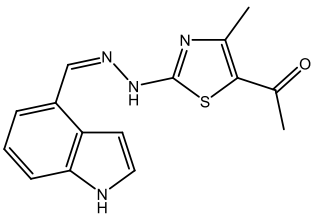

L24

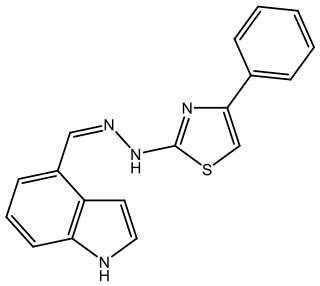

L25

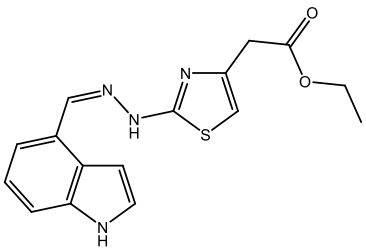

L26

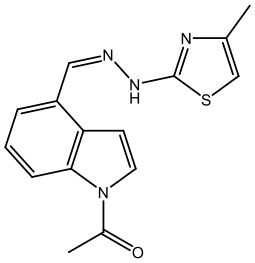

L27

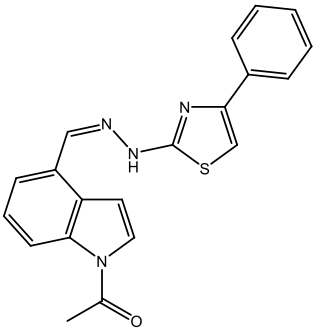

L28

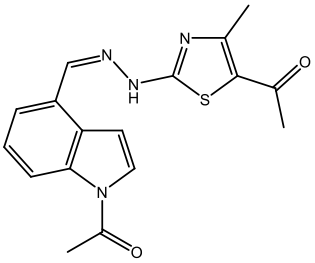

L29

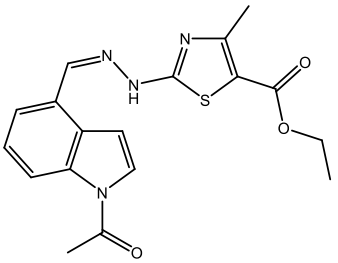

L30

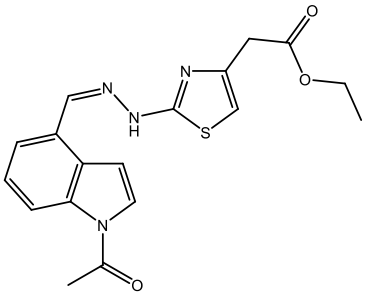

L31

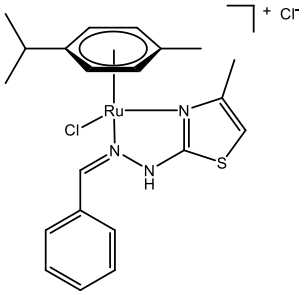

1

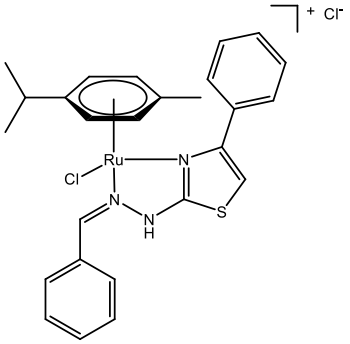

2

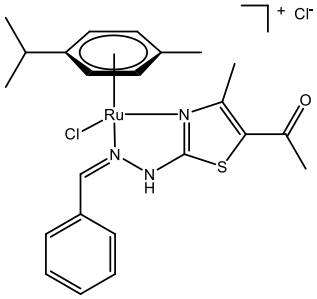

3

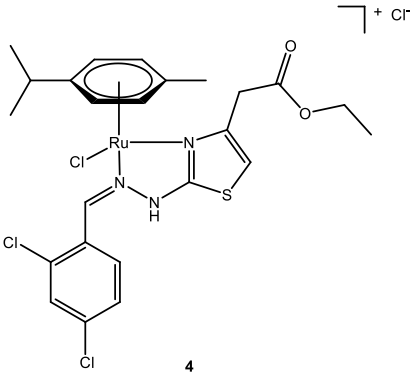

4

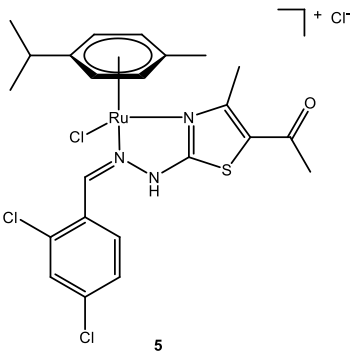

5

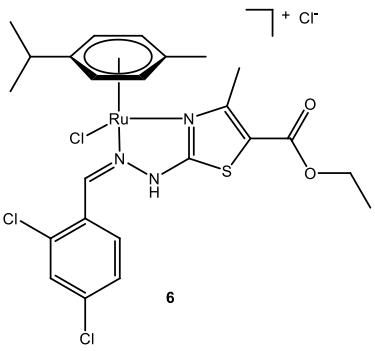

6

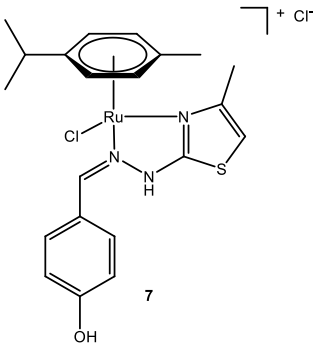

7

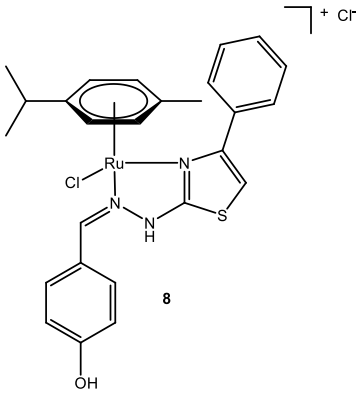

8

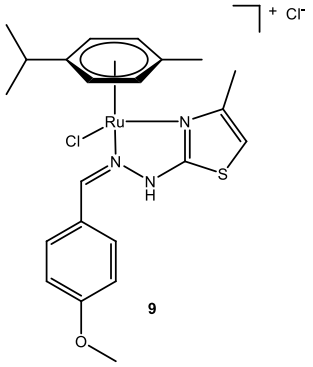

9

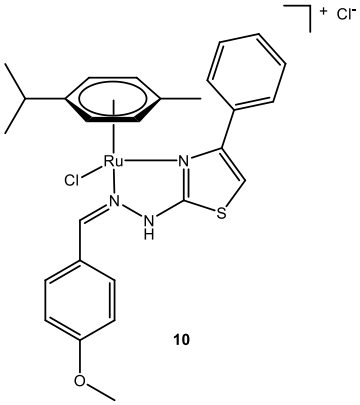

10

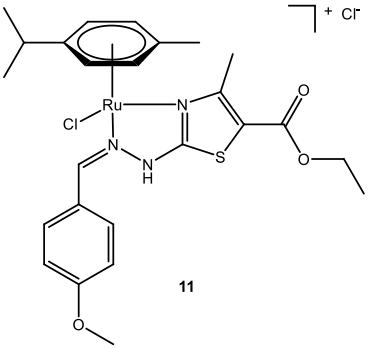

11

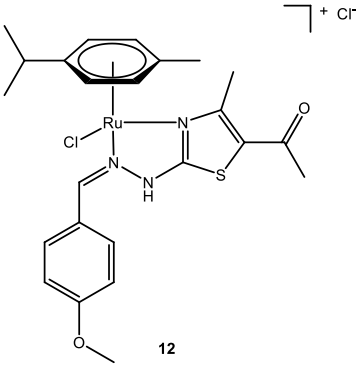

12

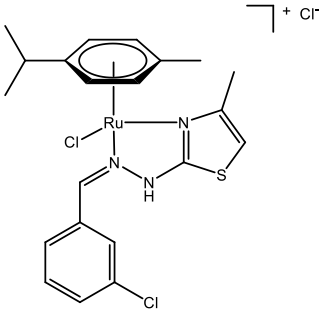

13

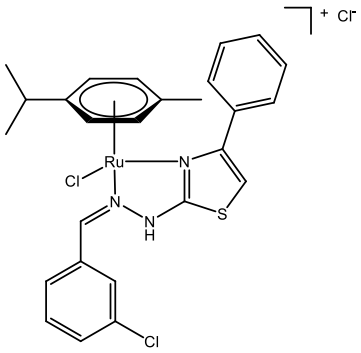

14

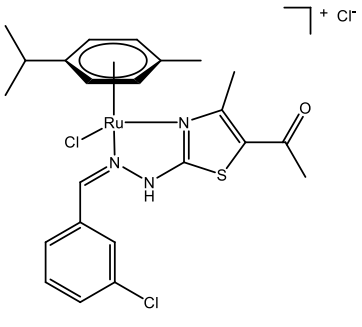

15

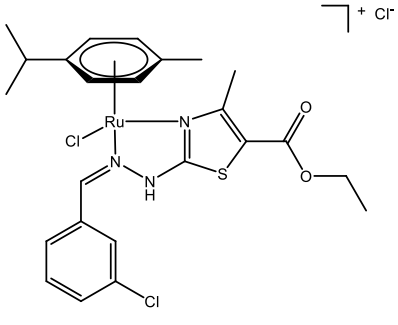

16

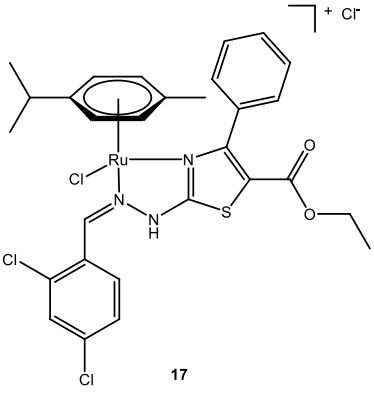

17

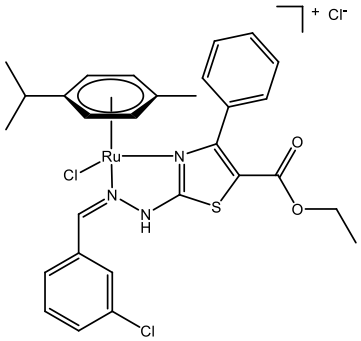

18

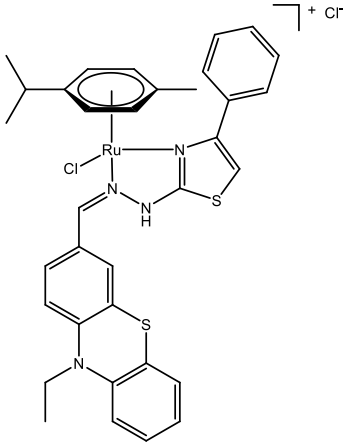

19

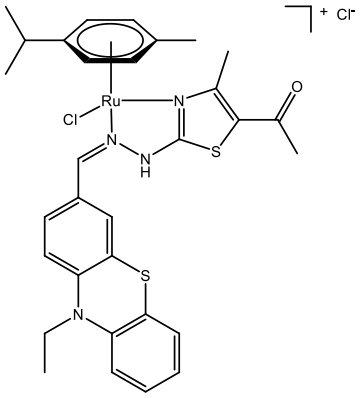

20

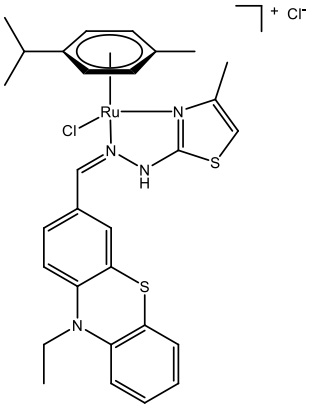

21

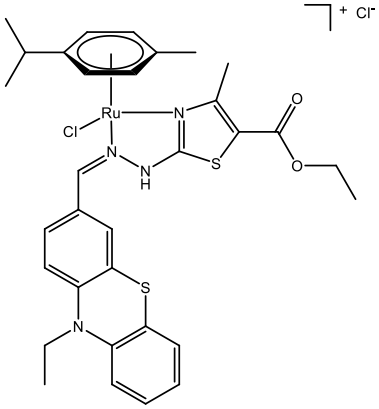

22

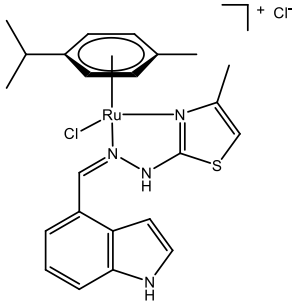

23

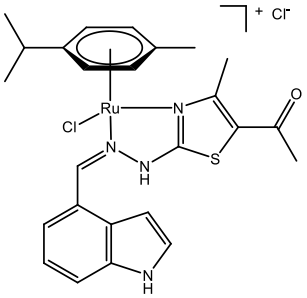

24

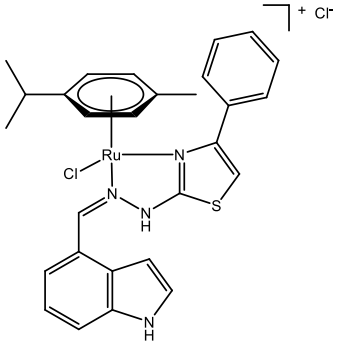

25

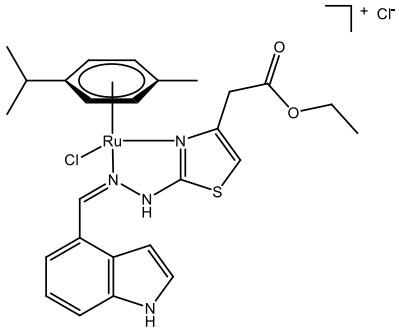

26

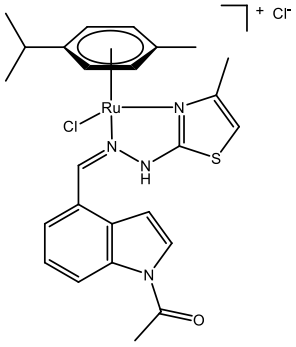

27

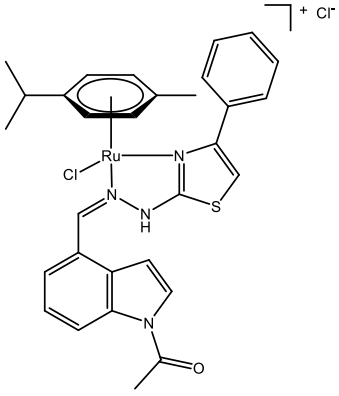

28

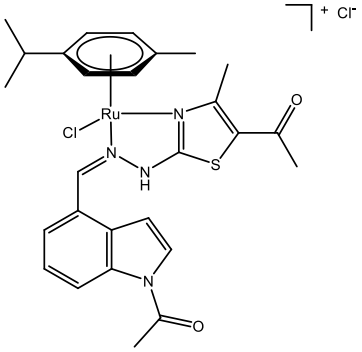

29

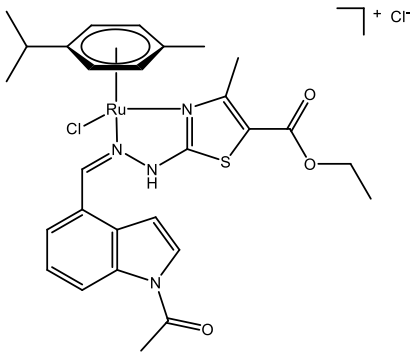

30

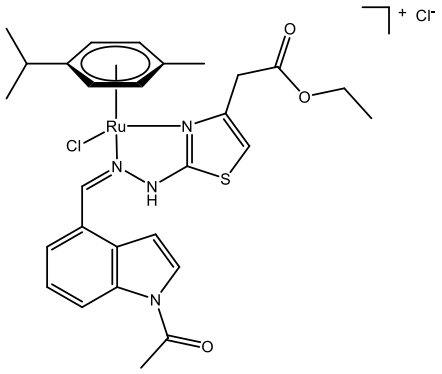

31

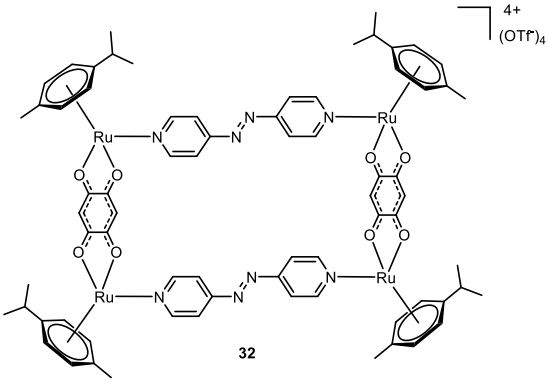

32

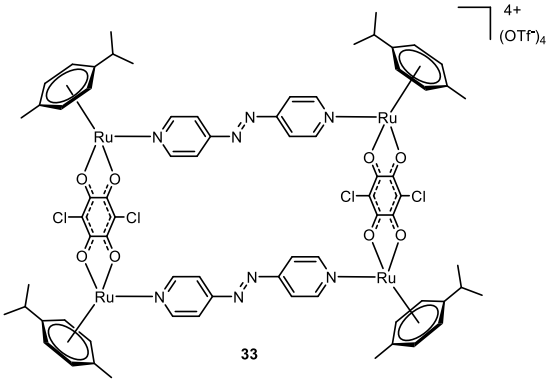

33

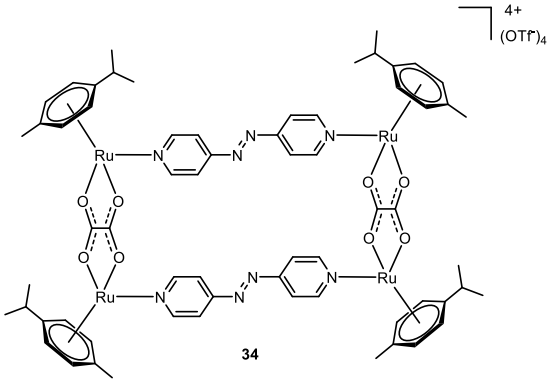

34

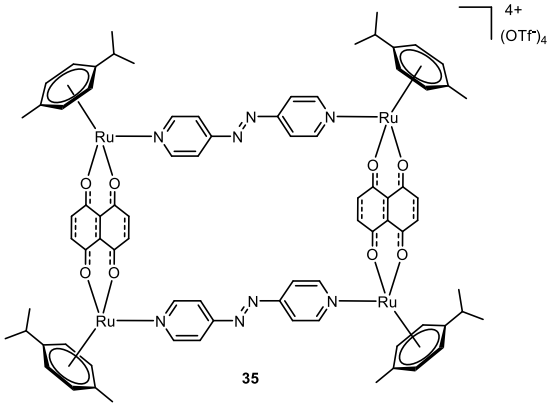

35

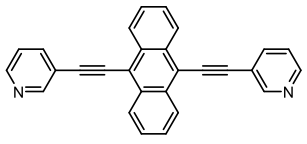

L36

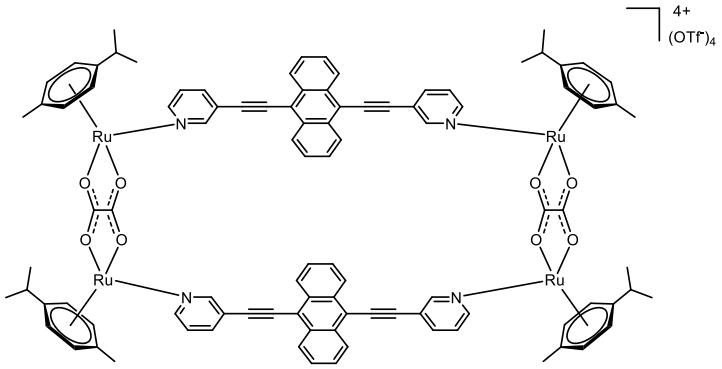

36

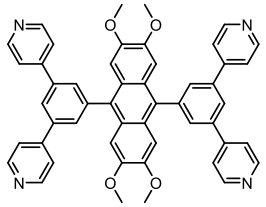

L37

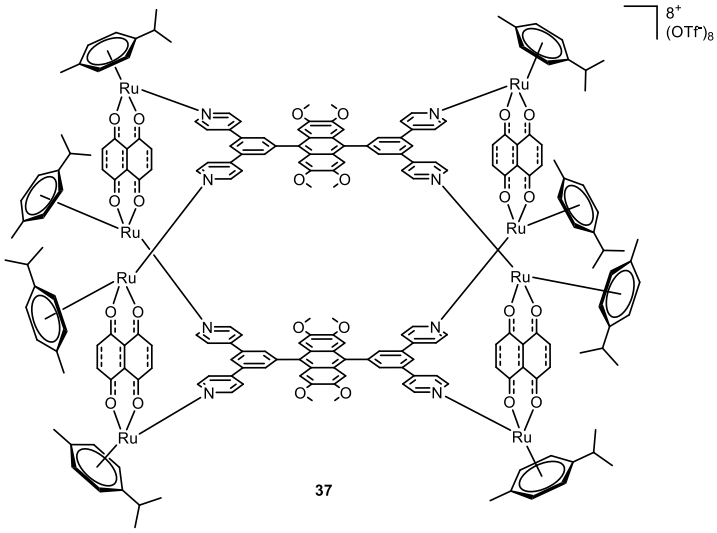

37

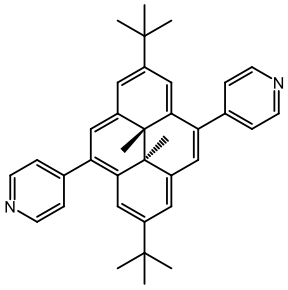

L38

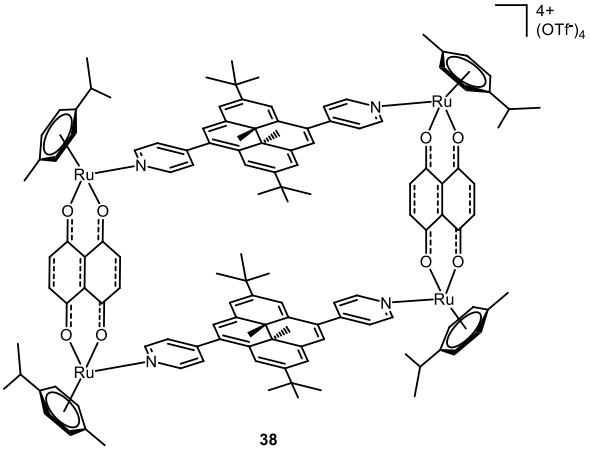

38

List of Publications and Conference Contributions

During the PhD studies:

Grozav, A., Balacescu, O., Balacescu, L., Cheminel, T., Berindan-Neagoe, I., Therrien, B., *Journal of Medicinal Chemistry*, **2015**, *58*, 8475-8490.

Previous work:

Moussa, J., Cheminel, T., Freeman, G.R., Chamoreau, L.-M., Williams, G.J.A., Amouri, H., *Dalton Transactions*, **2014**, *43*, 8162-8165.

Conference Contributions:

SCS Fall Meeting 2015, Lausanne, Switzerland – Poster

SGK-SSCr Annual Meeting and General Assembly 2015, Neuchâtel, Switzerland – Poster

SCS Fall Meeting 2014, Zürich, Switzerland – Poster

SCS Fall Meeting 2013, Lausanne, Switzerland – Poster

European Winter School on Physical Organic Chemistry 2013, Bressanone, Italy – Flash presentation + Poster – Best Poster Award